Institut für Angewandte Photophysik
Fachrichtung Physik
Fakultät Mathematik und Naturwissenschaften
Technische Universität Dresden

White Organic Light Emitting Diodes

Dissertation
zur Erlangung des
akademischen Grades
Doctor rerum naturalium,
(Dr. rer. nat.)

vorgelegt von
Thomas Conrad Rosenow
geboren am 09.04.1981 in Cottbus

Dresden 22.03.2011

TECHNISCHE UNIVERSITÄT DRESDEN

Eingereicht am 11.06.2010

1. Gutachter: Prof. Dr. K. Leo

2. Gutachter: Prof. Dr. K. Meerholz

Verteidigt am 21.03.2011

Contents

Publications

Articles

1. T. C. Rosenow, K. Walzer, and K. Leo. ”Near-infrared organic light emitting diodes based on heavy metal phthalocyanines”. *J. Appl. Phys.* **103**, 043105 (2008).

2. G. Schwartz, S. Reineke, T. C. Rosenow, K. Walzer, and K. Leo. ”Triplet harvesting in hybrid white organic light-emitting diodes”. *Adv. Funct. Mater.* **19**, 1319 (2009).

3. S. Reineke, T. C. Rosenow, B. Lüssem, and K. Leo. ”Improved high-brightness efficiency of phosphorescent organic LEDs comprising emitter molecules with small permanent dipole moments”. *Adv. Mater.* accepted (2010).

Conference Contributions

1. T. C. Rosenow, K. Walzer, K. Leo. ”Infrared light from organic light emitting diodes”. *DPG - Frühjahrstagung* **SYOE**, 8.64 (2007).

2. T. C. Rosenow, G. Schwartz, and K. Leo. ”OLEDs comprising different phosphorescent emitters in a single layer: a step towards triplet harvesting”. *ICEL 7*, 01.12 (2008)

3. T. C. Rosenow, S. Reineke, B. Lüssem, and K. Leo. ”Three colour triplet harvesting in white OLEDs”. *Plastic Electronics Europe* (2009).

4. T. C. Rosenow, S. Olthof, S. Reineke, B. Lüssem, and K. Leo. ”Four colour stacked white organic light-emitting diodes utilizing the concept of triplet harvesting”. *SPIE Photonics Europe* **7722**, 4 (2010).

5. B. Lüssem, S. Reineke, T. C. Rosenow, G. Schwartz, K. Leo. ”Novel concepts for OLED lighting”. *Proceedings of the SPIE - Light-Emitting Diodes: Materials, Devices, and Applications for Solid State Lighting XIV* **7617**, 761712 (2010).

List of Important Abbreviations

CCT	correlated color temperature
CIE	Commission Internationale de l'Éclairage
CRI	color rendering index
EBL	electron blocking layer
EML	emission layer
ETL	electron transport layer
HBL	hole blocking layer
HTL	hole transport layer
IAPP	Institut für Angewandte Photophysik, Technische Universität Dresden
ISC	intersystem crossing
ITO	indium tin oxide
HOMO	highest occupied molecular orbital
LCAO	linear combination of atomic orbitals
LED	light emitting diode
LUMO	lowest unoccupied molecular orbital
OLED	organic light-emitting diode
UPS	ultraviolet photoelectron spectroscopy
TTA	triplet-triplet annihilation
TPA	triplet-polaron annihilation

1 Introduction

Due to their low power efficiency, incandescent lamps are gradually banned in the European Union. Thus, there is a strong need for alternative highly efficient light sources for illumination and general lighting purposes. For indoor and workplace illumination, the requirements on colour and colour rendition are particularly high and the emission of a light source should be as close to black-body radiation/ sunlight as possible. Beside inorganic light emitting diodes (LEDs), fluorescent lamps are currently the strongest competitor to meet these requirements. However, organic light emitting diodes (OLEDs) are developing into a serious alternative in terms of efficiency, colour quality, and lifetime.

OLEDs have some general benefits compared with other light sources. They are area emitters and produce diffuse light. Hence, they do not glare a customer or produce sharp shadows. From a designers point of view OLEDs can be produced in almost any shape. Additionally, the thickness of an OLED product is only limited by the thickness of the substrate and the encapsulation. This allows for thin flexible devices with an overall thickness below 0.5 mm [1–3]. Due to their mercury content, fluorescent tubes need to be disposed separately from normal domestic waste after they have reached the end of their life cycle. OLEDs are free of mercury and therefore, provide a more ecological light source.

OLEDs can be distinguished between those based on small molecules and those based on polymers. Polymer OLEDs are processed by spin coating or wet printing technics [4]. Small molecule OLEDs are produced by the sublimation of the dye and subsequent condensation on a substrate under high vacuum conditions. This work focuses exclusively on the OLEDs consisting of small molecules.

Electroluminescence in organic material was first observed by Bernanose et al. in the 1950s, when a high-voltage alternating current field was applied to thin films of crystalline acridine orange and quinacrine [5, 6]. By improved carrier injection and the use of a two layer structure, Tang and Van Slyke were able to significantly decrease driving voltage and increase the efficiency of OLEDs in 1987 [7]. Further improvements concerning the charge carrier injection and transport were possible by electrically dop-

ing of the organic materials [8]. By systematically adding of impurities charge carrier density and mobility can be increased by several orders of magnitude [9, 10]. The improved mobility in the electrically doped transport layers allowed for optical optimisation of the microcavity of an OLED and increased external quantum efficiencies without an increase of the driving voltage [11]. A significant efficiency increase was possible by the introduction of heavy metal atoms into the organic molecules. In the presence of these metals, the spin conservation law is weakened and radiative transition of triplet excitons to the ground state is allowed. Hence, internal quantum efficiencies up to 100 % are possible [12]. Due to the radiative recombination of triplet excitons, these molecules are called phosphorescent emitters.

Stable and efficient phosphorescent emitters covering the spectral range from green to red are already well known and investigated [13, 14]. However, the available phosphorescent blue emitters do neither reach deep blue colour coordinates nor extended lifetimes [15, 16]. Consequently, fully phosphorescent OLEDs are currently limited in the achievable colour coordinates and the colour rendering index (CRI) [17, 18]. The more stable fluorescent emitters offer a rich variety of deep blue emission spectra [19–21]. The low efficiencies implied by quantum statistics can be overcome by the concept of triplet harvesting. By transferring otherwise unused triplet excitons from a fluorescent to a phosphorescent emitter, internal quantum efficiencies up to 100 % are possible [22, 23]. In this work the separation of singlet and triplet excitons is optimised and the simultaneous transfer of triplets to more than one phosphorescent emitter is investigated.

The stability of the spectrum against varying brightness is specifically of interest for lighting applications, because it provides the possibility to dim the light source to a brightness according to a given situation. A shift of the position of the charge carrier recombination zone can be the cause for a strong brightness dependence of the spectral shape if the OLED is composed of several emission layers with each comprising a single emitter [23]. The combination of several emitters in a single mixed layer bears the potential for good colour stability and, additionally, this approach simplifies the OLED architecture by the reduction of the number of layers. Here, different combinations of two phosphorescent emitters in a common matrix are investigated. The questions are addressed, in which way well balanced emission from both emitters can be achieved and in which way the second emitter can positively influence the quantum efficiency of the OLED.

Due to the low triplet gap of most fluorescent blue emitters, triplet transfer to a green phosphorescent emitter is not possible. OLEDs combining triplet harvesting and the emission of a phosphorescent green emitter are suffering from a loss of singlets to the green emitter [24]. A reduction of singlet-triplet splitting may result in fluorescent emitters, which allow for triplet harvesting to green phosphorescent emitters. However,

reducing the energetic difference between first excited singlet and triplet state, will increase the inter system crossing rate. Consequently, the already low blue emission is further reduced. A possibility to extend the spectrum of a red/blue triplet harvesting OLED in the green spectral region is the stacking of a second OLED on top of this device. In the last chapter, the optimised red/blue triplet harvesting OLED is combined with a full phosphorescent OLED which comprises the emission of a green and a yellow phosphorescent emitter. The resulting four colour white OLED features warm white colour coordinates, good colour rendition and high luminous efficacies.

2 Illumination and Colour Perception

This chapter gives an overview on the aspects of the anatomy of the human eye relevant to colour and intensity perception. The evaluation of a light source with respect to its application as illuminant is based on a handful of quantities, which correspond directly to the perception of human eye. The definition of those quantities and their relation to the anatomy of the human eye is elaborated in detail. Also, an overview on conventional light sources and their typical advantages and disadvantages is given.

2.1 Anatomy of the Human Eye

In the following section definitions for colour coordinates, white light, and colour rendering index will be presented. In order to understand the specification of these quantities, it is useful to summarise the light perception of the human eye. A cross-section of the human eye is shown in Figure 2.1. The eye is protected by an outer layer formed by the transparent cornea and the opaque sclera. The cornea, the anterior chamber, the lens, and the vitreous fluid form a lens system, which refracts light in a manner that it is focused on the retina. The shape of the lens can be adjusted to a specific focus by attached muscles.

The retina is the photosensitive part of the eye and consists of four different types of electrochemical receptors. The first one is the rod, which covers the largest part of the retina. Rods are very sensitive and are able to detect single photons. The rods are most sensitive to light at a wavelength of 510 nm and are used for monochrome vision under dark conditions, which is called scotopic vision. The rods are supplemented by three types of cones (named ρ, γ, and β for red, green, and blue) which enable colour vision. They are less sensitive than the rods and dominate the perception under bright light (photopic vision).The maximum of the sensitivity for the ρ-, γ-, and β-cones is at

590 nm, 540 nm, and 440 nm. The sensitivity curves are illustrated in Figure 2.2 [25].

The three types of cones are not represented equally. It was shown that the distribution can strongly vary between different individuals. For example, two test persons had the same share of β-cones of roughly 4 %, but totally different ratios between ρ- and γ-cones of $\rho/\gamma = 3.79$ and $\rho/\gamma = 1.15$ [26]. The quantitative lack of cones sensitive in the blue region is balanced by an increased sensitivity and a further amplification of the emitted signals with respect to the other ρ and γ type.

The cones are concentrated in the macula lutea. Macula lutea is the Latin word for yellow spot and describes the colour of this small area on the retina which has a diameter of roughly 5 mm. The highest concentration is near the centre of the macula lutea at the so called fovea. The average peak density is around 200 000 mm^{-2} and falls rapidly to the half maximum at a distance of roughly 150 µm. Within 1 mm the density decreases further to 20 000 mm^{-2} [27]. The yellow colour of the macula lutea is the result of a strong absorption in the ultraviolet and deep blue wavelength region which acts like natural sun glasses for the receptors. On an average, a human eye has 4.6 million cones and 92 million rods. The fovea and an area of 0.35 mm around fovea contains cones and is free of rods. The rods are not evenly distributed on the rest of the retina. The highest density of rods constitutes an oval ring with a radius of approximate 5 mm around the fovea [27].

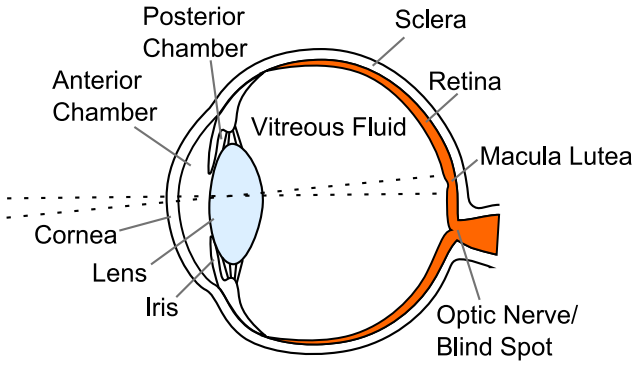

Figure 2.1: *The anatomy of the human eye. The transparent cornea and the opaque sclera form the outer protection layer of the human eye. The part of the retina with the highest receptor concentration is called the macula lutea (yellow spot). Most precise vision and sensitivity is given near the centre of the macula lutea in the fovea [28].*

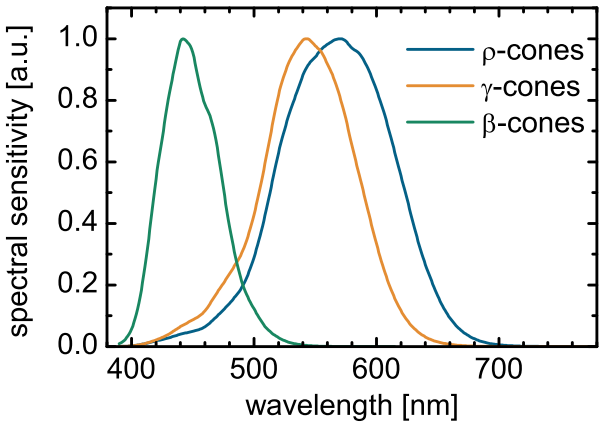

Figure 2.2: *Normalised spectral sensitivity of the three types of cones in the human eye [25].*

2.2 Quantification of Colour Perception

Caused by the difference in the sensitivity of rods and cones, light is differently perceived with regard to its intensity. Under dark conditions, the perception is dominated by the rods (scotopic vision) and under bright light it is dominated by the cones (photopic vision). If one intends to define quantities to describe colour, colour rendition, and intensity of a light source with respect to the human eye, these should relate to certain intensity range. The purpose of these quantities is to evaluate light sources as potential indoor illuminants. Therefore, they are related to the range of photopic vision. The Commission Internationale de l'Éclairage (CIE) gave recommendations as to which definitions should be used.

2.2.1 Colour Coordinates/Standard Observer

Colour perception is carried out exclusively by the cones. Every cone on its own is a monochrome receptor. Hence, colour perception occurs by means of three parameters termed as tristimulus values. Depending on their definition different colour spaces are spanned by the tristimulus values. The most often used model is the *CIE 1931 2° Standard Observer* (in the following referred to as Standard Observer). This model represents the colour perception within an angle of 2° around the centre of the field of vision. The Standard Observer is characterised by three colour matching functions (Figure 2.3) which were published by the CIE in 1931 [29] and are based on measurements by Guild [30] and Wright [31]. The tristimulus values (colour coordinates) result from a convolution of the spectrum of the light source with these functions.

An alternative way to describe the colour is a combination of a two dimensional chromaticity and a brightness parameter. An often used representation is the xyY-coordinate system. The chromaticity (x, y) is a projection of the X, Y and Z coordinate of the Standard Observer in a two dimensional space (Figure 2.4) and is given by:

$$x = \frac{X}{X+Y+Z},\ y = \frac{Y}{X+Y+Z}. \tag{2.1}$$

The Y coordinate is used as an additional brightness variable (This will be justified in section 2.2.4.). A model which is less often used, but closer to the actual perception of the human eye is the *CIE 1964 10° Standard Observer*. This model represents the colour perception within an angle of 10° around the centre of the field of vision. The *CIE 1960 Uniform Colour Space* and the *CIE 1964 Colour Space* are otherwise obsolete colour spaces, but are still used to evaluate the colour rendition of a light source.

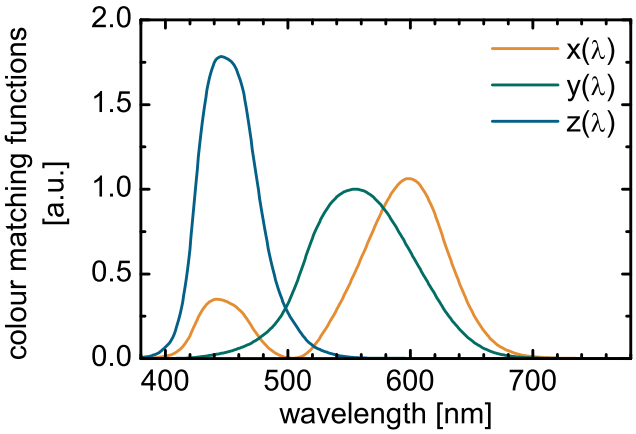

Figure 2.3: *Colour matching functions of the CIE 1931 2° Standard Observer [29].*

2.2.2 White Light

For the purpose of this work, it is important to clarify what can be understood by the term white light. The CIE defines white as the spectrum of a black body. Furthermore, light is considered as white if the Euclidean distance (in the *CIE 1960 Uniform Colour Space*) between its colour coordinates and the Planckian locus is below $5.4 \cdot 10^{-3}$.

$$\Delta E = \sqrt{\Delta u^2 + \Delta v^2} \leq 5.4 \cdot 10^{-3} \tag{2.2}$$

This definition implies that a black body with a low temperature is a white light source, although its colour would appear as red. Therefore, light sources are compared to

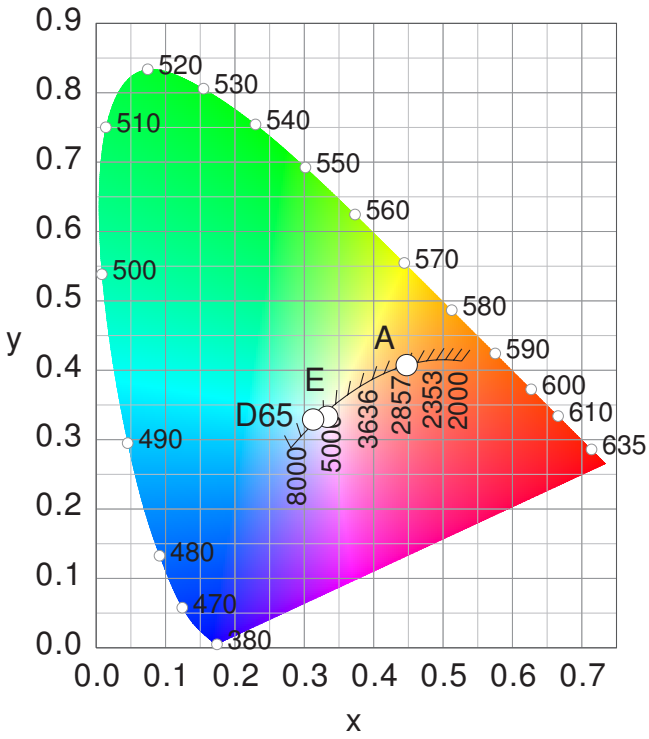

Figure 2.4: *The colour space which is defined by the x and y coordinates of the xyY-coordinate system. Monochromatic light sources form the outer border of the horse shoe. Black body emission at different temperatures is represented by the Planckian locus (plotted as black line, corresponding temperatures are stated in K). The chromaticity coordinates of important reference illuminants are highlighted.*

certain reference points on or close to the Planckian locus which bear a special meaning (Figure 2.4). These reference points are given by the CIE standard illuminants. They are referred to by a single letter or a combination of a letter and a number. The CIE standard illuminant A $(x,y) = (0.448, 0.407)$ is a black body with the temperature of 2856 K and represents the light of an incandescent lamp. The CIE standard illuminant E $(x,y) = (0.333, 0.333)$ is not a black body radiator. It is characterised by a constant spectral power distribution also known as the equal-energy radiator. The CIE standard illuminants D are a series of illuminants representing natural daylight at different times of a day. The most often used illuminant of the D series is D65 $(x,y) = (0.313, 0.329)$, which describes the sun light in Western or Northern Europe at midday.

2.2.3 Colour Rendering Index

Since entirely different spectra can be described by the same colour coordinates, an additional quantity is needed to evaluate the colour rendition properties of a light source. The colour rendition can only be described by comparison to another light source. In order to ensure comparability between different laboratories an independent reference is needed. A feasible reference is given by the black body. The temperature of the black body is chosen in a way that the Euclidean distance in the *CIE 1960 Uniform Colour Space* to the light source to be evaluated is minimised. This temperature is called the correlated colour temperature (CCT) of the light source. The black body is chosen as reference up to a CCT of 5 000 K. Above that point, a CIE Standard Illuminant of the D series is preferred.

The comparison of the colour rendition of a light source and its reference is based on eight test colour samples. The test colour samples are illuminated each at a time with the light source and the corresponding black body. The special colour rendering index (CRI) for each test colour sample is proportional to the Euclidean distance of the colour coordinates of the reflected light in the *CIE 1964 Colour Space*. The general CRI (R_a) is the arithmetic mean of the eight special CRIs.

For the estimation of the CRI, no actual test colour samples are illuminated. This is rather done by convolution of defined reflectivity curves with the spectra of the light source and its reference. The precise calculation was published by the CIE [32].

This definition of the CRI has some major drawbacks. The use of three different colour spaces makes the calculation very complicated. Furthermore, it is only defined for white light sources. Light sources which are not close enough to the Planckian locus do not deliver conclusive values. White light sources with different correlated colour temperatures render colours in a different way, but may result in the same CRI. For these and other reasons the CIE is currently working on an improved method to describe colour rendition properties [33].

2.2.4 Radiometric vs. Photometric Quantities

The human eye can perceive light in a small wavelength range and the sensitivity shows a strong dependence on the wavelength. Therefore, radiometric quantities can not describe the brightness of a light source as it is perceived. The luminous efficiency function V_λ (often only called V_λ function) reflects the spectral response of the human eye. It is important to distinguish between the rod dominated scotopic and the cone dominated photopic vision. The scotopic (V'_λ) and photopic (V_λ) luminous efficiency

functions are plotted in Figure 2.5. The photopic luminous efficiency function was measured by Gibson [34] and standardised by the CIE in 1926 [35]. Furthermore, it is used as the colour matching function of the Y coordinate of the *CIE 1931 2° Standard Observer*. Therefore, the Y coordinate is used as brightness variable in the xyY-coordinate system(Section 2.2.1). Although more precise measurements are published [36], this is still the common standard for brightness measurements. All radiometric quantities can be transfered into photometric quantities by the use of the photopic luminous efficiency function. This is done by convolution of the spectral radiometric quantity with the V_λ function and multiplication with a constant K_m. For instance the luminous flux Φ_v can be derived from the radiant flux Φ_e by:

$$\Phi_v = K_m \int_{380\text{nm}}^{780\text{nm}} \Phi_e(\lambda) V_\lambda \, d\lambda \,, \tag{2.3}$$

with $K_m = 683$ lm/W for photopic and $K_m = 1\,699$ lm/W for scotopic vision. Table 2.1 summarises the four fundamental radiometric and their corresponding photometric quantities.

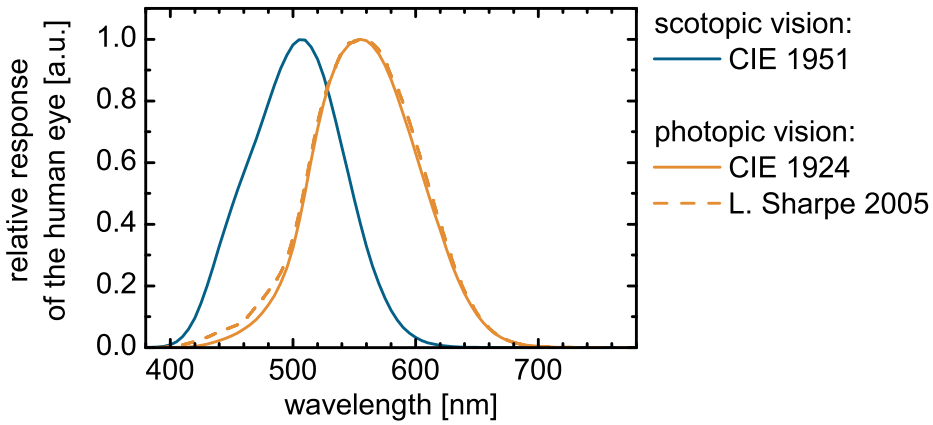

Figure 2.5: *The scotopic luminous efficiency as published by the CIE in 1951[37, 38], the photopic luminous efficiency as published by the CIE in 1926 [35] and the more precise measurement of the same done by Sharpe et al. in 2005 [36].*

2.3 Conventional Light Sources

The characteristics of different light sources are discussed in detail in this chapter. The properties of each light source make it more appropriate for a specific application and

radiometric quantity	symbol	unit	photometric quantity	symbol	unit
radiant flux	Φ_e	W	luminous flux	Φ_v	lm
radiant intensity	I_e	W/sr	luminous intensity	I_v	$cd = lm/sr$
irradiance	E_e	W/m^2	illuminance	E_v	$lx = lm/m^2$
radiance	L_e	W/m^2sr	luminance	L_v	cd/m^2

Table 2.1: *Radiometric and their corresponding photometric quantities. The photometric SI units are lumen (lm), candela (cd), and lux (lx).*

some of these light sources are direct competitors to OLEDs, while others target on different markets.

The Incandescent Lamp

Incandescent lamps are consisting of a glowing tungsten wire in an evacuated glass bulb. The luminous efficacy is as low as 14.8 lm/W and the typical device lifetime does not exceed 1 000 h. By filling the glass bulb with a halogen gas, the lifetime is extended to 2 000 h and the efficacy increases up to 19 lm/W [39]. These very low values imply that almost 95 % of all energy is lost as heat. However, incandescent lamps have the highest achieveable colour rendering index (CRI = 100), because an incandescent lamp can be considered as Planckian radiator (Section 2.2.3). These lamps are widely used for indoor and outdoor illumination as well as for design purposes. Due to their successive ban in the European Union and a generally increased ecological awareness, the incandescent lamp will vanish in the near future and will be replaced by alternative light sources.

The Fluorescent Lamp

The fluorescent lamp is based on the electrical excitation of mercury vapour at a low pressure (0.5 Pa [40]). The mercury vapour is emitting ultraviolet light. A fluorescent coating at the inner surface absorbs the ultraviolet radiation and emits light in the visual spectral region. Because the mercury vapour has to be ionised before operation, the fluorescent lamp needs additional electronics for starting. Furthermore, fluorescent lamps have a negative differential resistivity. Hence, they will fast be destroyed by too high currents, if they are connected to a constant power supply. Accordingly, a ballast is needed to limit the current flowing through the lamp. The benefit of fluorescent lamps are their high light output of up to 2 800 lm and their high efficacy of up to 87.5 lm/W.

Taking additionally their warming time into account, they are especially suited for permanent illumination of large rooms. For smaller rooms the compact fluorescent lamps with a screw base have been developed. These have a lower light output of around 900 lm and luminous efficacies of 60 lm/W and are often used to replace the incandescent lamp [39]. Therefore compact fluorescent lamps are direct competitors to OLEDs, because this is the market, which is also targeted by the white OLED.

The Sodium Vapour lamp

The working principle of the sodium vapour lamp is similar to that of the fluorescent lamp. The use of sodium instead of mercury makes the fluorescent coating obsolete, because sodium is emitting in the visible region. These lamps are characterised by efficacies of up to 130 lm/W [40] and a narrow emission line at 589 nm. Due to their high efficacy and long lifetime (up to 20 000 h), sodium vapour lamps are often used as street lights. However, their poor colour rendition of $\mathrm{CRI} = -44$ does allow only for a few other applications, such as greenhouse illumination [40].

The Light Emitting Diode

The light emitting diode (LED) was invented in 1962 by N. Holonyak Jr. [41]. The applications of this highly efficient, strongly directed point light source range from indicator lamps to illumination. Commercially available LEDs reach luminous efficacies around 70 lm/W and lifetimes of 50 000 h [39]. *Cree Inc.* announced in a recent press release (03.02.2010) a record luminous efficacy of 208 lm/W for a white LED with a CCT of 4 579 K at room temperature. Although the angular dependence of the emitted light varies with the package type, LEDs have a strongly directed emission in common. Hence, a costumer is easily glared at lighting relevant brightnesses.

Similar to fluorescent lamps, white light is produced by light conversion. The light of a blue LED is partly absorbed by a photoluminescent dye and emitted in the yellow wavelength region. The resulting two colour white light features colour coordinates close to the Planckian locus, but the colour rendition properties suffer from a gap in the green region. Therefore, LEDs are not suitable for indoor illumination, despite the fact that they are sold for this purpose. As in case of sodium vapour lamps the strength of white LEDs is in applications where good colour rendition is not the main requisite, e.g., car headlights or street lights.

2.4 White Light from OLEDs

OLEDs are area emitters. Hence, regarding illumination applications, their main benefit against other light sources is diffuse light emission. Due to diffuse emission with low luminance from a large area, they do not glare a customer or produce sharp shadows. White light emission can be achieved by different approaches with different advantages and disadvantages. They can be distinguished by the employed type of emitter materials (fluorescent or phosphorescent emitters) or specific physical concepts like the concept of triplet harvesting or the stacking. In the following paragraphs, the prevalently used approaches are summarised.

The first approach is the exclusive application of fluorescent emitters. The available fluorescent blue emitters reach deep blue colour coordinates and offer prolonged lifetimes in comparison with their phosphorescent counterparts [19–21]. Therefore, cold white colour coordinates as $(x,y) = (0.285, 0.406)$ and lifetimes up to $t_{1/2} = 40\,000\ h$ at an initial luminance of $L_0 = 300$ cd/m^2 can be achieved with this approach [42]. However, since the yield of fluorescent emitters is strongly limited by spin statistics, the luminous efficacy of such devices does not exceed 10 lm/W.

By restricting the OLED design to phosphorescent emitters, luminous efficacies up to $\eta_v = 124$ lm/W at $L = 1\,000$ cd/m^2, which already exceed the efficacies of fluorescent tubes, can be achieved [17]. However, lifetime and colour quality are limited by the available phosphorescent blue emitters. Due to their typical sky blue colour coordinates, the spectra of full phosphorescent white OLEDs exhibit increased green emission, which results in greenish colour coordinates as $(x,y) = (0.41, 0.49)$ [17, 18]. Recently, a phosphorescent blue emitter with deep blue colour coordinates was presented. With this emitter it was possible to reach the CIE standard illuminant E $(x,y) = (0.33, 0.33)$, but the luminous efficacy did not exceed $\eta_v = 20$ lm/W [43].

The concept of triplet harvesting combines the benefits of both approaches, by the simultaneous application of fluorescent and phosphorescent emitters. Here, the otherwise lost triplets of a fluorescent blue emitter are transferred to a phosphorescent emitter and internal quantum efficiencies up to 100 % are possible. In case of commercially available fluorescent blue emitters, the transfer of triplets is limited to phosphorescent yellow and red emitters, due to the low first excited triplet state of the blue emitter. Green emission can be achieved in a white triplet harvesting OLED by direct recombination of charge carriers in a green emission layer. Consequently, also singlets recombine on the green emitter and the fluorescent blue emission is reduced. However, it is still possible to reach warm white colour coordinates with a CRI above 80 and luminous efficacies up to $\eta_v = 25.4$ lm/W at $L = 1\,000$ cd/m^2 [23, 44]. Recently, the development of a new fluorescent blue emitter allowed for triplet transfer to phosphorescent green emitters, but the corresponding luminous efficacies was limited to $\eta_v = 21.4$ lm/W [45].

Another possibility to combine the emission of different emitters in an OLED is given by the concept of stacked OLEDs. Two or more individual devices are subsequently processed and connected by a charge generation layer, where pairs of electrons and holes are separated [46, 47]. The resulting device is electrically equivalent to a monolithic series connection of independent OLEDs. Because external quantum efficiency and driving voltage of the individual units add up, the luminous efficacy of a stacked OLED is comparable to the single OLEDs. The advantage is that each unit can be electrically optimised to the corresponding emitter material. Therefore, it is possible to increase the efficiency in comparison with OLEDs where all emitters are combined in a single unit. It was shown that by combining three units, which comprise the emission of a fluorescent blue, a phosphorescent green, and a phosphorescent red emitter, a luminous efficacy of $\eta_v = 35$ lm/W (with attached light extraction foil) at 1 000 cd/m^2 is possible. The same device exhibited warm white light emission at $(x, y) = (0.426, 0.435)$, good colour rendition CRI $= 89.7$, and a device lifetime of $t_{1/2} = 100\,000$ h at an initial luminance of 1 000 cd/m^2 [48]. The prolonged lifetime is possible by the application of the fluorescent blue emitter, which is a tradeoff regarding the efficiency, because a part of the excitons is recombining radiationless.

3 Organic Semiconductors and Light Emitters

In this chapter, the basic working principle of OLEDs is discussed. At first, the focus is on the electronic structure of organic semiconductors, charge carrier transport and excitation exchange between molecules. In the second part of the chapter, the general composition of a pin-OLED is explained in detail and an overview is given concerning the materials which are used in the OLEDs.

3.1 Organic Dyes

OLEDs are based on vapour-deposited, amorphous thin films of organic molecules. The electronic structure of such films is entirely different from that of classical semiconductors. This directly results from a lack of a periodic lattice and weak intermolecular bonds. This section attempts to summarise and explain their properties.

3.1.1 From Atomic to Molecular Orbitals

The intermolecular bonds in amorphous, organic thin films are limited to the weak van der Waals force. Therefore, energy states E^n are primarily determined by the structure of single molecules. The time independent Schrödinger equation for this problem:

$$H\psi^n(\vec{r}) = E^n\psi^n(\vec{r}), \tag{3.1}$$

with the molecule described by the eigenfunctions ψ^n of the Hamiltonian H, can not be solved analytically. Some approximations are necessary. A first step is the Born-Oppenheimer approximation, which is the separation of the movement of electrons and nuclei. This approach is reasonable, since the movement of the nuclei can be neglected

due to their high mass in comparison to the electrons. Hence, the Hamiltonian H can be separated into a Hamiltonian describing the electrons H_e and another one describing the nuclei H_n. The total wave function is a product of the corresponding eigenfunctions ψ_e and ψ_n:

$$H = H_e + H_n \tag{3.2}$$

$$\psi = \psi_e \cdot \psi_n \,. \tag{3.3}$$

The Hartree product assumes non-interacting electrons. Therefore, the total wave function can be written as a product of the wave functions of the single electrons ψ_i:

$$\psi_e = \prod_i \psi_i \,. \tag{3.4}$$

Considering the spin and the fermionic character of electrons, this product must be antisymmetric with regard to exchange of two electrons. The antisymmetry is ensured by means of the Slater determinant:

$$\psi_e = \frac{1}{\sqrt{N!}} \begin{vmatrix} \psi_1(1) & \psi_1(2) & \cdots & \psi_1(N) \\ \psi_2(1) & \psi_2(2) & \cdots & \psi_2(N) \\ \vdots & \vdots & \ddots & \vdots \\ \psi_N(1) & \psi_N(2) & \cdots & \psi_N(N) \end{vmatrix} . \tag{3.5}$$

It was found that the electron wavefunctions of hydrocarbons can be described by a series expansion with the atomic orbitals Φ_i as a set of basis functions [49]. This method is called linear combination of atomic orbitals (LCAO) [50]:

$$\psi_i(\vec{r}) = \sum_k c_{i,k} \Phi_i(\vec{r}) \,. \tag{3.6}$$

The band gap for light emission in the visible wavelength region is in the range of $2 \ldots 4$ eV, which is typical for aromatic compounds as benzene. The alternating arrangement of single and double bonds in these molecules results in remarkable electrical and optical properties. The sp^2 hybrid orbitals provide a good set of basis functions for applying the LCAO method on benzene. These orbitals are a superposition of the s-, p_x-, and p_y-orbital of the carbon atom. The bonding angles of the sp^2 orbitals equal the angle of 120° between the carbon atoms of the benzene (Figure 3.1) and form the so called σ bonds in the xy plane. Due to their strong overlap, the σ bonds are the strongest type of covalent bonds and mainly determine the chemical properties of a compound [51].

The p_z-orbitals overlap weakly and form a delocalised electron cloud. Furthermore, the lower overlap leads to a lower splitting of the resulting binding π and anti-binding π^*

states in comparison to the σ and σ^* states. As a consequence, the highest occupied molecular orbital (HOMO) and the lowest unoccupied molecular orbital (LUMO) are formed by the π and π^* orbitals, respectively. Therefore, the electronic and optical properties of a molecule are determined by its π electron system. The relative sharp states of a single molecule are broadened by intermolecular polarisation effects in a Gaussian way in a neat layer [52, 53].

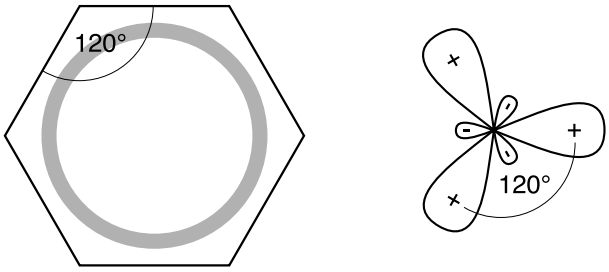

Figure 3.1: *The molecular orbitals of benzene are calculated by applying the sp^2 hybrid orbitals as basis for the LCAO method. The bonding angles of the sp^2 orbitals equal 120°, which is the angle between the carbon atoms of the benzene. The p_z orbitals are perpendicularly oriented to the sp^2 orbitals and form a delocalised electron cloud, which is illustrated by the grey circle.*

3.1.2 Fluorescence and Phosphorescence

Luminescence takes place as a molecule in an excited state, an exciton, relaxes to the ground state. An exciton can also be understood as a bound pair of an electron and a hole. Due to the weak intermolecular van der Waals forces and strong Coulomb coupling, these excitons show a strong localisation to a single molecule and are called Frenkel excitons. This is contrary to the Mott-Wannier excitons in inorganic semiconductors which can have radii of up to 10 nm (Figure 3.2). Furthermore, binding energies are higher in case of Frenkel Excitons. Due to strong Coulomb interaction between electrons and holes, binding energies are in the range of $0.1 \ldots 1.5$ eV [54, 55], while they reach only a few meV in case of Mott-Wannier excitons.

Excitons are created either by optically exciting an electron from the HOMO to the LUMO or electrically by recombination of an electron and a hole. Both electron and hole bear the spin $s = 1/2$. Therefore, the total spin of an exciton can be $S = 0$ or $S = 1$ (Figure 3.3). Since there is only a single realisation for the composition of the individual spins to a total spin of $S = 0$ and three realisations for $S = 1$, these excitons are called singlets and triplets, respectively. The factor of the wave function representing the spin can be written for singlet states as follows (with $\uparrow$ and $\downarrow$ representing the

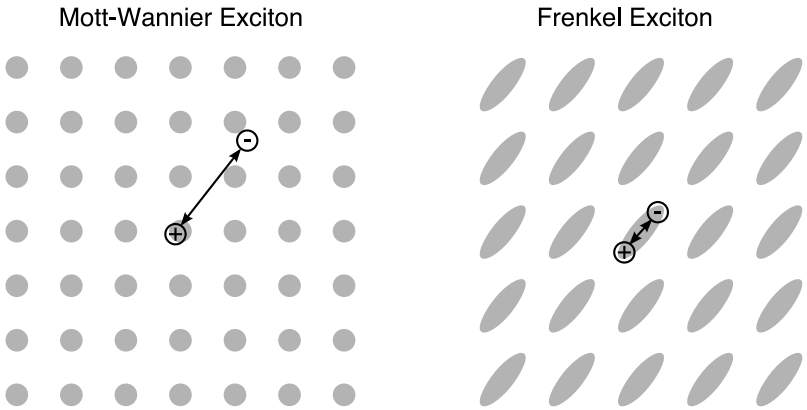

Figure 3.2: *Charges are delocalised and move freely in the lattice of classical semiconductors. The Mott-Wannier excitons which are typical for these systems can reach radii of* 10 *nm. Due to the weak intermolecular van der Waals forces and strong Coulomb coupling, excitons in amorphous organic semiconductors show a strong localisation to single molecules and are called Frenkel excitons.*

possible spin orientations):

$$^0\chi_S = \frac{1}{\sqrt{2}}[\uparrow(a)\downarrow(b) - \downarrow(a)\uparrow(b)], \tag{3.7}$$

and for the three realisations of triplet states:

$$^1\chi_T = \uparrow(a)\uparrow(b), \tag{3.8}$$

$$^2\chi_T = \frac{1}{\sqrt{2}}[\uparrow(a)\downarrow(b) + \downarrow(a)\uparrow(b)], \tag{3.9}$$

$$^3\chi_T = \downarrow(a)\downarrow(b). \tag{3.10}$$

The ground state of a molecule with an even number of π electrons is a singlet state, because every orbital up to the HOMO is filled and every electron has a complement with opposed spin orientation due to the Pauli principle. The conservation of angular momentum prohibits the transition between singlet and triplet states. Because triplets are not allowed to relax into the ground state, they have a longer lifetime and recombine radiationless in most molecules. These emitters, which emit exclusively from the singlet state, are called fluorescent emitters. However, by utilising heavy metal atoms in the molecular structure, it is possible to soften the rule of the conservation of angular

momentum. In these so called phosphorescent emitters, transitions between singlet and triplets states are possible by metal to ligand charge transfer.

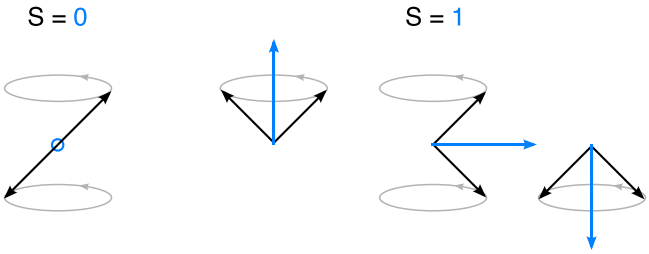

Figure 3.3: *The total spin of an exciton can be $S = 0$ or $S = 1$. Since there is only a single realisation for the composition of the individual spins to a total spin of $S = 0$ and three realisations for $S = 1$, these excitons are called singlets and triplets.*

Phosphorescent emitters play a major role if a molecule is excited electrically as it is the case in OLEDs. The spins of the injected electrons and holes are stochastically distributed. If electrons and holes recombine, they will form 25 % singlet excitons and 75 % triplet excitons. Singlet excitons will relax to the triplet state by intersystem crossing in case of phosphorescent emitters. Hence, the electroluminescent yield of such emitters is four times higher than for fluorescent emitters.

Nevertheless, the yield of fluorescent emitters can exceed the limit of 25 %, which is given by spin statistics. On the one hand, it was shown that the singlet-triplet ratio can be influenced by electric or magnetic fields [56, 57]. On the other hand, the formation of singlet excitons by the mutual annihilation of triplet excitons can increase the yield at high exciton densities. The theoretical limit for the internal quantum efficiency which may be achieved with this approach was calculated to be $\eta_{q,\mathrm{int}} \approx 40$ % [58, 59], which is still significantly below the efficiencies achieved with phosphorescent emitters.

It is important to understand that the lowest excitation energy does not result from the difference between HOMO and LUMO as given by the approach in the previous section:

$$\Delta E \neq E_{\mathrm{LUMO}} - E_{\mathrm{HOMO}} = \varepsilon_r - \varepsilon_a \tag{3.11}$$

with: ε_r electron affinity
ε_a ionisation potential .

The previously presented approach is based on single electron wave functions and electron-electron interactions are not taken into account. A more precise quantitative

description considers the interaction between the excited electron ψ_r in the π^* orbital and the remaining electrons ψ_a in the π orbital [60]. The Coulomb integral $J_{a,r}$ represents the energy of the electrostatic repulsive interactions between those electrons:

$$J_{a,r} = \iint \psi_a^*(r_1)\psi_r^*(r_2)\frac{e^2}{4\pi\varepsilon_o}\frac{1}{|r_1 - r_2|}\psi_a(r_1)\psi_r(r_2)d^3r_1 d^3r_2\,. \tag{3.12}$$

The Exchange integral $K_{a,r}$ is a consequence of the quantum mechanical exchange interaction between identical particles and is equivalent to the energy of the electrostatic repulsive interaction between the charge distributions $e\psi_a^*(r_1)\psi_r(r_1)$ and $e\psi_r^*(r_2)\psi_a(r_2)$:

$$K_{a,r} = \iint \psi_a^*(r_1)\psi_r^*(r_2)\frac{e^2}{4\pi\varepsilon_o}\frac{1}{|r_1 - r_2|}\psi_r(r_1)\psi_a(r_2)d^3r_1 d^3r_2\,. \tag{3.13}$$

Because of spin integration $K_{a,r}$ vanishes if ψ_a and ψ_r do not have the same spin factor. Pauli's principle delivers an explanation: Electrons with equally orientated spins can not come arbitrarily close. Consequently, the repulsive Coulombic interactions are smaller in case of triplet exciton. The corrected energies of the first excited singlet ΔE_S and triplet ΔE_T states are given by:

$$\Delta E_S = \varepsilon_r - \varepsilon_a - J_{a,r} + 2K_{a,r} \tag{3.14}$$

$$\Delta E_T = \varepsilon_r - \varepsilon_a - J_{a,r}\,. \tag{3.15}$$

Given that, the energetic position of the first excited triplet state is always somewhat below the first excited singlet state [60].

3.1.3 Exciton Transfer and Diffusion

Energy transfer between organic molecules can be classified into radiative and non-radiative energy transfer. Radiative energy transfer is a two step process which can be divided into the emission of a photon by one molecule and subsequent absorption by another. Because of the strong Stokes shift between absorption and emission in organic dyes, this loss process is negligible [61].

For the single-step non-radiative energy transfer, Dexter and Förster transfer can be distinguished. The Förster transfer is based on the Coulomb interaction and induced by resonant dipole interaction [62]. The Förster transfer rate constant k_F is proportional to the quotient between the overlap J between donor emission $\bar{I}_D$ and acceptor absorption

$\bar{\varepsilon}_A$ and the distance between both molecules R to the power of six:

$$k_f \propto \frac{J}{R^6}\,. \tag{3.16}$$

The overlap integral J is given by:

$$J = \int_0^\infty \bar{I}_D(\nu)\bar{\varepsilon}_A(\nu)d\nu\,. \tag{3.17}$$

Despite its dependence on the distance with an exponent of -6, Förster transfer is relevant up to a distance of $2\ldots10$ nm and the dominant process in matrix emitter systems. An important characteristic of the Förster transfer is the preservation of the spin of both participants. This is a consequence of the pure dipole-dipole interaction character of this transfer type. Allowed transitions between donor D and acceptor A are:

$$^1D^* + {}^1A \rightarrow {}^1D + {}^1A^* \tag{3.18}$$

$$^1D^* + {}^3A \rightarrow {}^1D + {}^3A^*\,. \tag{3.19}$$

Here, the number marks the spin and the asterisk the excitation state.

The Dexter transfer is based on the quantum mechanical exchange interaction between two charge distributions [63]. The Dexter transfer is a short range energy transfer, since the exchange interaction decreases exponentially with the overlap of the orbitals of donor and acceptor:

$$k_D \propto Je^{-2R_{DA}/L} \tag{3.20}$$

with L as the effective average orbital radius of donor and acceptor [64]. Since only the total spin has to be conserved in this case, the following transitions are permitted:

$$^1D^* + {}^1A \rightarrow {}^1D + {}^1A^* \tag{3.21}$$

$$^3D^* + {}^1A \rightarrow {}^1D + {}^3A^* \tag{3.22}$$

The Dexter type singlet-singlet transfer is of small relevance in comparison to the Förster transfer. On the other hand, the Dexter type triplet-triplet transfer is, despite its short range of ~ 1 nm, crucial for transfer processes at interfaces between different layers and the diffusion of triplet excitons. The exciton diffusion process is a series of incoherent jumps by means of Förster and Dexter transfer [65]. Fick's second law describes the time dependent diffusion of particles in continuous media caused by a concentration gradient. This is analog to the random walk problem of excitons[66].

The problem can easily be formulated in one dimension:

$$\frac{\partial n}{\partial t} = G(x,t) - \frac{n}{\tau} - Q(n,x,t) + D\frac{\partial^2 n}{\partial x^2} \tag{3.23}$$

with:
- n exciton density
- G exciton generation
- Q exciton quenching
- D diffusion coefficient
- τ effective exciton lifetime (radiative and non-radiative decay).

Neglecting all possible exciton quenching effects and assuming a sharp exciton recombination zone at the interface between emission layer and one of the blocking layers, the solution of this equation yields the exciton distribution in the emission layer for the steady state [67]:

$$n = n_0 \cdot e^{-x/L_D}. \tag{3.24}$$

The exciton diffusion length L_D is given as:

$$L_D = \sqrt{D\tau}. \tag{3.25}$$

While quenching effects are neglected above for the sake of simplicity, they show strong influence on device performance. Here, two important annihilation processes are discussed. A process occurring at high exciton densities is the triplet-triplet-annihilation (TTA). This process is responsible for the strong decrease of external quantum efficiency at high brightnesses [68, 69]. A molecule in an excited triplet state transfers its energy to another excited molecule. While the first one relaxes to the ground state, the later is excited to a higher state:

$$^3D^* + {}^3A^* \rightarrow {}^1D + {}^1A^{**} \tag{3.26}$$

$$^3D^* + {}^3A^* \rightarrow {}^1D + {}^3A^{**}. \tag{3.27}$$

Sharp recombination zones are often correlated with large charge accumulations. These accumulations give rise to another quenching process called triplet-polaron annihilation (TPA) [70]. During this process the energy of a triplet exciton is transferred to a positively or negatively charged molecule, a polaron, which subsequently relaxes non-radiatively:

$$^3D^* + {}^1A^{\pm} \rightarrow {}^1D + {}^1A^{\pm *} \xrightarrow{nr} {}^1D + {}^1A^{\pm}. \tag{3.28}$$

Both annihilation processes can be avoided by a broad charge carrier recombination zone, which is only achieved in ambipolar emission layers. This ambipolarity may

be achieved by a combination of materials with different transport properties in the emission layer.

3.1.4 Charge Carrier Transport

Transport in Amorphous Layers

Ohm's law describes the charge transport in a arbitrary medium in the most general way. The current density $\vec{j}$ is given as the product of the tensor of the conductivity $\hat{\sigma}$ and the electrical field $\vec{E}$:

$$\vec{j} = \hat{\sigma}\vec{E}\,. \tag{3.29}$$

In an isotropic medium the conductivity can be described by a scalar σ and is the product of the elementary charge e, the charge carrier density n, and the mobility μ:

$$\sigma = en\mu\,. \tag{3.30}$$

Thermally deposited organic layers are often amorphous and represent disordered systems. Band transport as it is observed in inorganic semiconductors and the associated high mobility ($\mu \gg 1$ cm^2/Vs) are only present in crystalline organics, where the molecular lattice forms a periodic potential for the electrons. Similar to inorganic semiconductors the electrons can be described by Bloch wave functions and the bonding and antibonding energy levels split into valence and conduction band [71, 72]. However, in the disordered system of an amorphous layer the Bloch theory cannot be applied. Here, charge transport happens almost exclusively by hopping, which is a stochastic charge transfer between the localised HOMOs and LUMOs of neighbouring molecules [53, 73]. Therefore, the mobilities which can be reached by hopping transport are limited to $\mu \ll 1$ cm^2/Vs [50].

Because of the low mobility, the layers will charge at the interfaces, if an ohmic contact is given. These charges are additionally hindering the transport. This effect is known as space charge limited current [74]. The Mott-Gurney law describes the current-voltage characteristics for unipolar transport under these conditions:

$$j = \frac{9}{8}\varepsilon_0\varepsilon_r\mu\frac{U^2}{d^3} \tag{3.31}$$

with:
- $\varepsilon_r \approx 3$ permittivity of the material
- d thickness of the layer
- U applied voltage
- μ mobility.

The transport is further restricted by charge trapping by impurities. These impurities can be impurities from the synthesis or reaction products with air and water. A high quality cleaning procedure and good encapsulation are crucial for successful OLED production.

Electrically Doped Layers

In analogy to classical semiconductors, systematical adding of impurities can enhance charge carrier density and conductivity by several orders of magnitude. The conductivities of electrically doped transport layers reach values of 10^{-5} S/cm [9]. First experiments concerning the electrical doping of organic semiconductors have been done by Maitrot et al. in 1986 [8]. They have demonstrated the electrically doping of nickel phthalocyanine by molecular dopants as dichlorodicyanoquinone and tetracyanoquinodimethan. For p-type doping a dopant is coevaporated with the matrix which has a LUMO energetically below the HOMO of the matrix material. Electrons from the HOMO of the matrix fill the unoccupied states of the dopant (Figure 3.4). Thereby, the concentration and the conductivity of holes in the matrix material are increased. For n-type doping a dopant is used, which has a HOMO above the LUMO of the matrix, in which case electrons are transferred from the dopant to the matrix. While many molecular p-type dopants are commercially available, there are less organic n-type dopants available. The reason is that the LUMO of a potential n-type dopant is very close to the vacuum level. Therefore, these molecules are very sensitive to oxidation. An alternative to molecular dopants is the use of alkali metals [75]. Cs-atoms are exclusively used for n-type doping for all OLEDs in this work.

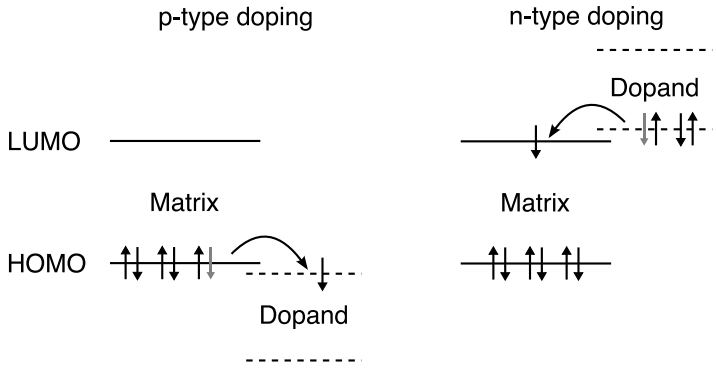

Figure 3.4: *The electrical doping of organic semiconductors is comparable to inorganic semiconductors. Charge carrier density and mobility of a layer are enhanced by systematical inclusion of impurities. A donor may transfer electrons to the electron conducting or a acceptor may accept electrons from the hole conducting matrix.*

The advantages of electrically doped layers are manifold. On the one hand, high charge carrier mobility reduces the voltage drop over the transport layers significantly. Hence, transport layer thicknesses can be varied to fit the optical cavity to the emission of the emitters. On the other hand, injection from cathode and anode is increased due to strong level bending at the interface between metal and organic. The thickness of the depletion layer scales with the dopant concentration $N_{D/A}$ according to:

$$d \propto \left(\frac{1}{N_{D/A}} \right)^{1/2} \tag{3.32}$$

and with decreased barrier width tunnel injection becomes more probable (Figure 3.5). One drawback is that many available dopants have a comparable small bandgap and absorb the light emitted by the emission layer. This effect has to be taken into account for large layer thicknesses.

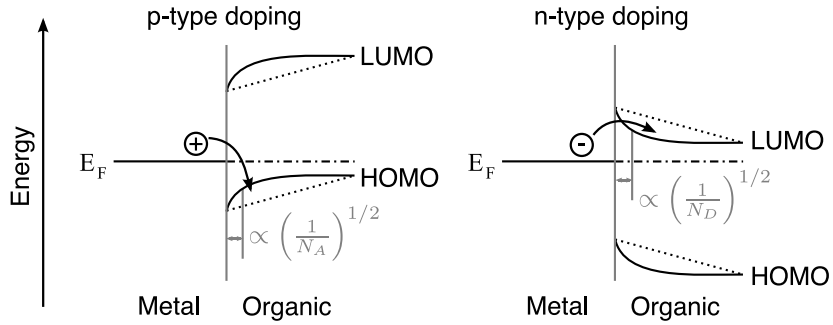

Figure 3.5: *Doping induced level bending increases the probability of tunnel injection at the interfaces to anode and cathode.*

3.2 Organic Light Emitting Diodes

3.2.1 The General Principle of Operation

A primitive approach to an organic electroluminescent device would be a single organic layer sandwiched between a cathode and an anode. Such a device would emit light on the basis of equal transport properties and injection efficiency for both kinds of charge carriers. Otherwise, recombination of holes and electrons would not take place inside the organic layer.

A more sophisticated approach was presented by Tang and Van Slyke [7]. Their OLED

consisted of two organic layers, one was formed by a primarily hole and the other by an electron conducting material. Charge Carriers accumulate and recombine at the interface between both layers. Because of the different band gaps of the utilised materials barriers are different for the injection of electrons into the hole conducting and the injection of holes into the electron conducting material. Hence, electroluminescence takes place on only one of the materials according to the barrier heights (compare Figure 3.6.).

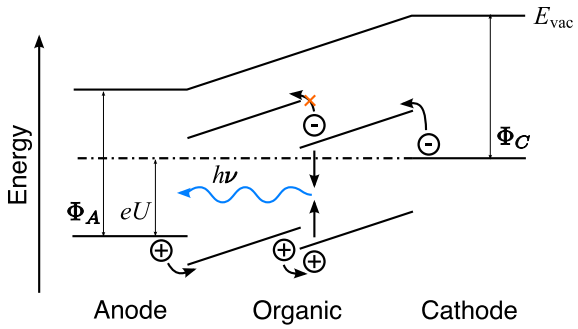

Figure 3.6: *Operation principle of a simple two layer OLED as presented by Tang and Van Slyke [7]. Holes and electrons are injected on two different materials with according transport properties. Charge carriers are accumulated at the interface between both organic layers, where excitons are formed and light is emitted. Due to the different barrier heights for the two charge carrier types at this interface, recombination only takes place on one of the materials.*

3.2.2 Electrically Doped Transport Layers

The high driving voltages of the above device need to be reduced. As discussed in section 3.1.4, injection and transport could be improved by electrical doping of organic materials. For hole transport the frequently used and well examined matrix dopant system of MeO-TPD and F_4-TCNQ [10] is applied. In some experiments these materials are replaced by NHT-5 doped with NDP-2 which is a commercially available hole conducting system and can be obtained from *Novaled AG*. Both systems reach comparable conductivities and the properties of OLEDs based on NDP-2 and F_4-TCNQ are identical. An advantage of the NDP-2 is that it yields better device stability and F_4-TCNQ tends to contaminate sources which are located in the same vacuum chamber. Thus, it is not used in any single chamber systems and is replaced in those tools by NDP-2.

Another dopant which is used for doping of materials with a deeper HOMO than MeO-TPD is the fluorinated fullerene derivative C60F36. It is known for its doping effect on the conjugated polymer poly-3-hexylthiophene [76]. Further investigations have shown

that it is also applicable for small molecules [77]. As mentioned above, for electron transport only Cs doped BPhen is used. In order to avoid reabsorption, electron as well as hole transport materials have a huge bandgap. The HOMO and LUMO values of the transport materials are summarised in Table 3.1. The corresponding molecular structures are shown in Figure 3.7.

Material	HOMO [eV]	LUMO [eV]
MeO-TPD	−5.1	−1.9
F_4-TCNQ	−8.34	−5.24
C60F36	−8.38	−5.40
BPhen	−6.38	−2.34

Table 3.1: *Values of the HOMOs and LUMOs of the materials used for charge transport. [77–79]*

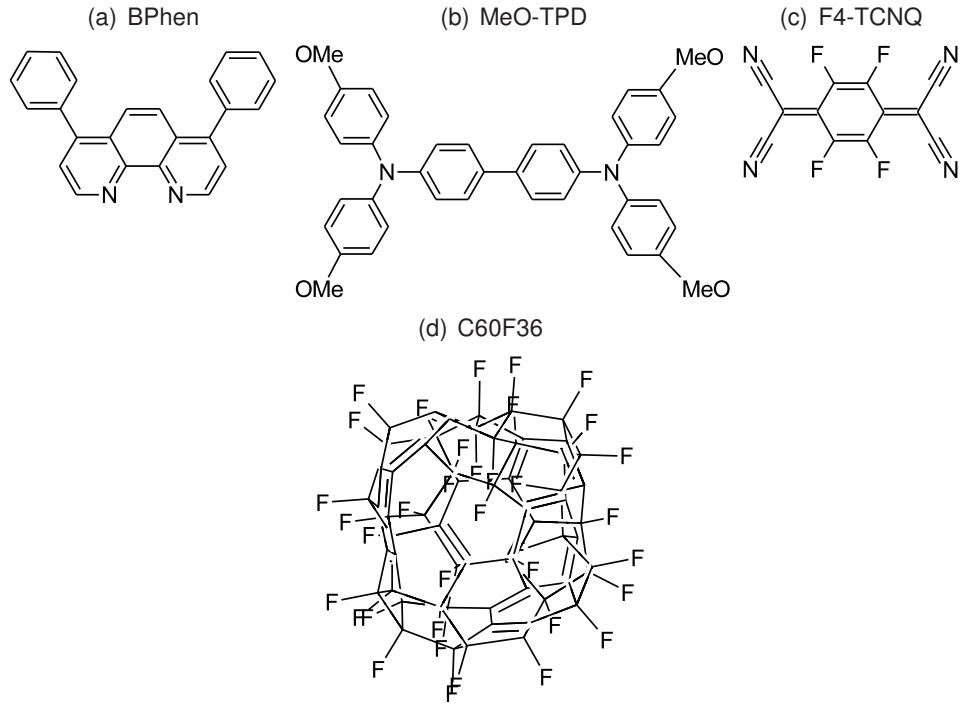

Figure 3.7: *Important transport materials and dopants: (a) 4,7-diphenyl-1,10-phenanthroline; (b) N,N,N',N'-tetrakis(4-methoxyphenyl)-benzidine; (c) 2,3,5,6-tetrafluoro-7,7,8,8-tetracyanoquinodimethane; (d) fluorinated fullerene derivative.*

3.2.3 Charge and Exciton Blocking Layers

Blocking layers are crucial for the device performance of an OLED with doped transport layers. They are used to confine charge carriers to the emission layer and to increase the quantum efficiency by improved charge carrier ballance. This task can be satisfied by appropriate energy barriers between the emission layer and the charge blocking layer or decreased mobility for the according charge carrier type in the charge blocking layer. On the other hand, excitons have to be separated from the high charge carrier densities in the transport layers to avoid charge exciton quenching mechanisms. In order to fulfil this task the excited states of the blocker material must be higher than the excited states of the emitter material. Working with phosphorescent emitters, also the triplet states of the blocker materials have to be considered. Important characteristics like energy levels and first excited states are summarised for the most important blocker materials (Figure 3.9) in Table 3.2. If the transport of one charge carrier type is favoured by the emission layer, these demands may be less important for the other type. Recombination will happen at one interface of the emission layer and excitons as well as the other kind of charge carriers most likely will not reach the other blocking layer. The operation principle of the resulting five layer OLED consisting of charge transport, charge blocking, and emission layers is explained in Figure 3.8.

Material	HOMO [eV]	LUMO [eV]	S_1 [eV]	T_1 [eV]
α-NPD	−5.4 [79]	−2.6 [79]	2.81	2.29 [15]
Spiro-TAD	−5.4 [80]	−2.3 [80]	3.06	?
TCTA	−5.9 [81]	−2.7 [81]	3.20	2.82 [15]
TAPC	−5.8 [82]	−2.4 [82]	3.35	2.87 [15]
Alq_3	−5.8 [83]	−3.1 [83]	2.30	2.03 [84]
BAlq	−6.1	−3.2	2.51	2.18 [84]
BPhen	−6.4 [79]	−2.3 [79]	3.20	2.58 [15]
TPBi	−6.2 [85]	−2.7 [85]	3.20	2.64 [15]

Table 3.2: *Values for HOMO, LUMO, singlet gap, and triplet gap for three primarily hole conducting and four electron conducting materials. S_1 is calculated from the fluorescence peak. The energy levels of BAlq are determined by Selina Olthof by optical gap and UPS-measurements at the IAPP.*

3.2.4 The Emission Layer

Up to now the emission layer was assumed to consist only of a single emitter material, but many materials can only be used when diluted in a matrix material. Such materials

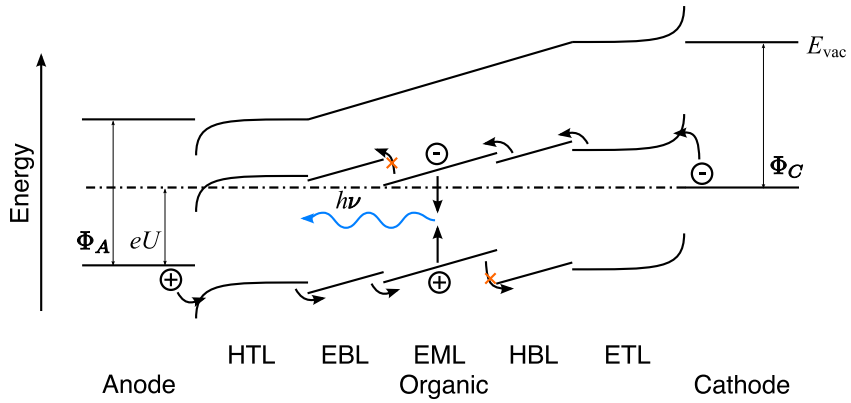

Figure 3.8: *Operation principle of a pin-OLED. Charges are injected by electron (ETL) and hole (HTL) transport layer. The blocking layers for electrons (EBL) and holes (HBL) confine charge carriers to the emission layer (EML), where they form excitons and recombine under light emission.*

would otherwise form aggregates and a red shift of the emission spectrum would be accompanied by a drop of quantum yield [86–88]. All triplet and several singlet emitters suffer from these effects and need an appropriate matrix material. In some of these matrix/emitter systems, excitons are formed on the matrix and are transferred by means of Förster transfer to the emitter molecules. In others, charge carriers are trapped by the emitter molecules and excitons are formed directly on the molecules where they emit light. Recent studies showed that the efficiency of a device can be improved by a mixed matrix, e.g. a mixture of a hole and an electron conducting material [89, 90]. A combination of different matrix materials can lead to a broader recombination zone and would yield higher efficiencies and stability due to reduced quenching effects. The benefits of combining several emitters in a common matrix are shown in section 5.3. The chemical structure of the emitter molecules used in this work are shown in Figure 3.10. HOMO and LUMO values as well as emission maxima are summarised in Table 3.3. Due to their importance for the later introduced concept of triplet harvesting a separate section is dedicated to the fluorescent blue emitters (Section 5.1).

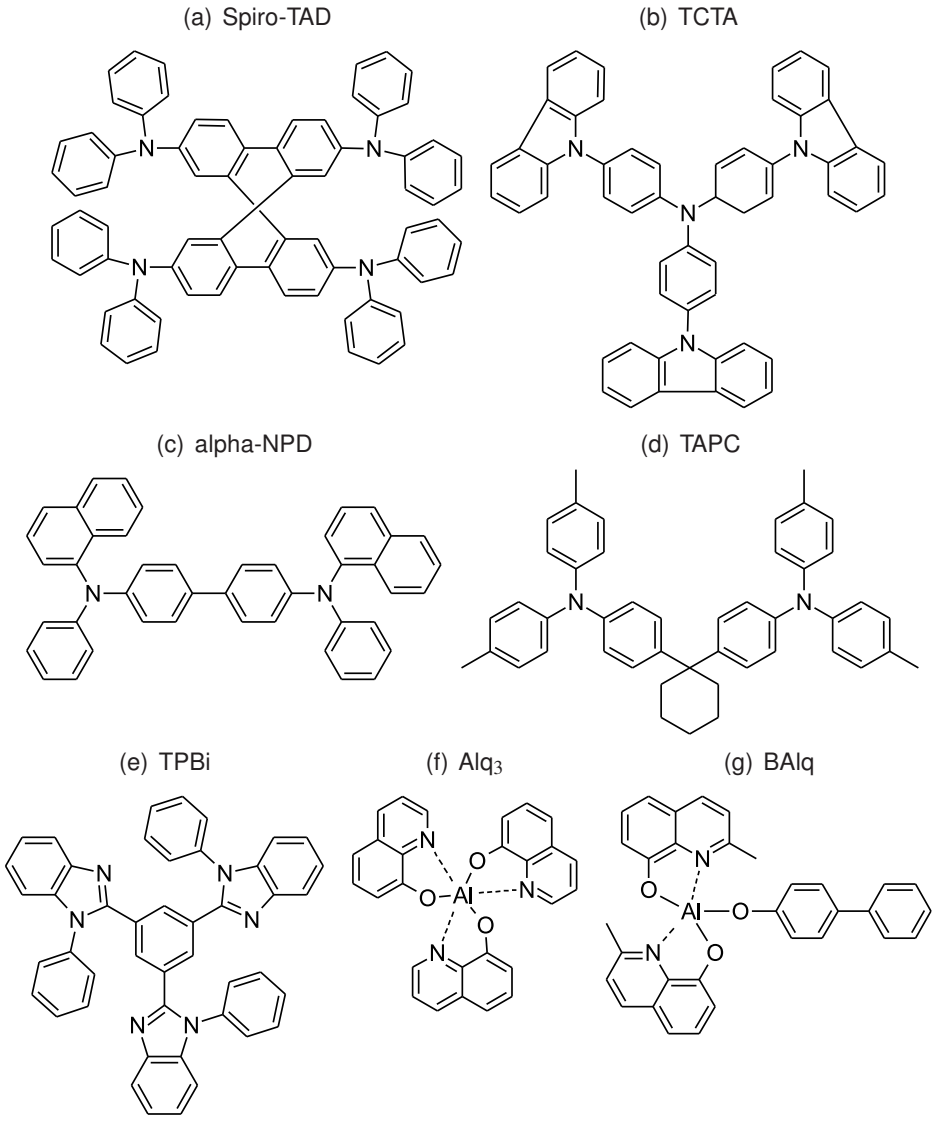

Figure 3.9: *Important charge and exciton blocking materials: (a) 2,2',7,7'-tetrakis(N,N-diphenylamino)-9,9'-spirobifluorene; (b) 4,4',4"tris(N-carbazolyl)-triphenylamine; (c) N,N'-di(naphthalen-1-yl)-N,N'-diphenyl-benzidine; (d) di-[4-(N,N-ditolyl-amino)-phenyl]cyclohexane; (e) 2,2'2"-(1,3,5-benzenetriyl)-tris[1-phenyl-1H-benzimidazole]; (f) aluminium tris(8-hydroxyquinoline); (g) bis(2-methyl-8-quinolinolato-N1,O8)-(1,1'-Biphenyl-4-olato)aluminium.*

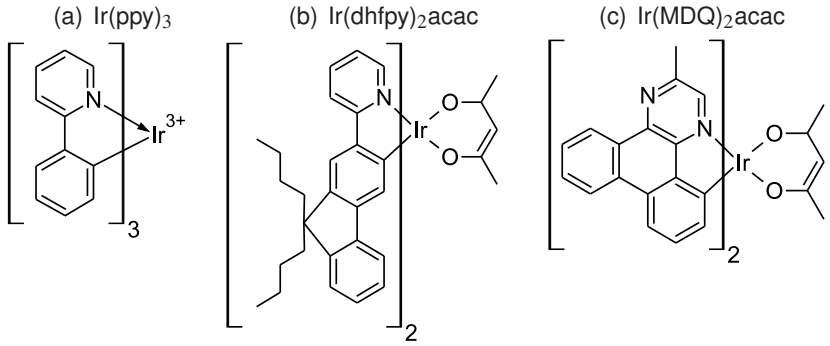

Figure 3.10: *Important phosphorescent emitter materials: (a) fac-tris(2-phenylpyridine) iridium(III); (b) bis(2-(9,9-dihexylfluorenyl)-1-pyridine)(acetylacetonate) iridium(III); (c) bis(2-methyldibenzo-[f,h]quinoxaline)(acetylacetonate) iridium(III).*

Material	HOMO [eV]	LUMO [eV]	λ_{max} [nm]/[eV]
$Ir(ppy)_3$	-5.6 [91]	-3.0 [91]	510/2.43
$Ir(dhfpy)_2acac$	-5.1	-2.4	557/2.23
$Ir(MDQ)_2acac$	-5.4	-2.8	603/2.06

Table 3.3: *The phosphorescent emitters utilised in this work are characterised by the above values for HOMO, LUMO and photoluminescence peak. The energy levels of $Ir(dhfpy)_2acac$ and $Ir(MDQ)_2acac$ are determined by Selina Olthof by the use of optical gap and UPS-measurement at the IAPP.*

4 Experimental Setup

This chapter gives an introduction into the experimental methods applied, including sample preparation as well as the characterisation of OLEDs and organic molecules in terms of their optical properties. The design of experiments by utilising optical simulations is explained and also a way to estimate the maximum external quantum efficiency of OLEDs with several emitters is elucidated.

4.1 Sample Preparation

In this work only bottom emitting OLEDs are investigated, where light is emitted through the substrate. Here, 90 nm indium tin oxide (ITO) pre-coated glass (*Corning Inc.*: Eagle XG $n_d = 1.51$) is used as transparent substrate. Our substrates are delivered by *Thin Film Devices Inc.* and are prestructured according to the layout shown in Figure 4.1. In order to improve light extraction, a special glass with high refractive index (*SCHOTT AG*: N-SF11 $n_d = 1.78$) was employed. Those substrates were coated with ITO at the *LFB* in Stuttgart and structured by the *Fraunhofer IPMS*.

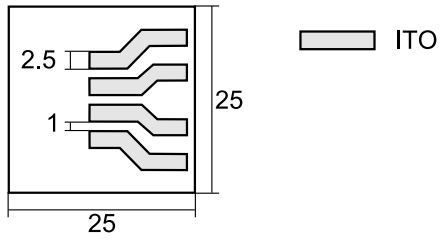

Figure 4.1: *Layout of the prestructured ITO on a 25 mm x 25 mm glass substrate.*

The glass is coated by thermal evaporation of the different organic molecules and the cathode material under high vacuum conditions (base pressure 10^{-8} mbar) after cleaning. Structuring is carried out by the use of shadow masks while calibrated crystal

quartz monitors allow to precisely control the thicknesses and doping ratios. In case of mixed layers the depositions of all materials are measured independently with separate crystal quartz monitors. Crosstalk between the thickness monitors is avoided by the geometrical arrangement. The deposition of the Cs doped BPhen layer is an exception, since the Cs rate cannot be measured by crystal quartz monitors. Adequate control is given by in situ measurement of the conductivity of the mixed layer.

For material deposition the following tools are available. The UFO-2 is a cluster tool acquired from *BESTEC GmbH*. Each chamber of the UFO-2 contains up to eight organic sources. An additional chamber contains metal evaporators for aluminium, silver, gold and other optional metals. Because all chambers can be switched off and vented independently, this tool is very well suited for tests of new materials. This tool is primarily used for testing new approaches concerning device architecture or material combination.

In addition to the cluster tool, two vacuum systems were purchased from *Kurt J. Lesker Company*®. These are single chamber tools with all organic and inorganic sources located in one chamber. It is possible to process four times four samples on these machines in the same time. The construction of these tools allows the separate coating of single rows and columns. Therefore, sixteen different samples can be processed in a single run. The advantage of these tools is that among the sixteen devices besides the varied layers all other layers are identical. Therefore, the optimisation of a device with respect to a selected parameter is simplified in comparison to the UFO-2.

4.2 Optical Measurements

For an optical simulation of the investigated OLED stacks some material properties have to be supplied. These properties are in particular the photoluminescence spectrum and the complex refractive index, which is often referred to as n&k values. This section is about the measurement of these properties.

4.2.1 Photoluminescence

For the measurement of photoluminescence spectra the following spectrometers are used: the Fluoromax from *SPEX*® and the FS 920 from *Edinburgh Instruments Ltd.*, which is more precise in the deep red wavelength region. All measurements are carried out on thin films on glass substrates. If the deep blue or the ultra violet wavelength region is of interest, quartz glass will be chosen instead of standard glass. To avoid

aggregation effects (Section 3.2.4), the photoluminescence spectra of emitter molecules are either measured in mixed layers or solutions.

4.2.2 Determination of n&k Values

An in-house collection of n&k values is used to describe the optical properties of OLEDs. A part of these values is based on ellipsometry (measurement of reflection with respect to the angle and the polarisation of incident and reflected beam) on thin films on glass substrates, which were carried out at the *Fraunhofer IPMS*. The remaining values as well as the values obtained for this work are based on a simplified measurement procedure. Considering transmission and reflection at normal light incidence, the Fresnel equations, which allow for the calculation of the n&k values, simplify in a manner that transmission and reflection are independent of the polarisation of the incident light. Therefore, polarisers are obsolete for measurements at normal light incidence [92]. While the measurement of transmission at normal light incidence is possible, such conditions can only be reached approximatively for the measurement of reflectivity. This is due to a restriction of our measurement system (SHIMADZU UV-3101PC) to a minimal angle of 5°. The calculation of the n&k values is done according to the algorithm published by Fritz et al. [93]. This is an adequate way of determining n&k values as is demonstrated by the good agreement of experimental data and optical simulations presented later in this work.

4.3 OLED Characterisation

4.3.1 IVL-Robot

Two similar measurement systems are available for automatically recording current-voltage-luminance curves. One system was designed and sold by *Novaled AG* and the other one by *Contronix GmbH*. Both are based on the same measurement equipment which consists of a silicon photodiode, a source measurement unit SMU2400 from *Keithley* and a spectrometer CAS140CT-153 from *Instrument Systems GmbH* calibrated in terms of absolute intensity. Spectrum and luminance are measured in accordance with the terms of the *CIE 1931 2° Standard Observer*. The 2° aperture is secured by means of a special measuring adapter. The luminance is measured by the photodiode. Photocurrent is amplified and transformed to a voltage value. This value is calibrated to a luminance value given in cd/m^2 by a spectrometer measurement at

roughly 1 000 cd/m^2. From these values the current efficiency η_c can be calculated:

$$\eta_c = \frac{K_m A}{I} \int_{\lambda} L_e^{\vartheta_0}(\lambda) d\lambda \tag{4.1}$$

$$\eta_c = \frac{L_v^{\vartheta_0} A}{I} \quad \left[\frac{\mathrm{cd}}{\mathrm{A}}\right]. \tag{4.2}$$

The current efficiency describes the luminous intensity emitted in forward direction for a given current.

4.3.2 Goniometer and Ulbricht sphere

For illumination purposes it is reasonable to state efficiencies which specify the total emitted light. A goniometer is used to measure the angular dependence of light emission. Spectral characterisation is done with the mini spectrometer USB4000 (*Ocean Optics, Inc.*), which is calibrated in terms of the spectral shape and relative intensity. The intensity calibration is given by comparison to the measurement done with one of the CAS140CT-153 spectrometers (see above). A step motor is rotating the OLED. A laser diode and a xyz-translation stage are used to adjust the active area to the rotation centre. Angle dependent spectral measurements allow the calculation of the integral quantities external quantum efficiency and luminous efficacy. The external quantum efficiency and luminous efficacy describe the efficiency of an OLED in terms of radiometric and photometric units, respectively. The external quantum efficiency is defined as the ratio between per unit of time emitted photons $\dot{n}_\gamma$ and injected electrons $\dot{n}_e$:

$$\eta_q = \frac{\dot{n}_\gamma}{\dot{n}_e}. \tag{4.3}$$

$\dot{n}_e$ can be calculated directly from the current at which the device is driven:

$$\dot{n}_e = \frac{I}{e}. \tag{4.4}$$

and $\dot{n}_\gamma$ can be derived as:

$$\mathrm{I}_e(\Omega,\lambda) = \frac{d^2\Phi_e(\Omega,\lambda)}{d\Omega d\lambda} \tag{4.5}$$

$$= \frac{d^2}{d\Omega d\lambda}\frac{hc}{\lambda}\dot{n}_\gamma \tag{4.6}$$

$$\Longrightarrow \dot{n}_\gamma = \frac{1}{hc}\int\limits_{\Omega}\int\limits_{\lambda}\lambda \mathrm{I}_e(\Omega,\lambda)d\Omega d\lambda\,. \tag{4.7}$$

Consequently, the external quantum efficiency is given by:

$$\eta_q = \frac{2\pi e}{Ihc}\int\limits_{\vartheta}\int\limits_{\lambda}\lambda \mathrm{I}_e(\vartheta,\lambda)\sin\vartheta d\vartheta d\lambda\,. \tag{4.8}$$

The quotient of luminous flux and electrical power defines the luminous flux η_v,

$$\eta_v = \frac{\Phi_v}{P} \tag{4.9}$$

$$\eta_v = \frac{2\pi K_m}{UI}\int\limits_{\vartheta}\int\limits_{\lambda}\mathrm{I}_e(\vartheta,\lambda)\mathrm{V}_\lambda\sin\vartheta d\vartheta d\lambda \quad \left[\frac{\mathrm{lm}}{\mathrm{W}}\right]. \tag{4.10}$$

In some cases a goniometer measurement is not possible due to geometrical reasons. For instance, this will be the case if an outcoupling enhancement structure has to be applied to the OLED. In this work an Ulbricht sphere connected to a CAS140CT-153 spectrometer (*Instrument Systems GmbH*) is employed. If both goniometer and Ulbricht sphere measurement are not possible, Lambertian emission may be assumed:

$$\mathrm{I}_e(\vartheta,\lambda) = \mathrm{I}_e^{\vartheta_0}(\lambda)\cos\vartheta\,. \tag{4.11}$$

The calculations of the efficiencies are reduced to the integrals over wavelength,

$$\eta_q = \frac{\pi e}{Ihc}\int\limits_{\lambda}\lambda \mathrm{I}_e^{\vartheta_0}(\lambda)d\lambda \tag{4.12}$$

$$\eta_v = \frac{\pi K_m}{UI}\int\limits_{\lambda}\mathrm{I}_e^{\vartheta_0}(\lambda)\mathrm{V}_\lambda d\lambda \quad \left[\frac{\mathrm{lm}}{\mathrm{W}}\right]. \tag{4.13}$$

This is often a good approximation. However, the relative error of the determined efficiencies can be as high as 15 % in some cases. Therefore, it is not recommended

to rely on the assumption of Lambertian emission for OLEDs. A goniometer was not available at the beginning of this work. Nevertheless, the samples of the individual sections have allways a similar architecture in common. Since the microcavity of these devices is not modified, they have a common angular emission dependence. Therefore, it is possible to compare the efficiencies of these devices among each other. In order to avoid confusion, goniometer and Ubricht sphere corrected measurements are allways identified as such.

4.3.3 Lifetime Measurement Setup

Lifetime measurements are carried out with a measurement system developed and sold by *Novaled AG*. The lifetime is defined as the time after which an OLED emits the half of its initial luminance when it is driven at a constant current. Hence, luminance is measured by three photodiodes in regular intervals. For luminance measurements a single photodiode would be enough, but the photodiodes are coated with colour filters in a way that the colour shift of the devices can be measured during degradation. Long living OLEDs are measured with an accelerated method. One takes advantage of the fact that initial luminance and lifetime show an exponential dependence:

$$t_{1/2} = \frac{C}{L_0^n} \tag{4.14}$$

with C and n as free parameters [94]. By applying this law, the lifetime at any initial luminance can be extrapolated. An initial luminance of 1 000 $\mathrm{cd/m^2}$ is commonly used as reference. An initial luminance of 500 $\mathrm{cd/m^2}$ is often used instead, assuming a possible enhancement of light extraction by a factor of two for OLEDs on standard glass substrates.

4.4 Calculations and Simulations

4.4.1 OLED Design by Optical Simulations

The thickness of an OLED results in an optical path length in the order of the wavelength of the emitted light. Thus, the cavity formed by substrate and cathode has a significant influence on the performance of an OLED. Even the internal quantum yield of an emitter can be enhanced by microcavity effects [11].

Due to the high mobility of charge carriers in electrically doped layers, the electrical

characteristics of an OLED are independent of the layer thickness of the transport layers, which can be adjusted in a manner that the microcavity of the OLED is optimised for the emission of the utilised emitters. An extensive optimisation by experimental variations would be tedious and expensive. By applying an optical model, the experimental optimisation process can be accelerated considerably. Sim-OLED (*sim4tec GmbH*) is a numerical tool which is able to simulate the optical behaviour of an OLED. The simulations shown in this thesis are done with the software version 1.1.1.

Sim-OLED is based on a model as published by Benisty et al. [95]. The model of dipole emission is used for the emitting molecules. The electric field is decomposed into plane waves. The transfer matrix formalism and the intensity matrix formalism are used for the physical description of the organic layers and the thick incoherent substrate, respectively [96, 97]. The simulation gives values in arbitrary units for emission affinity, spectral radiant intensity (CIE-coordinates are included), luminous efficacy, and external quantum efficiency. The emission affinity is an abstract quantity equivalent to the spectral radiant intensity of an OLED comprising an emitter which emits an unitary intensity in the whole visible wavelength range. In other words, the emission affinity describes the ratio between extracted and emitted photons at a specific wavelength.

Sim-OLED allows device optimisation with regard to the mentioned quantities by systematic layer thickness variation. An experiment which is based on the results of this optimisation can be used to calibrate the simulated quantities. This allows the estimation of the potential for improvement by thickness variations. Such an approach is well suited for the optimisation of white OLEDs with several emitters in terms of luminous efficacy, colour coordinates, and colour rendition properties. Furthermore, it is possible to determine the excitation distribution among the emitters by the use of the emission affinity. This information yields the possibility of determining the maximum external quantum efficiency as shown in the following section.

4.4.2 Estimation of the Maximum External Quantum Efficiency

The maximum external quantum efficiency of a monochrome OLED is predicted by the work of Greenham et al. [98]. They have proven that assuming Lambertian emission and following Snell's law, the outcoupling efficiency of an OLED on a flat standard glass substrate is 22 %. Since the microcavity of an OLED can never be optimised for all emitters at the same time, this does not hold for white devices as can be illustrated by the emission affinity. For the example given in Figure 4.2, a material emitting blue light at 440 nm would only result in half the efficiency of a green emitter which fits to the maximum of the emission affinity at 515 nm. Here, a way is presented to evaluate the photon distribution inside an OLED. Subsequently, the maximum quantum efficiency, which can be achieved with a given spectrum and OLED architecture, can be calculated

directly from the photon distribution.

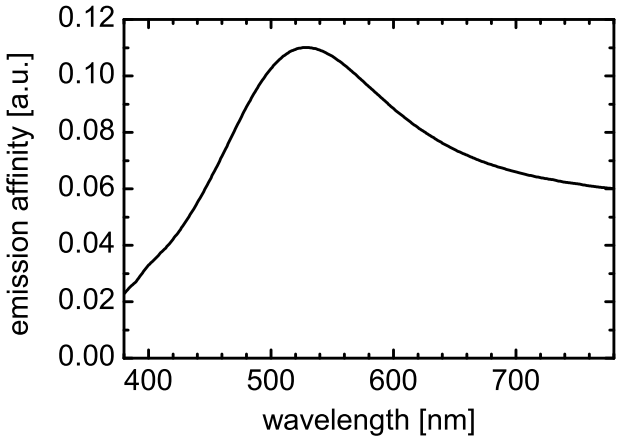

Figure 4.2: *An example for the emission affinity of a typical OLED. The external quantum efficiency of a white OLED is strongly limited in comparison to a monochrome device, since the microcavity can never be optimised for all emitters at the same time. A material emitting blue light at* 440 *nm would only result in half the efficiency of a green emitter which fits to the maximum of the emission affinity at* 515 *nm.*

Prerequisites

Besides the precise OLED stack and n&k-values for all layers, the following data have to be collected prior to the calculation:

- the spectral radiance L_λ [W/sr m^2 nm] of the OLED normalised to $\int L_\lambda \, d\lambda = 1$,
- the photoluminescence spectra PL_i of all emitters normalised to $\int PL_i \, d\lambda = 1$, and
- the internal efficiency of each emitter η_i. Due to spin statistics the maximum values are $\eta_i = 1$ for phosphorescent and $\eta_i = 0.25$ for fluorescent emitters.

Calculation

The calculation of the internal photon distribution starts with the simulation of the relative emission affinity $A_{r,i}$ in forward direction. In this work the software Sim-OLED (Version 1.1.1) is used for this purpose. Due to the dependence of the emission affinity

on the position of the emission zone relative to the cavity, this calculation has to be done separately for every emitter. In order to calculate the external quantum efficiency, a calibration of the emission affinity by a factor κ is crucial

$$\mathrm{A}_{a,i} = \kappa \cdot \mathrm{A}_{r,i}\,. \tag{4.15}$$

This calibration is valid, if Lambertian emission is assumed. The estimation of the calibration factor κ will be discussed later. The spectrum of the OLED can be fitted by:

$$\mathrm{L}_{\lambda,\mathrm{calc}} = \frac{\sum\limits_{i=r,g,b(,\dots)} \alpha_i \cdot \mathrm{PL}_i(\lambda) \cdot \mathrm{A}_{r,i}(\lambda)}{\sum\limits_{i=r,g,b(,\dots)} \int \alpha_i \cdot \mathrm{PL}_i(\lambda) \cdot \mathrm{A}_{r,i}(\lambda)\,\mathrm{d}\lambda}\,. \tag{4.16}$$

The coefficients α_i are identical to the internal photon distribution and the emission of each emitter PL_i is coupled out according to the corresponding emission affinity $\mathrm{A}_{r,i}$. The integral in the denominator normalises the Spectrum to $\int \mathrm{L}_{\lambda,\mathrm{calc}}\,\mathrm{d}\lambda = 1$. It is important for the following calculations to normalise the coefficients to

$$\sum_{i=r,g,b(,\dots)} \alpha_i = 1. \tag{4.17}$$

The internal quantum efficiency equals the ratio of generated photons to injected electrons. Assuming that the whole spectrum is emitted by an averaged photon, the internal quantum efficiency can also be expressed as the inverse of the number of electrons needed to emit a single white photon:

$$\eta_{q,\mathrm{int}} = \frac{1 \text{ white photon}}{\text{number of needed electrons}} \cdot 100\,\% = \frac{1}{\mathrm{N}_e} \cdot 100\,\%\,. \tag{4.18}$$

Assuming perfect charge balance and neglecting all exciton quenching mechanisms, the number of injected electrons is equal to the number of excitons. The number of per photon injected electrons can be calculated directly from the coefficients α_i, but two cases have to be differentiated:

1. **With triplet-harvesting:**
   The principle of triplet harvesting and its implementation are explained in detail in Section 5.2. Here, otherwise unused triplet excitons on fluorescent emitters are transferred to phosphorescent emitters, where they can emit light. Therefore, N_e equals one if the share of singlet emission α_{fl} is below one quarter and is otherwise four times this value.

$$\mathrm{N}_e = \begin{cases} 1, & \alpha_{fl} < 1/4 \\ 4 \cdot \alpha_{fl}, & \alpha_{fl} > 1/4 \end{cases} \tag{4.19}$$

2. **Without triplet-harvesting:**
   Every exciton recombines on the molecule on which it was created and triplet excitons created on fluorescent emitters recombine radiationless. Every emitter is emitting according to its share on the average photon α_i with its own internal efficiency η_i:
   $$N_e = \sum_{i=r,g,b(,\dots)} \frac{\alpha_i}{\eta_i}. \tag{4.20}$$

For calculation of the external quantum efficiency, the outcoupling of the light out of the device has to be taken into account, which is achieved by the use of the calculated emission affinities:

$$\eta_q = \frac{\sum_{i=r,g,b(,\dots)} \int \alpha_i \cdot PL_i(\lambda) \cdot A_{a,i}(\lambda)\, d\lambda}{N_e} \tag{4.21}$$

$$\eta_q = \frac{\kappa \sum_{i=r,g,b(,\dots)} \int \alpha_i \cdot PL_i(\lambda) \cdot A_{r,i}(\lambda)\, d\lambda}{N_e}. \tag{4.22}$$

Estimation of the Calibration Factor κ

The calculation of the emission affinity with Sim-OLED does not result in absolute values. As mentioned above, a calibration factor κ has to be applied for determination of the external quantum efficiency. It was shown that the maximum outcoupling efficiency is 22 % for a monochrome OLED on a flat glass substrate [98], if the refractive index of the glass was $n = 1.51$ and Lambertian emission was assumed. Hence, κ can be calculated as follows. At first, the maximum of the emission affinity has to be estimated. Afterwards, a virtual emitter $PL_{virtual}$ is designed as Gaussian function with the maximum at this wavelength and a width of 1 nm. Assuming perfect outcoupling for the emission of this virtual emitter, κ is given by the following equation:

$$\kappa = \frac{0.22}{\int A_r \cdot PL_{virtual}\, d\lambda}. \tag{4.23}$$

5 Results

This chapter summarises the results of the experimental work. At first different fluorescent blue emitters are presented and there properties are discussed with respect to their application in white OLEDs.

Afterwards the concept of triplet harvesting is introduced. From the examined blue emitters a suitable candidate is chosen, which allows for triplet transfer to yellow and red phosphorescent emitters. The influence of the most important parameters is investigated and an optimised triplet harvesting OLED comprising a fluorescent blue and phosphorescent red emitter is presented. Furthermore, the simultaneous triplet transfer to two different phosphorescent emitters is shown.

The focus of the third section is on the combination of different phosphorescent emitters in a single emission layer. This approach leads to increased colour stability and simplifies the architecture of a white OLED. It is shown in detail, how to achieve well balanced emission from both emitters at the same time and increase overall efficiency by adjusting the doping concentrations.

To achieve three-colour white light emission from a single emission layer, a stack is examined, which is based on the experiments in the previous section. By mixing a fluorescent emitter with two phosphorescent emitters white emission with exceptional colour stability is achieved.

In the last section the concept of stacked OLEDs is utilised to circumvent the limitations of triplet harvesting regarding the triplet transfer to phosphorescent green emitters. A fully phosphorescent unit comprising the emission of a yellow and a green emitter in a single emission layer is stacked on top of the optimised triplet harvesting OLED, which combines a fluorescent blue and a phosphorescent red emitter. An independent optimisation of the connecting charge generation layer, results in a strong decrease of the driving voltages. The efficiencies are further improved by

the use of a substrate with enhanced refractive index and outcoupling enhancement by a macro extractor and a pyramid pattern.

5.1 Blue Dyes

Several fluorescent blue emitting dyes are examined with regard to their application in white OLEDs. These investigations are summarised by a comparison of the most important properties of each emitter at the end of this section.

For application in white OLEDs stable deep blue dyes with colour coordinates around $(x, y) = (0.15, 0.15)$, long lifetimes, and high efficiency are needed. Despite their high yield, currently available phosphorescent blue emitters have the drawbacks of sky-blue colour coordinates and a short lifetime of a few hours only [17, 18]. However, deep blue fluorescent dyes are stable and offer a rich variety of emission spectra [19–21]. Therefore, this work focusses on white OLEDs which utilise fluorescent blue emitters. Besides the colour coordinates, the positions of the HOMO and LUMO levels play an important role, because a disadvantageous position will hinder charge injection. One way to classify blue emitters is to distinguish between host-guest emitter systems and bulk emitters. Two representatives of each class are discussed in the following paragraphs and the chemical structures are shown in Figure 5.1. A comparison concerning their advantages and drawbacks will be presented at the end of the chapter.

5.1.1 Host-Guest Systems

In this section the properties of the two blue fluorescent host-guest systems MADN: TBPe and Spiro-Pye: DBzA are discussed (Figure 5.1). The influence of emitter concentration and the choice of blocker materials are investigated in detail.

MADN:TBPe

The matrix material MADN (Figure 5.1) doped with the emitter TBPe is a highly efficient deep blue emitter system [99]. As for most anthracene derivatives MADN is also ambipolar. The mobility of electrons and holes is identical, but varies with respect to field ($\mu_{e/h} = 2 \ldots 3 \cdot 10^{-7}$ cm^2/Vs [100]). The energy levels of MADN

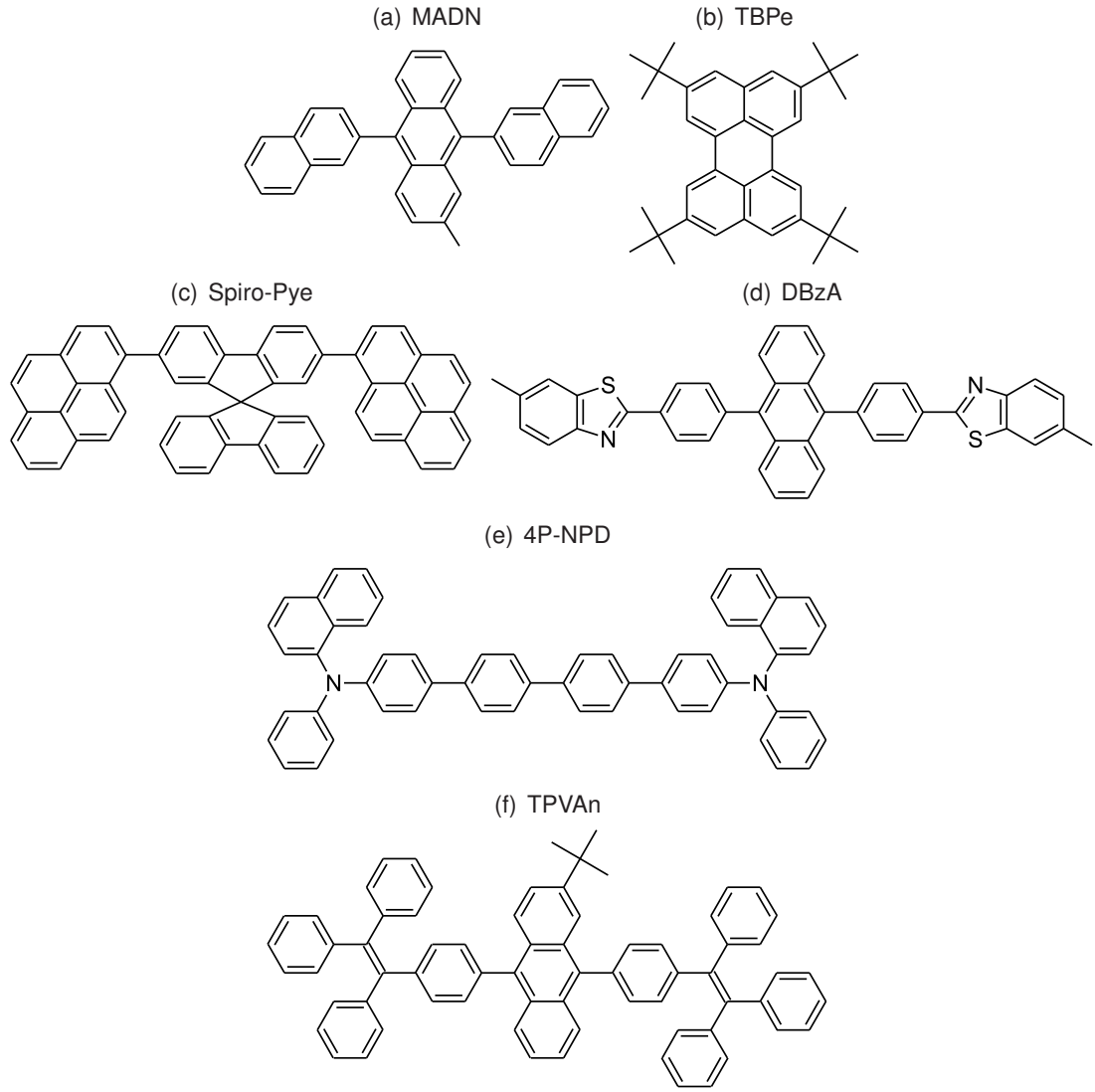

Figure 5.1: *Chemical structures of the fluorescent blue emitters of interest: (a) 2-methyl-9,10-bis(naphthalen-2-yl)anthracene; (b) 2,5,8,11-Tetra-tert-butylperylene; (c) 2,7-Di-pyrenyl-9,9-spirobifluorene; (d) 6-Methyl-2-(4-(9-(4-(6-methylbenzo[d]thiazol-2-yl)phenyl)anthracen-10-yl)phenyl)benzo[d]thiazole; (e) N,N'-di-1-naphthalenyl-N,N'-diphenyl-[1,1':4',1":4",1"'-Quaterphenyl]-4,4"'-diamine; (f) 2-tert-butyl-9,10-bis[4-(1,2,2-triphenylvinyl)phenyl]anthracene.*

(HOMO$= -5.6\ eV$, LUMO$= -2.6\ eV$ [100]) and TBPe (HOMO$= -5.3\ eV$, LUMO$= -2.3\ eV$ [19]) are appropriate for hole injection, but may hinder electron injection.

A good spectral overlap between matrix emission and emitter absorption is crucial for

Material	d [nm]
Glass substrate	
ITO	90
MeO-TPD: F_4-TCNQ	20: (4 mol%)
α-NPD	10
MADN: TBPe	10: (X wt%)
HBL	10
BPhen:Cs	35
Al	100

Table 5.1: *Common structure of the blue OLEDs investigated in this section. The emitter concentration is varied to verify its influence on efficiency and lifetime. TPBi, BPhen, BAlq or Alq_3 are applied consecutively as hole blocking layer (HBL) in order to reduce the electron injection barrier towards the emission layer and by this means to enhance the lifetime.*

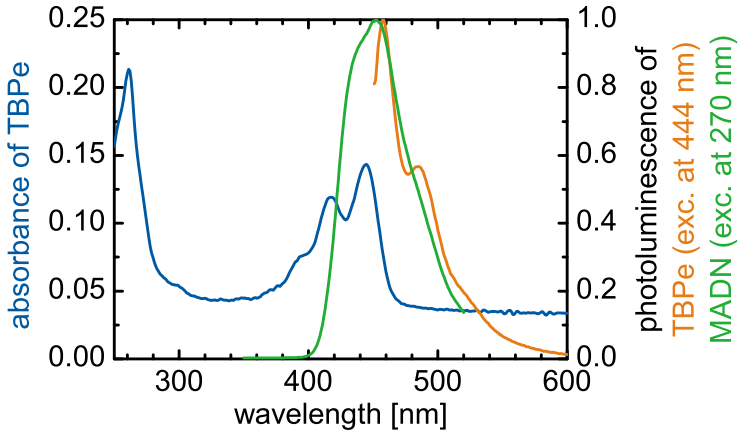

Figure 5.2: *Absorbance and photoluminescence of TBPe as well as the photoluminescence of MADN. In each case a thin film of 20 nm on quartz glass was investigated. MADN and TBPe have a good spectral overlap between matrix emission and emitter absorption, which is crucial for efficient energy transfer. The Stokes shift of TBPe is rather small and may limit the efficiencies by allowing reabsorption, but can be neglected for low emitter concentrations.*

efficient energy transfer between host and guest, which is illustrated for MADN and TBPe in Figure 5.2. The Stokes shift of TBPe is small, which may limit the efficiencies by allowing for reabsorption. However, this effect can be neglected for lower emitter

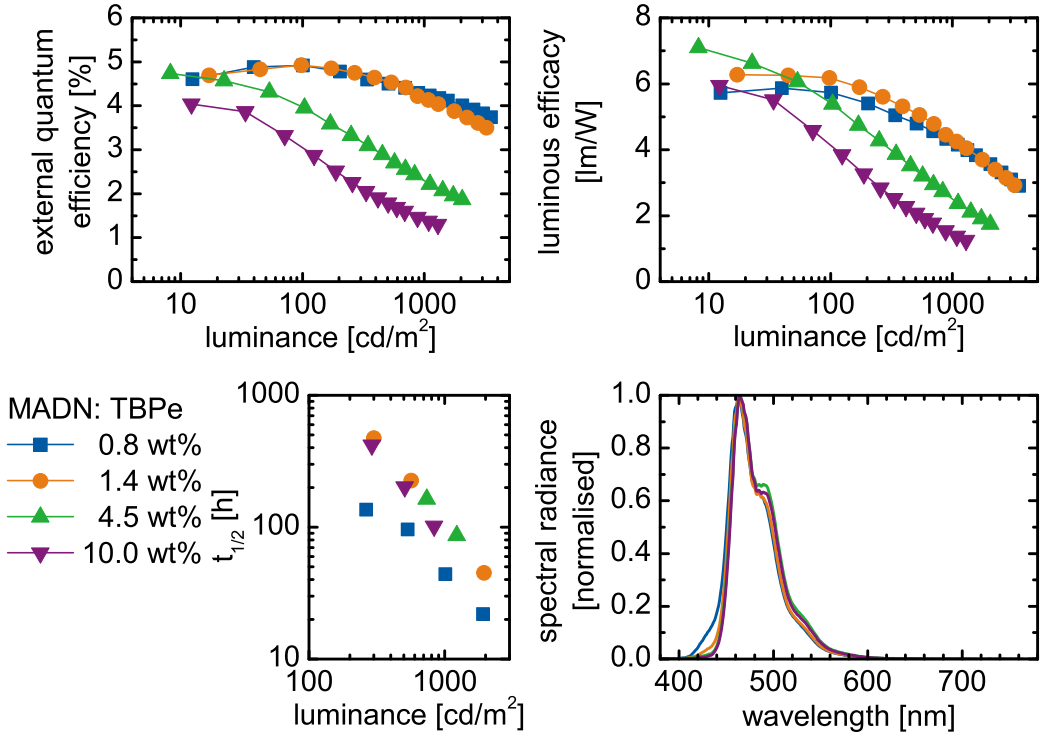

Figure 5.3: *Efficiencies, lifetimes, and spectra of OLEDs based on the stack presented in Table 5.1 with varying emitter concentration and TPBi as hole blocking layer. Highest efficiencies are reached for a TBPe concentration of* 1.4 *wt%. Due to incomplete energy transfer MADN emission occurs for lower concentration values, which effects the lifetime negatively.*

concentrations.

Beside the cavity length, two other parameters are expected to have a strong influence on the device lifetime and efficiency. The first one is the concentration of the emitter. Because the HOMO of TBPe is 0.3 eV above the HOMO of MADN, TBPe may trap holes at lower and contribute to the hole transport at higher concentrations. Hence, the concentration of TBPe has a significant influence on the charge carrier balance inside the emission layer. Furthermore, aggregation effects may reduce the efficiency for higher emitter concentration (Section 3.2.4). Due to difficulties with the electron injection which is correlated to the high lying LUMO level, the second is the choice of the hole blocking material. The device performance as a function of the TBPe concentration will be shown first. Later, the influence of the hole blocking material will be discussed. The following OLEDs are based on the stack presented in Table 5.1 with TPBi as hole blocking layer. The cavity is optimised for emission at 460 nm. The emitter concentration is varied from 0.8 wt% to 10 wt%. The efficiencies, spectra, and

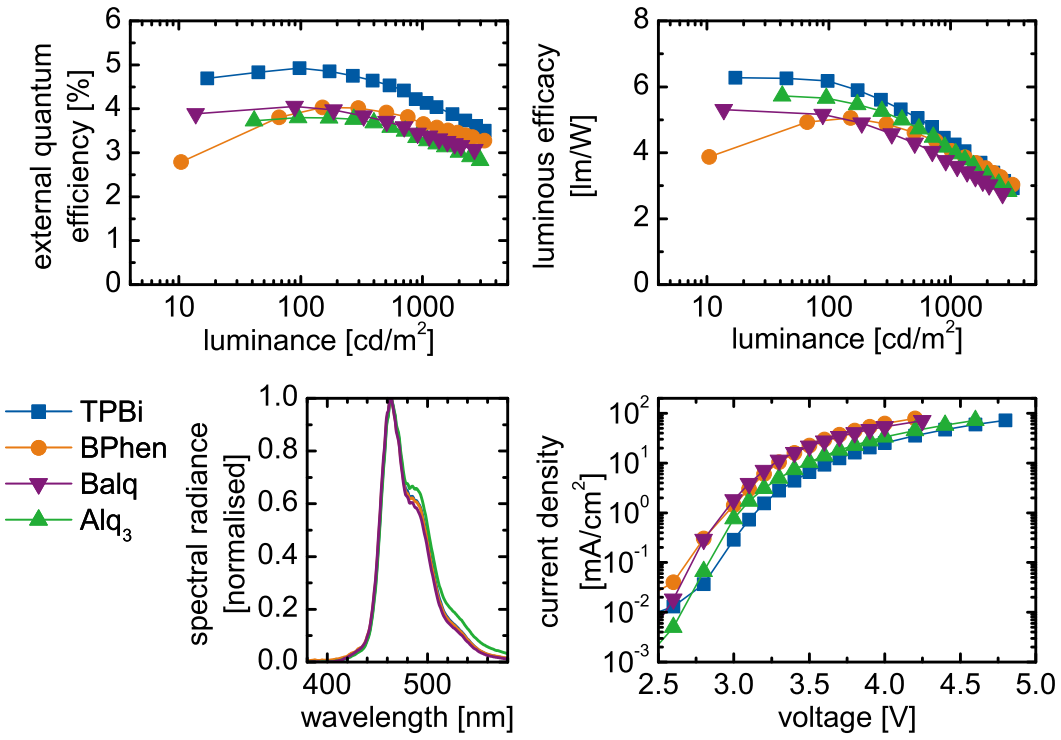

Figure 5.4: *Most important characteristics of OLEDs based on the stack presented in Table 5.1 with varying hole blocking material and a constant emitter concentration of* 1.4 *wt%. Highest efficiencies are achieved with TPBi. Despite its low external quantum efficiency, the Alq_3 OLED is second best in terms of luminous efficacy. This is due to a weak green shift of the spectrum.*

lifetimes of these OLEDs are summarised in Figure 5.3. The external quantum efficiency as well as the luminous efficacy decrease at higher concentrations of TBPe. No additional emission peaks appear in the spectrum for higher concentrations. Hence, aggregation effects can be excluded. A charge carrier imbalance induced by an increased contribution of the TBPe to the hole transport explains this behaviour. The highest efficiencies are reached at a TBPe concentration of 1.4 wt%. An external quantum efficiency of 5 % is reached at 100 cd/m^2, which drops to 4.2 % at 1000 cd/m^2. For white light emission at 1000 cd/m^2, less than 100 cd/m^2 are contributed by the blue emitter, which is due to the low sensitivity of the human eye in the blue region, and the low contribution in terms of radiance that is needed to achieve white colour coordinates. If the TBPe concentration is reduced to 0.8 wt%, not all excitons are transferred to TBPe, which leads to MADN emission in the spectrum and a decrease of lifetime. However, lifetime and spectrum are fairly independent of the TBPe concentration for higher percentages.

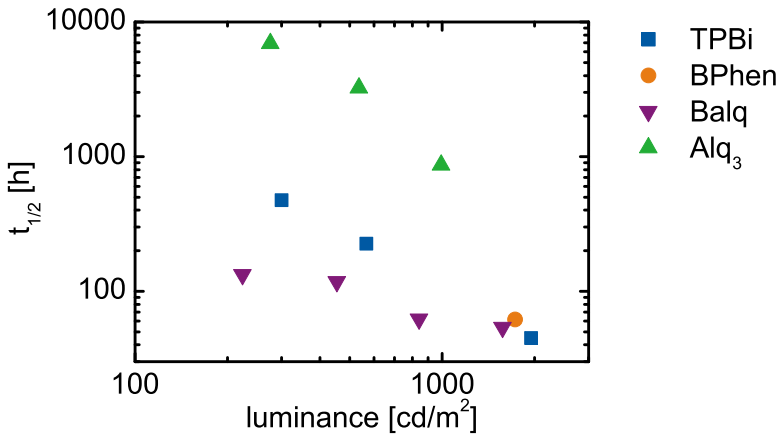

Figure 5.5: *Lifetime of blue OLEDs based on the stack presented in Table 5.1. $t_{1/2} = 850$ h can be reached at 1 000 cd/m^2 by applying Alq_3 as hole blocking layer.*

The position of the LUMO (-2.9 eV[1]) of TPBi is too low in comparison with the LUMO of other materials in the emission layer. A large barrier at the emission layer for one kind of charge carriers usually leads to a very thin recombination zone close to the interface between emission and blocking layer. The increased exciton density will accelerate the aging process of the emission layer. To improve the injection of electrons the hole blocking material TPBi is exchanged by BPhen, Alq_3, and BAlq. For better comparison with the above results, the concentration of TBPe is kept constant at 1.4 wt%. The LUMO levels of the hole blocking materials (BPhen: -2.9 eV, BAlq: -3.2 eV[2], Alq_3: -3.0 eV [101]) are similar to that of TPBi, but because of Fermi level alignment instead of alignment of the vacuum levels, the corresponding injection barriers do not equal the differences of the LUMO values. To further complicate the situation, also the barrier between the electron transport and the hole blocking layer is effected by the choice of the hole blocking material. Figure 5.4 shows the most important characteristics and Figure 5.5 the lifetimes of these OLEDs.

In the current voltage dependence, one can observe improved electron injection in case of BPhen and BAlq. In case of Alq_3 this effect is present, but is not that pronounced. All three blockers have in common that the improved electron injection is accompanied by a reduction of the external quantum efficiencies compared to the device which contains TPBi. In terms of luminous efficacy this loss is smaller, because operating voltages are decreased as well.

OLEDs with Alq_3 achieve the longest lifetimes and reach 850 h at 1 000 cd/m^2. Further-

[1] Optical gap and UPS-measurement done by Selina Olthof at the IAPP.
[2] Optical gap and UPS-measurement for BPhen and BAlq done by Selina Olthof at the IAPP.

more, the spectrum is slightly green shifted. This results in luminous efficacies, which are comparable to the TPBi devices, despite the lower external quantum efficiencies. A possible cause for the green shift is exciton transfer from the emission layer to the Alq_3. It is very likely that a broader recombination zone is responsible for the enhanced lifetime of the Alq_3 containing OLEDs.

Spiro-Pye:DBzA

When applied as bulk layer, DBzA shows good electron transport properties and can be used as electron injection layer [102]. On the other hand, mixed into an appropriate matrix material, DBzA emits light with deep blue colour coordinates $(x, y) = (0.150, 0.135)$ and reaches a lifetime of 1 100 h at an initial brightness of 500 cd/m^2 [20]. Its HOMO level is at -5.7 eV and its LUMO level is at -2.8 eV [103]. Here, Spiro-Pye, a perylene derivative, is used as matrix material. The chemical structures of both materials are presented in Figure 5.1. The LUMO of Spiro-Pye (-2.7 eV [104]) is 0.1 eV above the LUMO of DBzA. Therefore, the electron transport might be assisted by the DBzA molecules. The HOMO level of Spiro-Pye (-5.6 eV [104]) is also above the HOMO level of DBzA. Since DBzA is also used as hole blocking material, it can be assumed that the hole transport is exclusively taking place via the Spiro-Pye. Motivated by the fact that pure DBzA is applicable as electron transport layer, the photoluminescence of a 40 nm thick layer on quartz glass is measured. Unfortunately, a second peak at 536 nm appears additionally to the expected emission at 446 nm in the spectrum (Figure 5.6). This can be attributed to aggregation effects, which are generally connected with a loss of efficiency (Section 3.2.4). Hence, DBzA can not be applied as bulk emission layer.

Material	d [nm]
Glass substrate	
ITO	90
MeO-TPD: F_4-TCNQ	20: (4 mol%)
α-NPD	10
Spiro-Pye: DBzA	10: (X wt%)
TPBi	10
BPhen:Cs	35
Al	100

Table 5.2: *Architecture of a blue OLED based on the emitter system Spiro-Pye doped with DBzA. The concentration of the blue emitter is varied from* 1 *wt% to* 10 *wt%.*

The concentration dependence of the electroluminescence is examined by OLEDs based

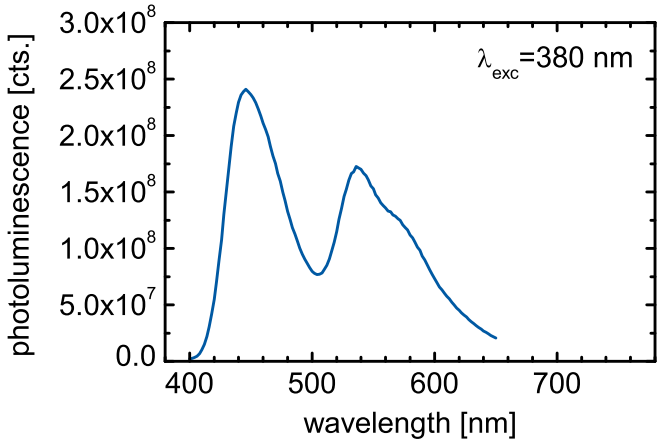

Figure 5.6: *Photoluminescence of a* 40 *nm thick DBzA layer on quartz glass excited at a wavelength of* 380 *nm. Due to aggregation effects, a second emission peaks arises at* 536 *nm. Therefore, DBzA can not be applied as bulk emission layer.*

on the stack presented in Table 5.2. The concentration of DBzA is varied from 1 wt% to 10 wt%. The most important properties of these OLEDs are summarised in Figure 5.7.

The spectrum of the OLED with a DBzA concentration of 10 wt% has a slight shoulder where the aggregate emission is observed in the photoluminescence measurement of the bulk layer. A maximum external quantum efficiency of 5.1 % is reached, for a concentration of 1 wt%. Although no aggregation effects are apparent in the spectrum for 5 wt%, the efficiency is decreased by 1 %. This can be explained by the change of the current voltage characteristics. As the current densities are slightly decreasing with increasing DBzA concentration and DBzA shows good electron transport properties [102] one can conclude that DBzA is hindering the hole transport in the emission layer. Accordingly, DBzA concentrations above 1 wt% result in a charge carrier imbalance and decreased efficiencies. The operational lifetime of the OLED with 1 wt% DBzA is only 40 h at an initial luminance of 1 000 cd/m^2. This is less than half of the lifetime of a device with the emitter system MADN:TBPe and the same blocker materials, which is about 100 h at an initial luminance of 1 000 cd/m^2 (Figure 5.5). Therefore, the investigation of the lifetime dependence on the choice of the blocking materials is omitted for this emitter system.

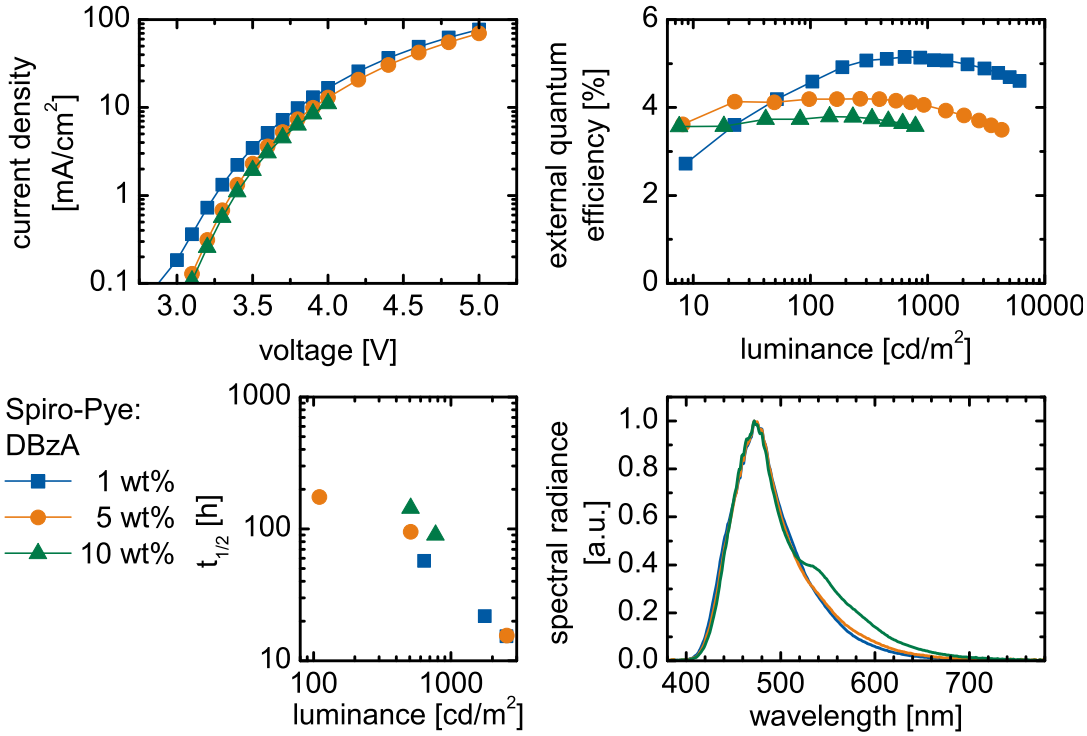

Figure 5.7: *Most important properties of the OLEDs introduced in Table 5.2. Aggregation of DBzA is taking place for concentrations above* 10 *wt%. Well balanced charge carrier injection results in external quantum efficiencies of up to* 5.1 *% for a concentration of* 1 *wt%.*

5.1.2 Bulk Emitters

Bulk emitters are emitters which are applicable as pure layer, because their yield is not limitted by aggregate effects. In this section the two representatives 4P-NPD and TPVAn (Figure 5.1) are investigated in detail.

4P-NPD

4P-NPD is a primarily hole conducting material. The hole mobility in 4P-NPD $\mu_{0h} = 6.6 \cdot 10^{-4}$ cm^2/Vs is four orders of magnitude higher than the electron mobility $\mu_{0e} = 3.6 \cdot 10^{-8}$ cm^2/Vs [23]. It is applicable as bulk emitter and provides fluorescent deep blue emission with the maximum of the photoluminescence spectrum at 425 nm [105]. The energy of the first excited triplet gap is 2.3eV [105]. The HOMO and LUMO levels of 4P-NPD are at -5.4 eV and -2.3 eV, respectively [106]. Hence, good hole injection can be achieved, but electron injection is hindered. Taking its primarily hole conducting character into account, it can be concluded that the charge carrier recombination zone in an OLED with 4P-NPD as emission layer will be close to the hole blocking layer.

Material	d [nm]
Glass substrate	
ITO	90
MeO-TPD: NDP-2	20: (4 wt%)
EBL	10
4P-NPD	10
HBL	10
BPhen:Cs	35
Al	100

Table 5.3: *Common structure of the 4P-NPD OLEDs investigated in this section. In order to improve the charge carrier balance in the emission layer several materials are consecutively applied as electron (EBL) or hole blocking layer (HBL). As electron blocking layer TAPC, α-NPD, and Spiro-TAD are used and as hole blocking layer TPBi and BPhen are applied.*

In order to estimate the influence of the blocker materials on quantum efficiency, luminous efficacy, and lifetime, some devices with an architecture according to Table 5.3 are produced and characterised. Whereas the thickness of each layer is kept constant, TPBi and BPhen are consecutively applied as hole blocking and TAPC, α-NPD, and Spiro-TAD as electron blocking layer. Due to the primarily hole conducting character of 4P-NPD, the electron blocking layer will not have to block any electrons and is

rather used as exciton blocking layer.

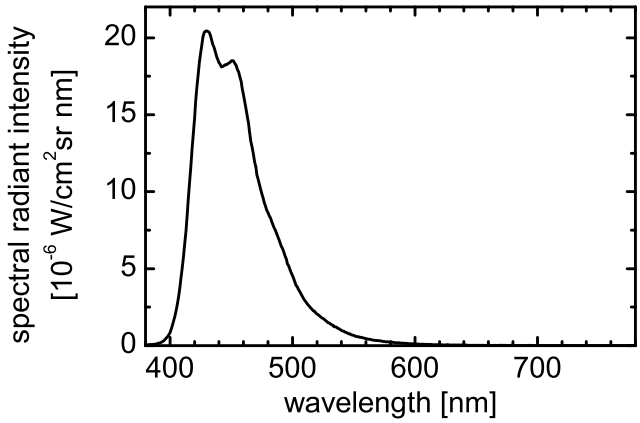

Figure 5.8: *Emission spectrum of the OLED with BPhen and Spiro-TAD as blocking materials measured at a luminance of* 1000 *cd/m*^{2}*. The corresponding colour coordinates are* $(x,y) = (0.152, 0.071)$.

The spectra of the devices are almost identical. Therefore, only the spectrum of the OLED with BPhen and Spiro-TAD as blocking materials is shown in Figure 5.8. The electroluminescent spectrum features a maximum at 430 nm and a second peak at 450 nm. The corresponding colour coordinates are $(x,y) = (0.152, 0.071)$.

For both hole blocking layers, the lowest driving voltage is achieved with Spiro-TAD as electron blocking layer (Figure 5.9). α-NPD is second best and the use of TAPC results in the highest voltages. In order to achieve a current density of 10 mA/cm^2, a voltage of 3.1 V, 3.4 V, and 3.9 V is needed with TPBi as hole blocking layer and Spiro-TAD, α-NPD, and TAPC as electron blocking layer, respectively. This can be interpreted as improved hole injection with Spiro-TAD in comparison to α-NPD and TAPC. Spiro-TAD and α-NPD have the same HOMO level of -5.4 eV [79, 80]. The HOMO level of TAPC is decreased by 0.4 eV (-5.8 eV [82]). This results in an increased barrier for hole injection into this material, which explains the increased driving voltages in case of TAPC. The hole mobility in α-NPD ($\mu_{h,\alpha-\mathrm{NPD}} = 2.2 \cdot 10^{-3}$ cm^2/Vs at a field of $2.5 \cdot 10^5$ V/cm) [82] is one order of magnitude higher than in Spiro-TAD ($\mu_{h,\mathrm{Spiro-TAD}} = 3.0 \cdot 10^{-4}$ cm^2/Vs at a field of $2.0 \cdot 10^5$ V/cm) [107], which is in contradiction to the observed driving voltages. At the interface between the doped MeO-TPD and the α-NPD no interface dipoles were observed [79]. Hence, the voltage increase in case of α-NPD in comparison with Spiro-TAD may be induced by interface dipoles at the 4P-NPD interface.

In case of TPBi, the highest external quantum efficiency is achieved with TAPC as electron blocking layer ($\eta_q = 5.4$ %), in which case the hole injection is worst. Whereas,

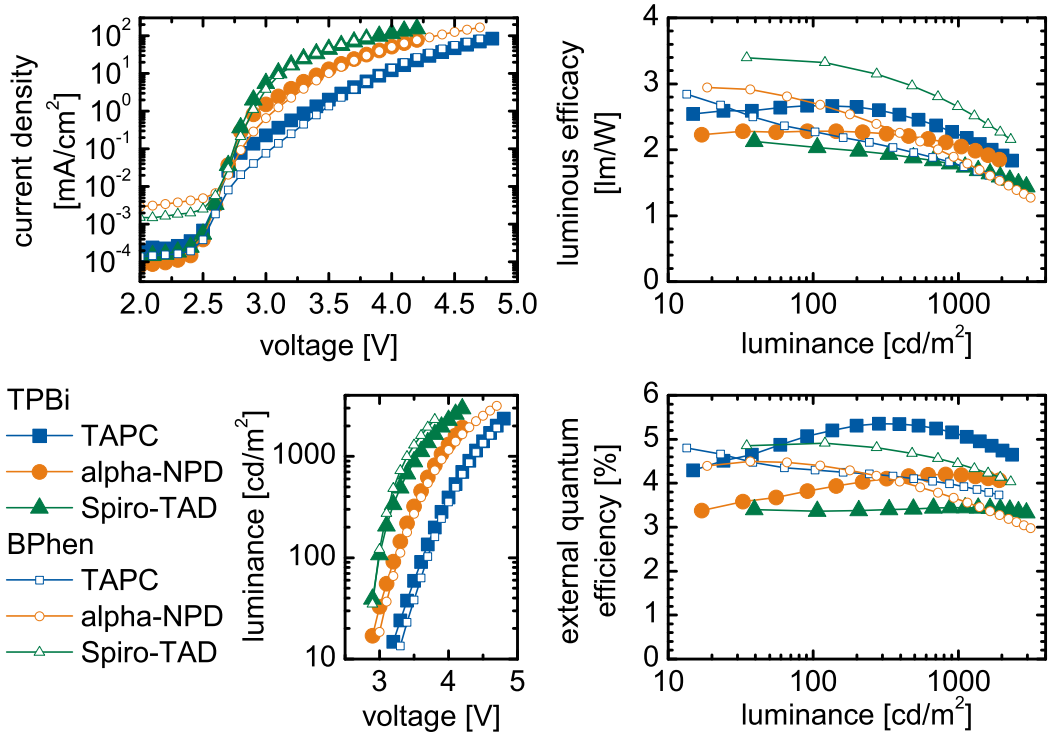

Figure 5.9: *Most important properties of 4P-NPD OLEDs as described in Table 5.3. The lowest driving voltage is achieved with Spiro-TAD as electron blocking layer, followed by α-NPD and TAPC. The highest external quantum efficiency is achieved with TPBi and TAPC and the highest luminous efficacy with BPhen and Spiro-TAD.*

for BPhen the highest external quantum efficiency is achieved with Spiro-TAD ($\eta_q = 4.9$ %), in which case the hole injection is best. By correlating enhanced quantum efficiency with improved charge carrier balance, it can be concluded that the electron injection with BPhen is better than with TPBi. Due to the driving voltage increase in case of the TPBi/TAPC blocker combination in comparison to the BPhen/Spiro-TAD combination (by $\Delta U = 0.8$ V for $j = 10$ mA/cm^2), the luminous efficacy is increased for the combination BPhen/Spiro-TAD ($\eta_{v,\mathrm{BPhen/Spiro-TAD}} = 2.7$ lm/W, $\eta_{v,\mathrm{TPBi/TAPC}} = 2.2$ lm/W at 1 000 cd/m^2). For illumination applications high luminous efficacies are preferred against high external quantum efficiencies. From this point of view the combination of BPhen as hole blocking and Spiro-TAD as electron blocking material is best.

The device lifetime is measured for the four blocker combinations with the highest luminous efficacy (Figure 5.10). The combination of TPBi and α-NPD reaches the longest lifetime, which is $t_{1/2} = 1$ h at an initial luminance of 1 000 cd/m^2. If charge

transport was not carried by 4P-NPD, the device lifetimes might be improveable. This can be achieved by an appropriate matrix material. Experiments with TCTA, TPBi or CBP (4,4'-N,N'-dicarbazole-biphenyl) as matrix material for 4P-NPD were not successful and resulted in very low external quantum efficiencies around $\eta_q = 1$ %.

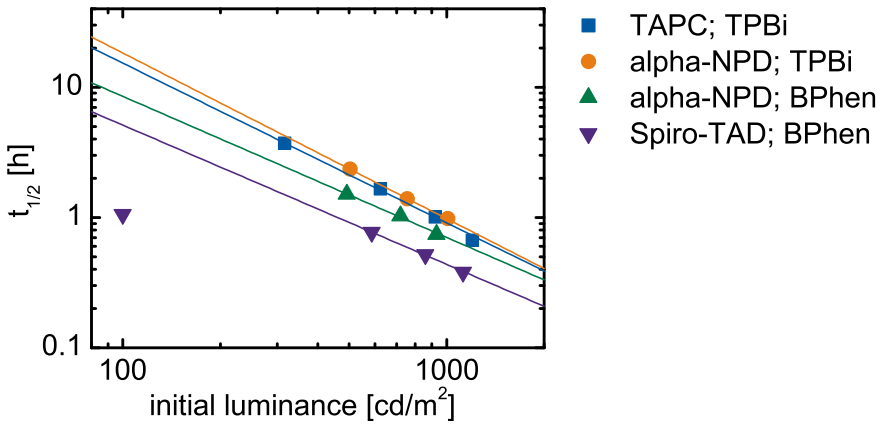

Figure 5.10: *Device lifetime of the four OLEDs with the highest luminous efficacy. None of the devices exceeds a lifetime of $t_{1/2} = 1$ h at an initial luminance of 1 000 cd/m^2.*

TPVAn

TPVAn is an anthracene derivative, which is applicable as bulk emitter (Figure 5.1). It forms a smooth layer after thermal deposition and exhibits deep blue light emission with a photoluminescence maximum at 450 nm (Figure 5.11) [21].

The HOMO and LUMO level are at -5.7 eV and -2.9 eV, respectively [21]. Due to the low HOMO level, it is likely that hole injection into the emission layer is hindered. Therefore, different combinations of hole transporting and electron blocking materials are tested in order to optimise the hole injection (Table 5.4).

The HOMO level of TCTA is -5.9 eV, so that hole injection from TCTA to TPVAn should not be hindered by high barriers. Hence, TCTA is used as electron blocking layer. For improved injection of holes into the TCTA layer, either α-NPD (HOMO$=$ -5.4 eV) doped with 10 wt% of C60F36 or MeO-TPD (HOMO$=$ -5.1 eV) doped with 2 wt% of NDP-2 is used as hole transport layer. Because of the deeper HOMO of α-NPD a reduced injection barrier to the TCTA is expected. Consequently, the driving voltage for a current density of $j = 10$ mA/cm^2 reduces from 4.30 V to 3.55 V when substituting the doped MeO-TPD for C60F36 doped α-NPD (Figure 5.12). The improved charge balance results in external quantum efficiencies of up to $\eta_q = 4$ %.

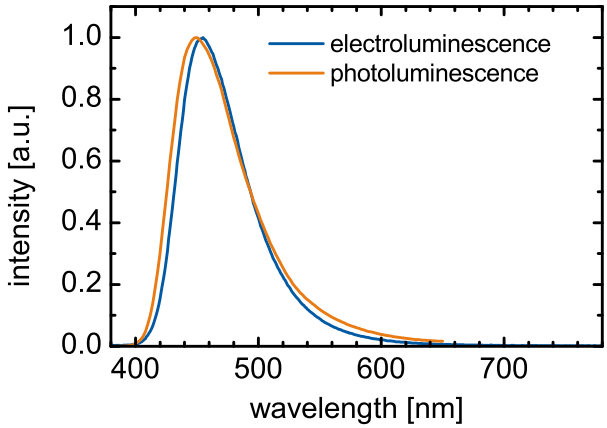

Figure 5.11: *Photoluminescence spectrum of* 1 *mg/ml TPVAn in toluol excited at* $\lambda_{\text{exc.}} = 350$ *nm and the common electroluminescence spectrum of the devices presented in Table 5.4.*

Material	d [nm]
Glass substrate	
ITO	90
HTL	20
TCTA or α-NPD	10
TPVAn	10
TPBi	10
BPhen:Cs	35
Al	100

Table 5.4: *Blue OLEDs based on the anthracene derivative TPVAn. In order to improve the hole injection, two different hole transport layer systems are applied. The first is MeO-TPD: (2 wt%) NDP-2 and the second is* α*-NPD: (10 wt%) C60F36.*

The HOMO of TCTA is below the HOMO of TPVAn, which results in an unnecessary high difference between the HOMO of the hole transport layer and this electron blocking layer. In order to further decrease the driving voltage, the TCTA layer is replaced by a pure layer of α-NPD. With α-NPD as electron blocking layer the voltage for a current density of $j = 10$ mA/cm^2 reduces to 3.49 V. The achieved efficiencies are comparable to the sample with TCTA as electron blocking layer.

The spectra of the investigated samples are identical. Therefore, only the spectrum

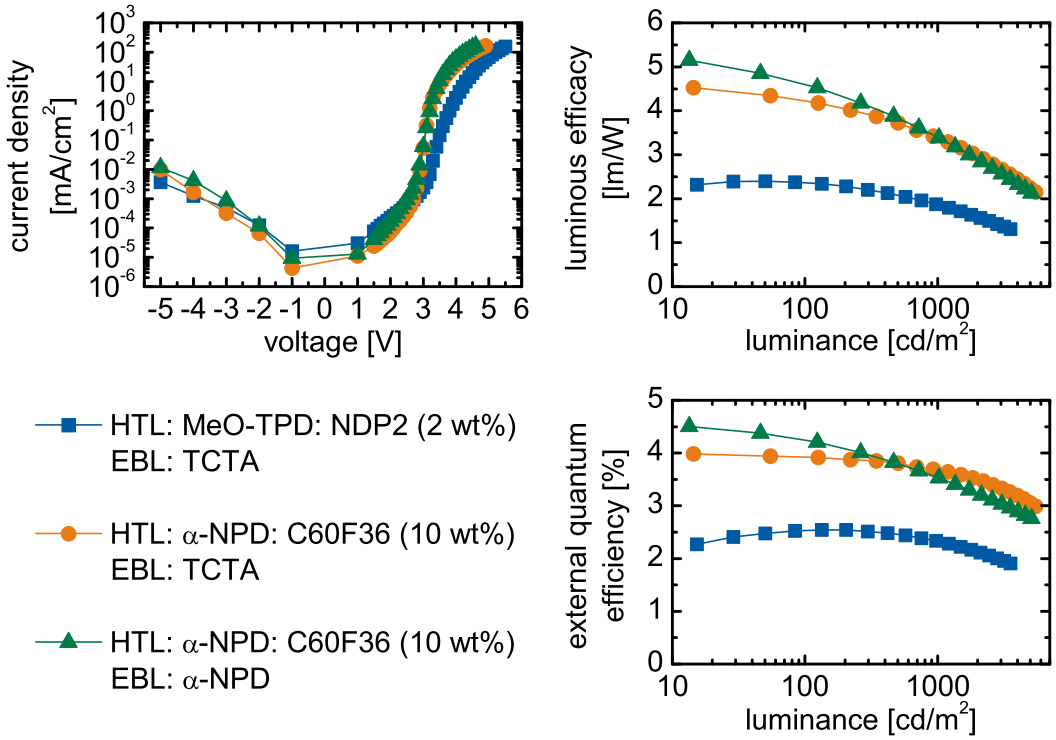

Figure 5.12: *Characteristics of the TPVAn based OLEDs as presented in Table 5.4. By choosing C60F36 doped α-NPD as hole transport layer the driving voltage decreases significantly. The enhanced hole injection results in improved charge carrier balance and increased external quantum efficiencies. Substitution of the electron blocking material TCTA with α-NPD does not yield a strong improvements.*

of the OLED with C60F36 doped α-NPD as hole transport layer and α-NPD as electron blocking layer is shown in Figure 5.11. The corresponding colour coordinates are $(x,y) = (0.151, 0.131)$. This OLED reaches a lifetime of 7.5 h at an initial luminance of 1 000 cd/m^2 (Figure 5.13), which is several orders of magnitude too low for application in a product.

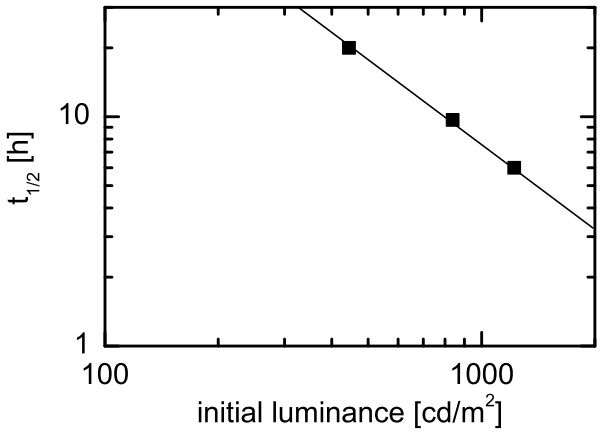

Figure 5.13: *Lifetime of the TPVAn based OLED as presented in Table 5.4 with C60F36 doped α-NPD as hole transport layer and pure α-NPD as electron blocking layer. At an initial luminance of* 1000 *cd/m*^{2} *this device reaches a lifetime of* 7.5 *h.*

5.1.3 Comparison

The presented collection of fluorescent blue emitters shows that it is possible to achieve high efficiencies with host-guest systems as well as bulk emitters. However, among the four presented fluorescent blue emitters the host-guest systems yield longer lifetimes. With the combination of MADN and TBPe lifetimes of up to 850 h at an initial luminance of 1 000 cd/m^2 are reached. Concentrations of 1 wt% are typical for emitters in fluorescent host-guest systems. Whereas it might be difficult to deposit layers with these low emitter concentrations homogeneously, the neat layers of bulk emitters are more easily processable. Table 5.5 summarises the most important properties of the OLEDs which were examined in this section.

Material	λ_{EL} [nm]	(x, y)	η_q [%]	η_v [lm/W]	$t_{1/2}$ [h]
MADN: TBPe					
α-NPD/ TPBi	463	(0.130, 0.168)	4.2	4.3	100
α-NPD/ Alq_3	463	(0.140, 0.199)	3.3	4.0	850
Spiro-Pye: DBzA	472	(0.168, 0.230)	5.1	7.1	40
4P-NPD					
TAPC/ TPBi	430	(0.152, 0.071)	5.1	2.2	0.9
Spiro-TAD/ BPhen	430	(0.152, 0.071)	4.4	2.7	0.4
TPVAn	455	(0.151, 0.131)	3.5	3.4	7.5

Table 5.5: *A collection of the properties of the examined fluorescent emitters including the emission peak of the electroluminescence, colour coordinates, external quantum efficiency, luminous efficacy and device lifetime at* 1 000 *cd/m*^{2}*. In case of MADN:TBPe and 4P-NPD, the results achieved with two different blocker combinations are presented (electron blocking layer/ hole blocking layer).*

5.2 Triplet Harvesting

In this section the concept of triplet harvesting is introduced. After discussing the basic principle and a possible implementation, three-colour devices based on this principle will be demonstrated. The parameters which have the strongest influence on the efficiency and the spectral shape of light emission are investigated in detail by means of a simplified two colour device. For these experiments, the transfer of triplets is limitted to a single phosphorescent emitter.

Stable phosphorescent blue emitters with deep blue colour coordinates are not yet available. Hence, the achievable colour coordinates and the colour rendering index (CRI) of white OLEDs is limited [17, 18]. Fluorescent emitters achieve deep blue emission and improve the colour quality of white OLEDs. However, due to spin statistics three out of four excitons are triplet excitons (see Section 3.1.2) and recombine non-radiatively. Thus, efficiencies of OLEDs based on fluorescent emitters are limited.

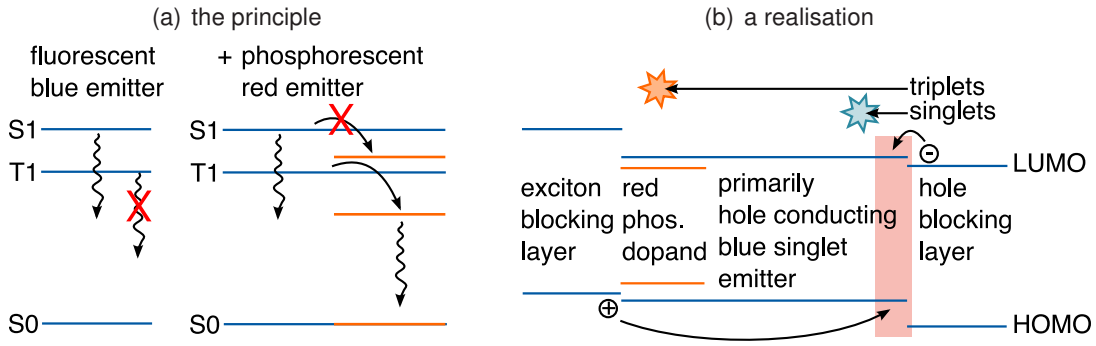

Figure 5.14: *(a) The principle of triplet harvesting: By transferring otherwise unused triplet excitons from the fluorescent to a phosphorescent emitter, internal quantum efficiencies of up to* 100 *% are possible. (b) An implementation of the concept of triplet harvesting: Applying a primarily hole conducting fluorescent blue emitter will result in an exciton generation zone close to the hole blocking layer. Having a shorter lifetime, singlets will rapidly recombine close to the place where they are generated, whereas triplets may diffuse inside the emission layer towards a phosphorescent red emitter.*

The idea behind the concept of triplet harvesting is to transfer these otherwise lost triplets to a phosphorescent emitter, where they can emit light (Figure 5.14 (a)). By implementing this principle in a white OLED, internal quantum efficiencies of up to 100 % are possible despite the use of a fluorescent blue emitter.

In order to achieve efficient white light emission with a strong blue fraction, triplet transfer has to be optimised and singlet transfer hindered simultaneously. The different lifetimes of singlets, which are in the range of nanoseconds, and triplets, which exceed microseconds, result in different diffusion lengths [108, 109]. This difference can be utilised to separate singlets and triplets [23]. Figure 5.14 (b) illustrates the implementation of this approach. If a blue fluorescent bulk emitter is chosen which is favouring the transport of one charge carrier type, the exciton generation zone will be located close to the interface of the corresponding blocking layer. Singlets, having a shorter lifetime, will rapidly recombine close to the place where they are generated, whereas triplets may diffuse inside the emission layer. If a part of the emission layer close to the opposite blocking layer is doped with a phosphorescent emitter, triplets will be transferred to this emitter and emit light. It is apparent that the success of this approach depends on the choice of the blue emitter. Therefore, the process of selecting an appropriate candidate is discussed in the following section.

5.2.1 Choice of Blue Emitter

An efficient bulk emitter is important for separation of singlets and triplets. Along with the bulk emitters TPVAn and 4P-NPD introduced in Section 5.1.2 the matrix material MADN was considered as potential emitter. The main criteria for selecting the emitter is its triplet gap, which should be above the triplet gap of the applied phosphorescent emitter, to allow for triplet transfer. However, a direct measurement of the triplet gap by delayed phosphorescence was not possible for MADN and TPVAn because of the effects of strong delayed fluorescence [110]. Therefore, an indirect approach was chosen for the determination of the triplet gap. Both were tested as matrix material for different phosphorescent emitters. In case of the MADN, light output was too low for device evaluation, which implies that the transfer of singlets from the MADN to the phosphorescent emitters and the back transfer of triplets are very efficient. Therefore, MADN is not suitable as matrix material for phosphorescent emitters in the visible wavelength region.

TPVAn was tested as matrix material for two different phosphorescent emitters. The samples have an architecture corresponding to Table 5.4 with C60F36 doped α-NPD as hole transport material and pure α-NPD as electron blocking layer. In the first OLED, 10 wt% of Ir(dhfpy)$_2$acac and in the second, 10 wt% of Ir(MDQ)$_2$acac are mixed into the TPVAn layer. Both emitters were introduced in Section 3.2.4. The contribution of Ir(dhfpy)$_2$acac emission in the electroluminescent spectrum is very small (Figure 5.15). In case of Ir(MDQ)$_2$acac, the phosphorescent emission is stronger, but still below the fluorescent emission. The external quantum efficiencies of both devices are below 0.1 %. Hence, TPVAn is also not applicable as host for phosphorescent emitters in

the visible wavelength region.

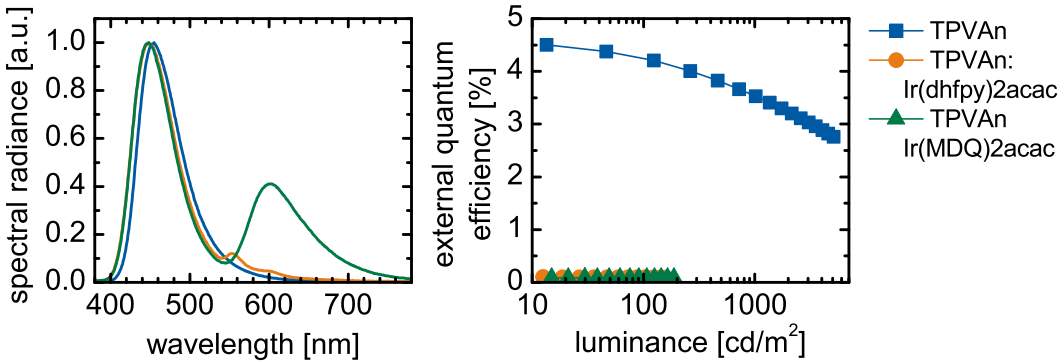

Figure 5.15: *Spectra and external quantum efficiencies of OLEDs using TPVAn as matrix material for the phosphorescent emitters Ir(dhfpy)$_2$acac and Ir(MDQ)$_2$acac. The low share of the phosphorescent emission and the low efficiencies imply that TPVAn is not suitable as matrix for these phosphorescent emitters, because of a too low triplet energy of the fluorescent emitter.*

A small triplet gap seems to be typical for anthracene derivatives as Singh et al. were able to measure a triplet gap of 1.83 eV for anthracene crystals [111]. Instead of TPVAn and MADN, 4P-NPD is chosen as blue emitter for the following experiments. For triplet transfer to a phosphorescent green emitter, a blue emitter is needed, which features a triplet above 2.45 eV. 4P-NPD does not meet this requirement. However, the triplet gap of 4P-NPD (2.3 eV [23]) allows for triplet transfer to emitters emitting in the yellow and red wavelength region ($\lambda > 540$ nm). The highly efficient emission with deep blue colour coordinates is advantageous for application in white OLEDs. Furthermore, the primarily hole transporting 4P-NPD fulfils the prerequisite of a sharp exciton generation zone close to one of the blocking layers.

5.2.2 Harvesting by Two Phosphorescent Emitters

Combining two emitters is sufficient for achieving white colour coordinates. However, the gap in the spectrum of a two-colour OLED will result in poor colour rendition properties. In order to achieve high quality white light, the emission of at least three emitters, covering the blue, green, and red wavelength range, has to be mixed.

The approach of triplet harvesting after diffusion is a possible way to realise an efficient three-colour white OLED. Because 4P-NPD does not allow for triplet transfer to a phosphorescent green emitter, triplet harvesting from a fluorescent emitter to two different phosphorescent emitters will be investigated by the use of a model. This model

OLED will illustrate how to design a three-colour white triplet harvesting OLED. 4P-NPD is used as blue emitter and matrix for the red emitter Ir(MDQ)$_2$acac as well as the yellow emitter Ir(dhfpy)$_2$acac, which represents the green emitter in this model. Both emitters were introduced in Section 3.2.4. The complete architecture of this OLED is presented in Table 5.6. The excitons are generated at the interface to the hole blocking material BPhen and diffuse towards the anode. Exciton transfer to BPhen can be excluded, because the singlet ($S_1 = 3.2$ eV) and the triplet energy ($T_1 = 2.58$ eV) of BPhen are higher than those of 4P-NPD ($S_1 = 2.85$ eV, $T_1 = 2.3$ eV) [15]. Two sections of the 4P-NPD close to the Spiro-TAD are doped with the phosphorescent emitters. While diffusing towards the anode, triplets will first arrive at the emitter with the larger triplet energy (Ir(dhfpy)$_2$acac) and afterwards at the emitter with the lower triplet energy (Ir(MDQ)$_2$acac). Direct excitation of the phosphorescent emitters can be neglected, because of the low electron mobility in 4P-NPD (Section 5.1.2).

Material	d [nm]
Glass substrate	
ITO	90
MeO-TPD: NDP-2	20: (2 wt%)
Spiro-TAD	10
4P-NPD: Ir(MDQ)$_2$acac	10: (8 wt%)
4P-NPD: Ir(dhfpy)$_2$acac	0/5/10: (10 wt%)
4P-NPD	10
BPhen	10
BPhen:Cs	35
Al	100

Table 5.6: *Stack of the three-colour triplet harvesting OLED investigated in this section. Excitons are generated at the interface between 4P-NPD and BPhen. The excitation distribution between the two triplet emitters Ir(MDQ)$_2$acac and Ir(dhfpy)$_2$acac is controlled by the thickness of the layer doped with the latter.*

The spectra in Figure 5.16 show that Ir(MDQ)$_2$acac (the peak at 605 nm) as well as Ir(dhfpy)$_2$acac (the peak at 557 nm) are excited and that the excitation distribution between them can be controlled by the thickness of the Ir(dhfpy)$_2$acac doped layer. Applying the optical simulation which is introduced in Section 4.4, the internal excitation distribution can be calculated. It is presented in Figure 5.17 for varying thickness of the layer doped with the yellow emitter. For a layer thickness of 10 nm, 36 % of the harvested triplets reach the red emitter. Figure 5.18 illustrates how the shift of excitation from the red to the yellow emitter affects the colour coordinates of the OLED. The colour coordinates of the OLED without the yellow emitter are $(x,y) = (0.403, 0.252)$. For a thickness of Ir(dhfpy)$_2$acac doped 4P-NPD of 5 nm and 10 nm the colour coordinates shift to $(x,y) = (0.382, 0.287)$ and $(x,y) = (0.363, 0.323)$, respectively. With

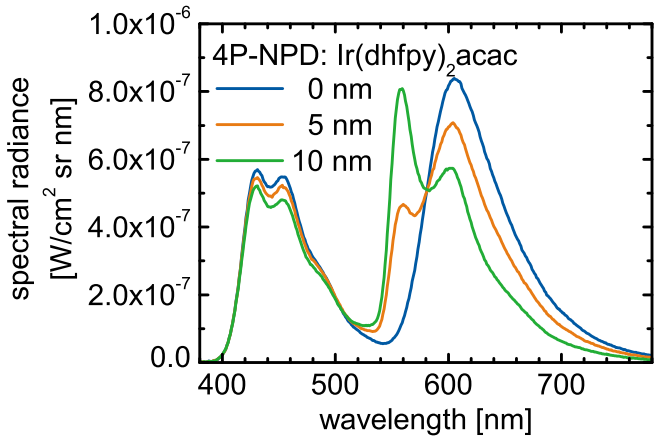

Figure 5.16: *Spectra of three-colour triplet harvesting OLEDs at a constant current density of* $j = 1.48$ *mA/cm*^{2}*. The corresponding architecture is presented in Table 5.6. Both triplet emitters are excited. The excitation distribution can be controlled by the thickness of the Ir(dhfpy)*$_2$*acac doped layer.*

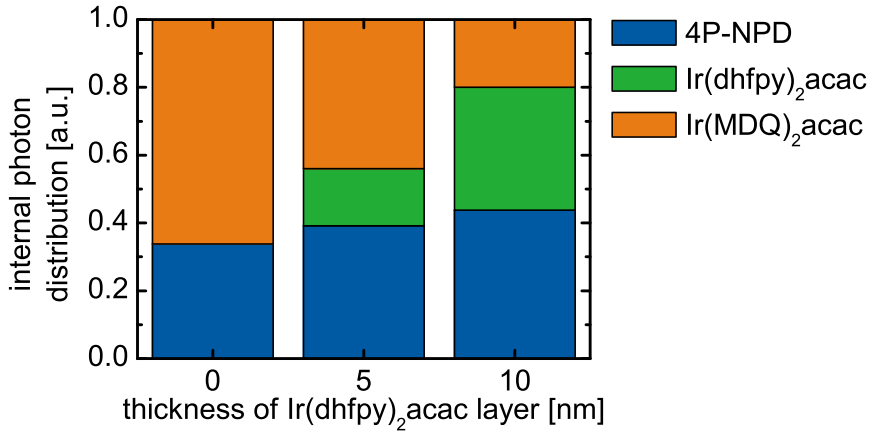

Figure 5.17: *Internal excitation distributions corresponding to the spectra presented in Figure 5.16 and calculated according to the algorithm which was presented in Section 4.4.2. The stacks of these devices are introduced in Table 5.6. For a layer thickness of* 10 *nm,* 36 *% of the harvested triplets reach the red emitter.*

this emitter combination, the Planckian locus can only be reached, if the $Ir(MDQ)_2acac$ is completely suppressed. Precise colour point control can be accomplished by layer thickness variation within the order of magnitude of a typical layer thickness in an OLED. Hence, no special requirements concerning the precision have to be met by the

deposition tools. Presuming that a blue emitter can be found which allows for triplet transfer to a green phosphorescent emitter, this approach is well suited for the development of a white OLED stack for large-scale production.

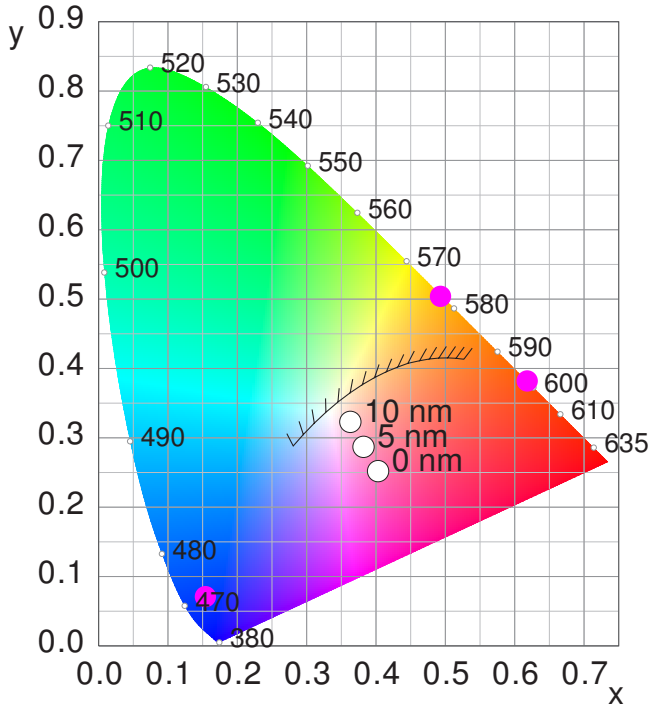

Figure 5.18: *Colour coordinates of the discussed three-colour triplet harvesting OLEDs. The variation of the Ir(dhfpy)$_2$acac layer thickness allows for precise colour point control. Because this variation is in the order of magnitude of a typical layer thickness in an OLED, no special requirements concerning the precision have to be met by the deposition tools.*

The external quantum efficiency and the luminous efficacy of the three OLEDs are summarised in Figure 5.19. For Ir(dhfpy)$_2$acac a decreased quantum efficiency was observed in comparison with Ir(MDQ)$_2$acac [105]. Consequently, the external quantum efficiency at 1 000 cd/m^2 decreases with an increasing amount of triplets recombining on the yellow emitter from $\eta_q = 11$ % for the device without Ir(dhfpy)$_2$acac to $\eta_q = 9$ % for the device with a 10 nm interlayer of Ir(dhfpy)$_2$acac doped 4P-NPD. This is a problem connected to this particular emitter and not to the stack design. Despite a decreasing external quantum efficiency, the luminous efficacy increases from $\eta_v = 13.4$ lm/W ($d_{Ir(dhfpy)_2acac} = 0$ nm) to $\eta_v = 15.4$ lm/W ($d_{Ir(dhfpy)_2acac} = 10$ nm), because of the beneficial position of the yellow emitter with regard to the maximum of the V_λ function. Although the achieved efficiencies are comparable low, one should keep in

mind that this approach bears the potential for higher efficiencies, because the optical cavities of these OLEDs are not adjusted to the emission of the emitters. Furthermore, the thickness of the pure and the doped 4P-NPD layer as well as the concentration of the emitters are not optimised for the triplet harvesting process. The large potential of this approach will be demonstrated in the next section.

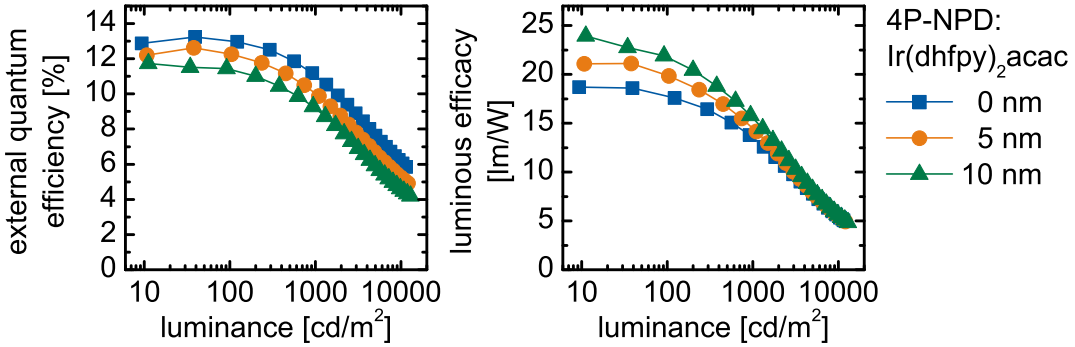

Figure 5.19: *External quantum efficiency and luminous efficacy of the devices introduced in Table 5.6. The corresponding electroluminescence spectra are presented in Figure 5.16.*

5.2.3 Detailed Investigation of the 4P-NPD/Ir(MDQ)$_2$acac System

For illumination purposes the above achieved efficiencies need to be improved. For reasons of simplicity, the optimisation is done for an OLED with only a single phosphorescent emitter. Due to its higher efficiency, the red emitter Ir(MDQ)$_2$acac is chosen for these experiments. Although triplet harvesting to a phosphorescent green emitter is not possible, the optimised 4P-NPD/Ir(MDQ)$_2$acac system can be used to design a white OLED. An approach to achieve highly efficient white light emission is presented in Section 5.5, where the spectral gap in the green range of the optimised 4P-NPD/Ir(MDQ)$_2$acac system is filled by stacking of a second full phosphorescent unit on top of this device.

The parameters besides the right choice of blocking materials, which influence the efficiency and the spectral shape of the emission, are the concentration of the red emitter and the thickness of the red doped emission layer. These parameters have to be chosen such that all triplets, which diffuse to this layer, are transferred to the red emitter and contribute to the emission of light. The thickness of the pure 4P-NPD layer is equivalent to the diffusion length. A reduction of this thickness will enhance the amount of triplets which are available for harvesting at the cost of additional transfer of singlets to the red emitter. The optimisation of the stack with respect to these parameters will

be presented in the following paragraphs. The charge and exciton blocking materials BPhen and Spiro-TAD are chosen according to Section 5.1.2, where the highest luminous efficacy for blue 4P-NPD OLEDs was achieved with this blocker combination. The cavity of the test devices is optimised for red emission, because three out of four excitons are triplets and in the ideal case all triplets are transferred to the phosphorescent red emitter. Table 5.7 illustrates the common stack of the OLEDs presented in the following paragraphs. The thickness variations of the two sections of the emission layer are compensated by the transport layers, in order to keep both the cavity length and the position of the red emission inside the cavity constant.

Material	d [nm]
Glass substrate	
ITO	90
MeO-TPD: NDP-2	70−X: (2 wt%)
Spiro-TAD	10
4P-NPD: Ir(MDQ)$_2$acac	X: (C wt%)
4P-NPD	Y
BPhen	10
BPhen:Cs	60−Y
Al	100

Table 5.7: *Common stack of the triplet harvesting OLEDs discussed in this section. The thickness variations of the two sections of the emission layer are compensated by the transport layers, in order to keep the cavity length constant and the red emission at a constant position inside the cavity.*

Influence of the Ir(MDQ)$_2$acac Concentration

To study the influence of the Ir(MDQ)$_2$acac concentration, the thickness of each layer is kept constant. The thickness of the mixed layer is 20 nm and the thickness of the pure 4P-NPD layer is 5 nm. The concentration of Ir(MDQ)$_2$acac is varied in the range of 2…15 wt%. The spectra in Figure 5.21 exhibit a dependence of the blue peak on the red emitter concentration. Additionally, the rising Ir(MDQ)$_2$acac concentration is accompanied by a decrease of the external quantum efficiency for values above 5 wt%. This can be explained by Ir(MDQ)$_2$acac participating in charge transport and thereby influencing the charge balance. The situation is illustrated in Figure 5.20. Because the HOMO of Ir(MDQ)$_2$acac (−5.4 eV[3]) is 0.3 eV higher than the HOMO of 4P-NPD (−5.7 eV [106]), hole transport may be hindered by trapping on the red emitter molecules for low concentrations. The decreased hole concentration at the interface

[3] UPS-measurement done by Selina Olthof at the IAPP

to the hole blocking layer results in an improved charge carrier balance, which is indicated by an increased external quantum efficiency and blue emission. For higher concentrations hopping transport on the red emitter becomes more likely because of an alignment of the HOMO levels of Spiro-TAD (-5.4 eV [80]) and Ir(MDQ)$_2$acac. Due to this alignment, the barrier for hole injection into Ir(MDQ)$_2$acac is lower than for injection into 4P-NPD. Due to the increased hole injection, the quantum efficiency decreases for higher Ir(MDQ)$_2$acac concentration.

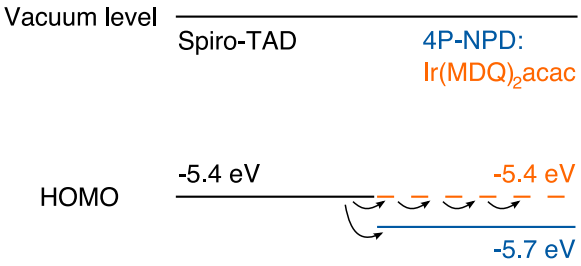

Figure 5.20: *Illustration of the charge injection at the interface between the emission layer and Spiro-TAD assuming vacuum level alignment. Due to good alignment of the HOMO levels of Spiro-TAD and Ir(MDQ)$_2$acac, hopping transport via the dopant is getting more likely for higher concentrations of Ir(MDQ)$_2$acac.*

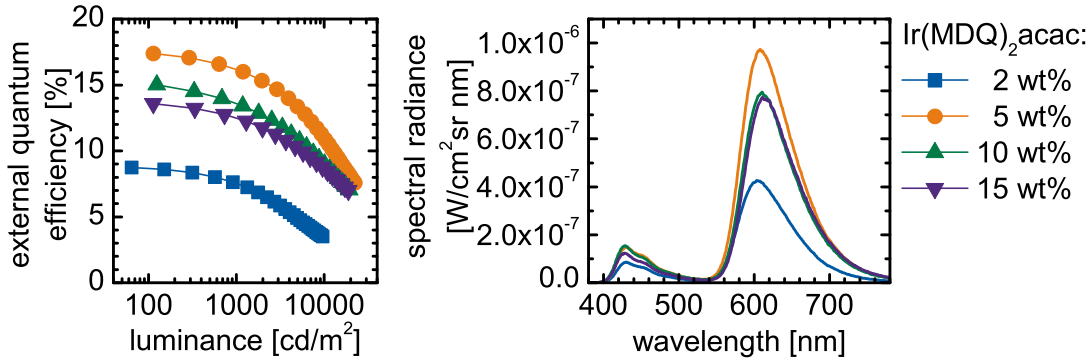

Figure 5.21: *External quantum efficiencies and spectra for OLEDs with varying Ir(MDQ)$_2$acac concentration. The external quantum efficiencies are determined by a goniometer measurement. All spectra are measured at a constant current density of $j = 0.77$ mA/cm^2. Highest efficiencies and strongest red emission are achieved for a concentration of 5 wt%.*

For concentrations below 5 wt% the red emission decreases. The ratio between the peak heights of Ir(MDQ)$_2$acac and 4P-NPD decreases from red/blue $= 6.50$ at 5 wt% to red/blue $= 4.94$ at 2 wt%, which means that for a concentration of 2 wt% less triplets are harvested. Highest efficiencies and strongest red emission are achieved with an concentration of 5 wt% for Ir(MDQ)$_2$acac.

Influence of the Thickness of the Ir(MDQ)$_2$acac layer

By reducing the thickness of the Ir(MDQ)$_2$acac layer, it is possible to reduce driving voltages, which results in increased luminous efficacies. However, a thin layer can at the same time result in a loss of triplet excitons. Here, the thickness of the Ir(MDQ)$_2$acac doped part of the 4P-NPD is varied in the range of 5…20 nm. The red emitter concentration is 5 wt% and the thickness of the pure 4P-NPD layer is 5 nm. The corresponding spectra are plotted in Figure 5.22. The spectral shape is independent of the thickness of the Ir(MDQ)$_2$acac layer. The conclusion is that already at a thickness of 5 nm all triplets which reach the mixed layer are transferred to the red emitter. As expected, luminous efficacies are slightly increasing for decreasing thickness. Due to the high hole mobility in 4P-NPD, this effect is rather weak. Further reduction of the layer thickness will not result in closed layers. Therefore, 5 nm is the minimum required layer thickness.

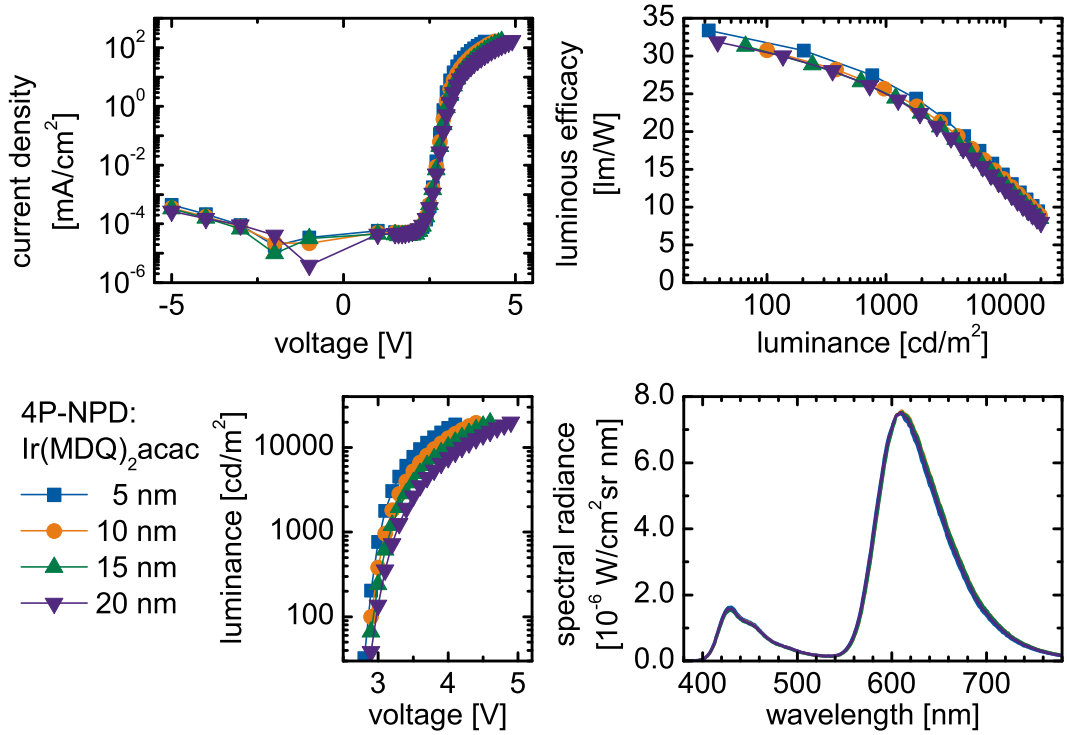

Figure 5.22: *Current-voltage and luminance-voltage characteristic, luminous efficacy, and emission spectrum depending on the thickness of the Ir(MDQ)$_2$acac doped layer. The luminous efficacies are determined by goniometer measurements. The shape of the spectrum does not change, but the driving voltage decreases with the thickness of the emission layer. Therefore, the highest luminous efficacy is achieved with a thickness of 5 nm.*

Influence of the Thickness of the 4P-NPD layer

Adjusting the thickness of the pure 4P-NPD layer is related with a trade off between efficient triplet transfer and low singlet transfer to the red emitter. The dependence of the excitation distribution on this layer thickness is investigated in steps of 3 nm starting from 5 nm. The other parameters are chosen according to the results of the previous paragraphs. The thickness of the $Ir(MDQ)_2acac$ layer is 5 nm and the emitter concentration is 5 wt%. As mentioned above, the total cavity length is constant and red emission is at a constant position inside the cavity. Because singlets recombine close to the interface between BPhen and 4P-NPD, the position of blue emission will change inside the cavity. Therefore, it is impossible to derive a statement about the exciton distribution directly from the shape of the external spectra (Figure 5.23), but it has to be deduced from optical simulations.

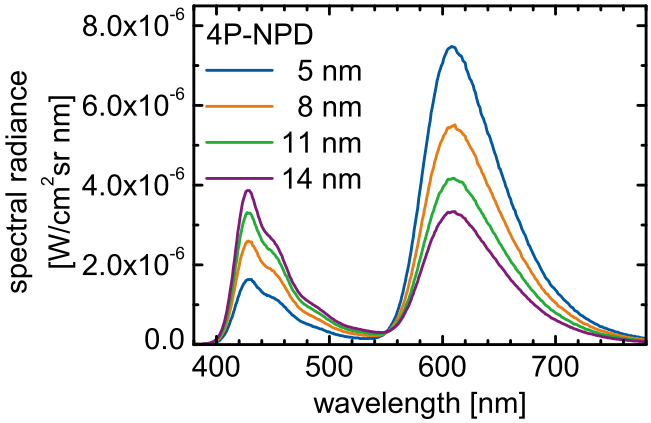

Figure 5.23: *Spectra of triplet harvesting OLEDs with different diffusion path length. Measurement is done at a constant current density of $j = 7.7$ mA/cm^2. With decreasing diffusion path length, red emission increases. The internal excitation distribution can be derived according to Section 4.4.2 and is presented in Table 5.8.*

By applying the method which was introduced in Section 4.4.2, internal excitation distribution and maximum quantum efficiencies can be calculated. The results of these calculations are summarised in Table 5.8. For a layer thickness of 5 nm, the ratio between emitting singlets and triplets is close to the ideal value of 3 : 1. If triplet-harvesting is taking place, the internal quantum efficiency can reach 100 %. The maximum of the external quantum efficiency of this device according to the calculation presented in Section 4.4.2 can roughly be estimated to be $\eta_q \approx 18$ %. Figure 5.24 demonstrates that this value is almost reached for low brightness. Hence, only an insignificant part of the singlets is transferred to the red emitter and the decreasing blue peak is induced by the

above mentioned change of optics for blue emission (Figure 5.23). Due to a small roll-off, the external quantum efficiency decreases to a value of $\eta_q = 16$ % at 1000 cd/m^2. These values are determined by a goniometer measurement.

d_{4P-NPD} [nm]	red [%]	blue [%]	$\eta_{int,noTH}$ [%]	$\eta_{int,TH}$ [%]
14	50.9	49.1	40.4	50.9
11	57.4	42.6	43.9	58.7
8	65.6	34.4	49.2	72.6
5	78.0	22.0	60.3	100.0

Table 5.8: *Internal excitation distribution corresponding to the spectra presented in Figure 5.23. The maximum internal quantum efficiency with and without the effects of triplet harvesting is calculated by the use of the method introduced in Section 4.4.2. For a layer thickness of the pure 4P-NPD of* 5 *nm, the ratio between emitting triplets and singlets is close to the triplet harvesting optimum of* 3 : 1 *and an internal quantum efficiency of* 100 % *is possible.*

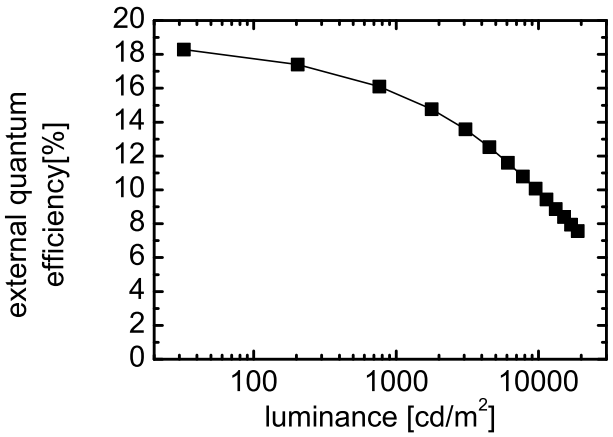

Figure 5.24: *External quantum efficiency against luminance for the best triplet-harvesting OLED. The external quantum efficiencies are determined by a goniometer measurement. The stack is presented in Table 5.7. The Ir(MDQ)$_2$acac concentration is* 5 *wt%. The thickness of the Ir(MDQ)$_2$acac and the thickness of the pure 4P-NPD layer are both* 5 *nm.*

This OLED is the final result of the optimisation process. Besides highly efficient triplet harvesting, this device comprises good colour stability with respect to different driving conditions. This can be explained by a strong pinning of the exciton generation zone to the interface between emission and hole blocking layer, caused by the difference between hole and electron mobility (Section 5.1.2). This pinning of the exciton gen-

eration to the interface results in a constant diffusion path length for different driving voltages and high colour stability is achieved (Figure 5.25).

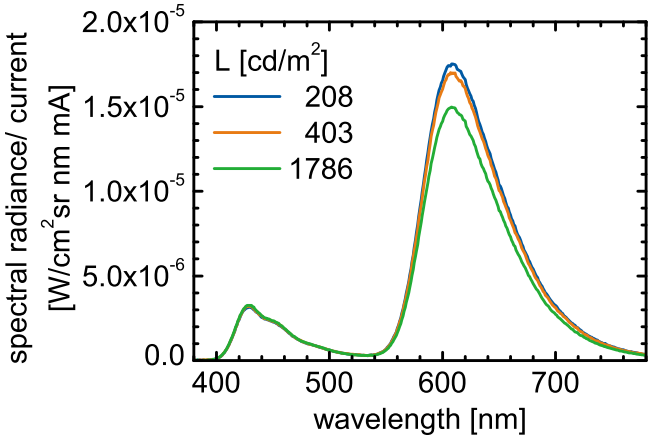

Figure 5.25: *Spectrum of the optimised triplet-harvesting OLED at different brightness values. The spectra are divided by the driving current and describe a spectral efficacy. The stack is presented in Table 5.7. The Ir(MDQ)$_2$acac concentration is 5 wt%. The thickness of the Ir(MDQ)$_2$acac and the thickness of the pure 4P-NPD layer are both 5 nm.*

5.3 Electroluminescence of Different Phosphorescent Materials in a Single Layer

In this section the combination of different phosphorescent emitters in a common matrix material is investigated. It will be shown in detail, how to achieve well balanced emission from both emitters at the same time and increase the overall efficiency by adjusting the doping concentrations.

Minimising the number of layers can highly contribute to reduce the production costs of a future product. Regarding three-colour hybrid white OLEDs, it should be possible to simplify the OLED architecture by combining both phosphorescent emitters in a single layer. The production costs of stacked OLEDs would be reduced as well, if it were possible to combine more than one emitter in a single unit in a colour stable and reproducible way. In Section 5.5 it will be shown, that a combination of the triplet harvesting OLED from Section 5.2.3 and the OLEDs from the present section in a stacked OLED will result in highly efficient white light-emitting OLEDs.

Several points have to be addressed concerning the combination of two different phosphorescent emitters in a single layer. How does the excitation of two different emitters in triple blend layers happen? Is it possible to distinguish between direct charge carrier recombination on the emitter molecules and recombination on the matrix with subsequent exciton transfer to the dopants? Which are the proper parameters for adjusting the emission to desired colour coordinates? Is it possible to reach desired colour coordinates without compromising on efficiencies?

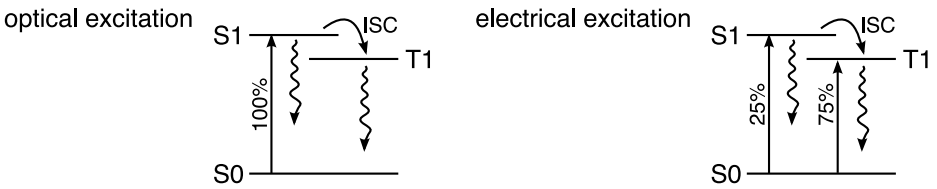

Figure 5.26: *The sketch illustrates the difference between photo- and electroluminescence concerning the generation of singlet and triplet excitons. By optical excitation, only singlets are generated and triplet states are excited by intersystem crossing. In case of electrical excitation only one quarter of the generated excitons are singlets.*

These questions have to be addressed by experiments with electroluminescent devices rather than photoluminescence measurements on thin films. This is due to several reasons. The main difference between photoluminescence and electroluminescence is the

ratio between generated singlets and triplets (Figure 5.26). Due to spin statistics this ratio is fixed to one to three in electroluminescent devices. This is in contrast to optical excited thin films, where only singlets are generated. Another point is the increased generation of excitons directly on the emitter molecules at high doping concentrations. This leads to an excitation distribution among the involved materials which strongly differs from the one achieved by optical excitation. In the latter case, the materials are excited according to their absorbance at the excitation wavelength.

5.3.1 Combination of Highly Efficient Emitters

In the following, the energy transfer from the green emitter $Ir(ppy)_3$ to the red emitter $Ir(MDQ)_2acac$ will be investigated. Both materials are well known phosphorescent emitters with a photoluminescence yield close to unity [14, 112]. If this transfer is lossless, this material combination has the potential of emitting any spectrum being a combination of the emission of both emitters with an internal quantum efficiency of 100 %.

All devices discussed in this section have the common stack presented in Table 5.9. The choice of matrix and blocker materials is based on a standard green single emission layer OLED. The emission layer is doped with an additional amount of the red emitter $Ir(MDQ)_2acac$. The influence of both emitter concentrations is discussed in the following paragraphs. The thickness of the transport layers is optimised for emission in the yellow wavelength region. Hence, it is ensured that the light of both emitters is almost equally coupled out of the OLED. For this purpose the emission affinity of the stack was calculated beforehand (see Figure 5.27). This quantity describes the amount of light which is coupled out of the device depending on the wavelength.

Material	d [nm]
Glass substrate	
ITO	90
NHT5: NDP-2	25: (4 wt%)
Spiro-TAD	10
TCTA: $Ir(ppy)_3$: $Ir(MDQ)_2acac$	20: (X wt%): (Y wt%)
TPBi	10
BPhen:Cs	55
Al	100

Table 5.9: *Common structure of the devices investigated in this section. The emitter concentrations are varied, in order to clarify their influence on the device characteristics, especially on the excitation distribution between both emitters.*

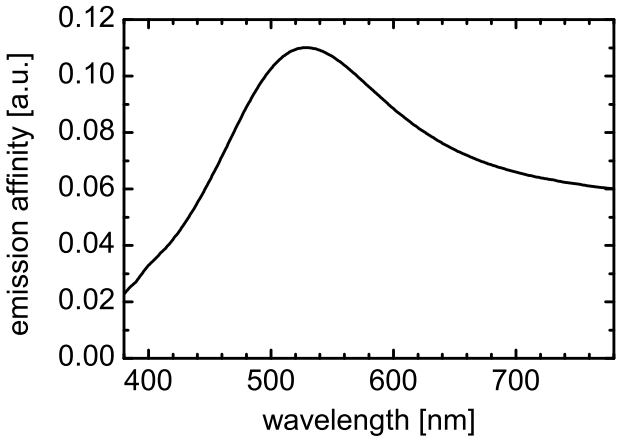

Figure 5.27: *Simulated emission affinity for OLEDs as presented in Table 5.9, with the light generation at the interface between emission and hole blocking layer.*

Variation of the Ir(ppy)$_3$ Concentration

In this paragraph the influence of the Ir(ppy)$_3$ concentration on the device performance is discussed. While the Ir(ppy)$_3$ concentration is varied, the Ir(MDQ)$_2$acac concentration is kept constant at a low value of 0.5 wt%, to reduce the effects of Ir(MDQ)$_2$acac on the electrical device properties.

The emission of Ir(MDQ)$_2$acac decreases with decreasing Ir(ppy)$_3$ concentration (Figure 5.28). Due to the low concentration of the red emitter, direct recombination of charge carriers on the Ir(MDQ)$_2$acac is unlikely. In the presence of higher concentrations of Ir(ppy)$_3$, a part of the charge transport takes place on the green emitter molecules. This assumption is backed by higher current densities for higher values of Ir(ppy)$_3$ concentration (Figure 5.30). Considering the position of the HOMO levels of the electron blocking layer Spiro-TAD (-5.4 eV [4]), the matrix TCTA (-5.9 eV [81]) and the emitter Ir(ppy)$_3$ (-5.1 eV [113]), one can conclude that direct hole injection to the Ir(ppy)$_3$ is energetically favourable. This was confirmed by measuring the concentration dependence of the current density in hole only devices [105]. Thus the excitons are formed on the Ir(ppy)$_3$ and transferred to the red emitter. As illustrated in Figure 5.29, this excitation path is lost for low Ir(ppy)$_3$ concentrations and red emission decreases.

In conclusion, efficiencies benefit from higher Ir(ppy)$_3$ concentrations. Best results are achieved with the established value of 8 wt% [13, 17, 114]. The efficiencies (up to $\eta_q =$

[4] UPS-measurement done by Selina Olthof at the IAPP in 2009

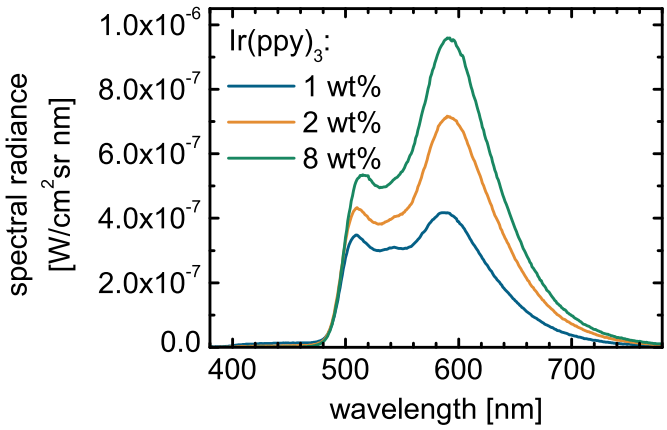

Figure 5.28: *Spectra of OLEDs with a stack according to Table 5.9. The $Ir(ppy)_3$ concentration is varied between 1 and 8 wt%, while the $Ir(MDQ)_2acac$ concentration is kept constant at 0.5 wt%. At this time, the measurement system was not able to measure different spectra at the same current. Therefore, all spectra are scaled to the measured radiant intensity at $j = 1$ mA/cm^2 afterwards. The excitons are formed on the $Ir(ppy)_3$ and transferred to the red emitter. This excitation path is lost for low $Ir(ppy)_3$ concentrations and red emission decreases (Figure 5.29).*

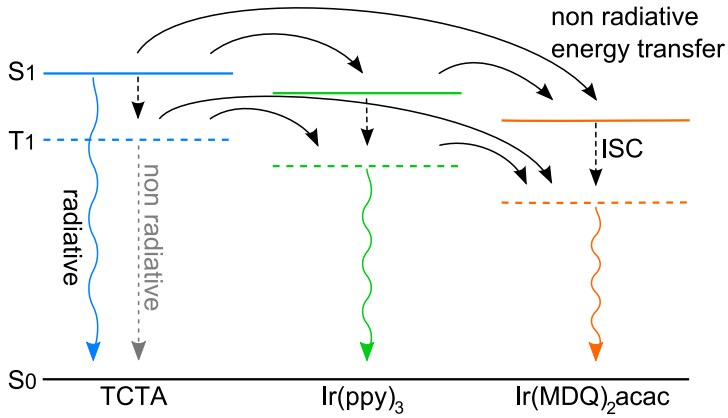

Figure 5.29: *Schematic representation of the excitation of $Ir(MDQ)_2acac$ doped into an emission layer consisting of a mixture of TCTA and $Ir(ppy)_3$. Due to its low concentration, direct recombination on $Ir(MDQ)_2acac$ is less likely. With decreasing $Ir(ppy)_3$ concentration the important excitation path via these molecules breaks down.*

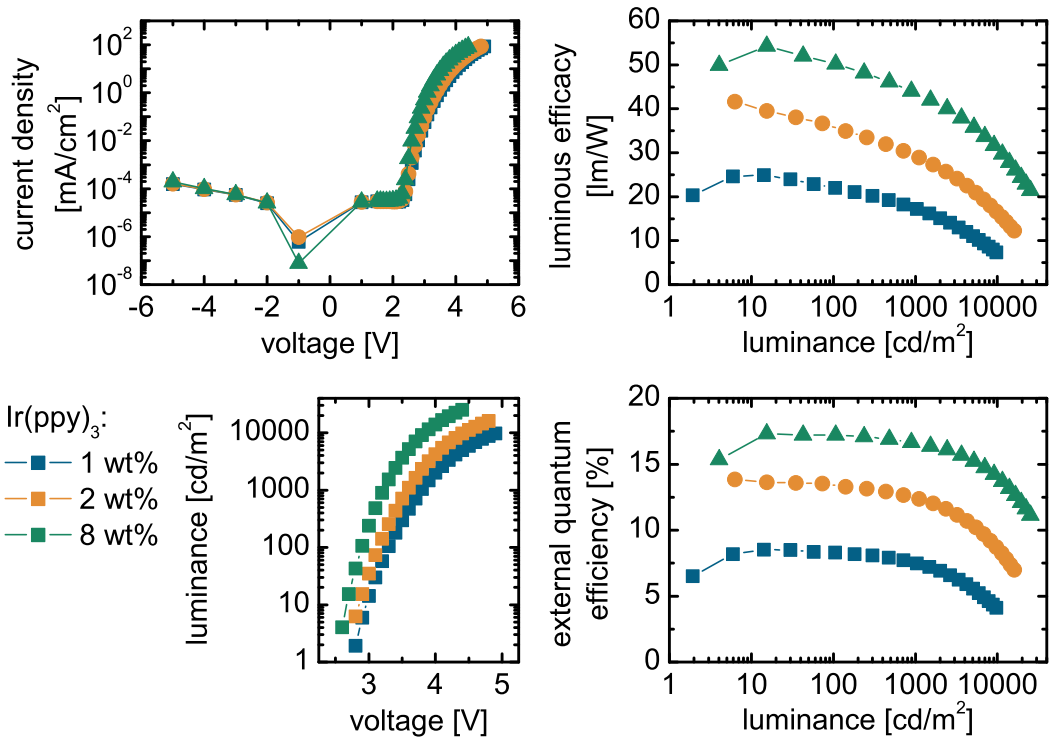

Figure 5.30: *Most important characteristics of the OLEDs discussed in this paragraph. The stack is the same as presented in Table 5.9. While the Ir(ppy)$_3$ concentration is varied, the Ir(MDQ)$_2$acac concentration is kept constant at 0.5 wt%. The current dependence reveals the strong contribution of the Ir(ppy)$_3$ molecules to the charge transport. Efficiencies decrease with the Ir(ppy)$_3$ concentration, because fewer excitons are formed directly on the emitter and the transfer of excitons to the emitter becomes less likely.*

16.5 % and $\eta_v = 43$ lm/W at 1000 cd/m^2; see Figure 5.30), reached with this OLED design, exceed the efficiencies of normal single emission layer green OLEDs and are comparable to those of the more sophisticated double emission layer OLEDs [13]. This is a hint for Ir(MDQ)$_2$acac having a positive influence on the charge carrier balance, despite its low concentration.

Variation of the Ir(MDQ)$_2$acac Concentration

Another parameter influencing the shape of the emitted spectrum is the concentration of the red emitter. Its influence will be investigated in this paragraph. For the following experiments, the Ir(ppy)$_3$ concentration is kept constant at 8 wt%, which is the optimum value derived in the previous paragraph. Figure 5.31 demonstrates the influence

of the Ir(MDQ)$_2$acac concentration on the emitted spectrum. As one would expect, red emission increases with increasing Ir(MDQ)$_2$acac concentration. While the spectral shape strongly changes, the external quantum efficiencies stay almost constant at 16.5 % (Figure 5.32). It is evident that the energy transfer between both emitters is very efficient and not attached to significant loss mechanisms.

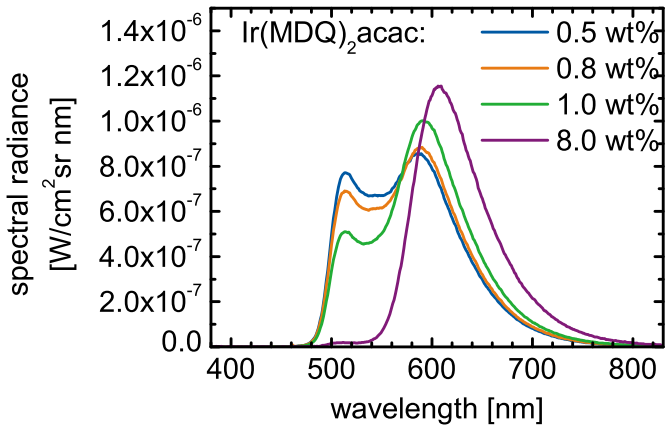

Figure 5.31: *Spectra of OLEDs with a stack according to Table 5.9. The Ir(MDQ)$_2$acac concentration is varied between* 0.5 *and* 8 *wt%, while the Ir(ppy)$_3$ concentration is kept constant at* 8 *wt%. At this time, the measurement system was not able to measure different spectra at the same current. Therefore, all spectra are scaled to the measured radiant intensity at* $j = 1$ *mA/cm^2 afterwards.*

The influence of the Ir(MDQ)$_2$acac concentration on the current-voltage dependence is not very strong, but the presence of the red emitter has some positive influence on the device performance. As already mentioned above, the devices perform better due to enhanced charge carrier balance, compared with standard green single emission layer OLEDs. Another striking feature is the weak roll off of the external quantum efficiency, which is attributed to suppressed triplet-triplet annihilation as a result of a broadened charge carrier recombination zone.

Because both emitters are homogeneously distributed in the emission layer, the spectral shape is independent of the spatial position of the recombination of the charge carriers. Therefore, high colour stability against changes in driving conditions is typical for all OLEDs in this section. This is shown by an example device with an Ir(MDQ)$_2$acac concentration of 1 wt% in Figure 5.33, which presents the normalised spectra of this OLED at different luminance. The slight spectral changes result in a very low shift of the corresponding CIE-coordinates from $(0.484, 0.491)$ at 100 cd/m^2 to $(0.489, 0.487)$ at 1 000 cd/m^2.

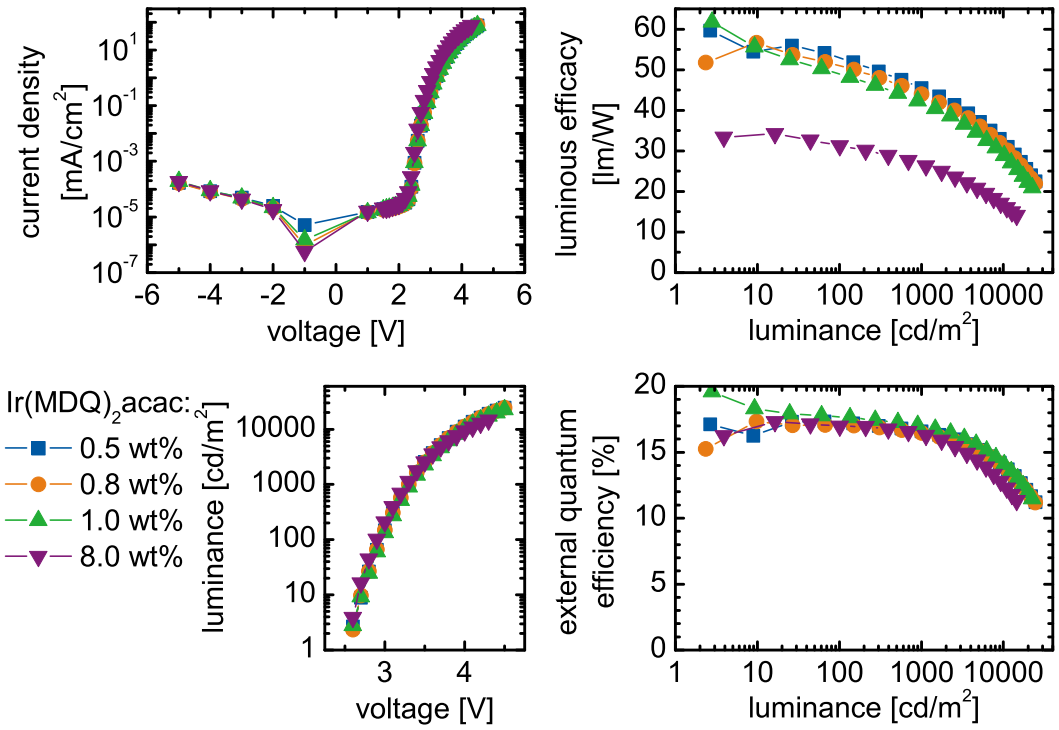

Figure 5.32: *Most important characteristics of the OLEDs discussed in this paragraph. The stack is the same as presented in Table 5.9 with a constant Ir(ppy)$_3$ concentration of 8 wt%. The external quantum efficiency is almost independent of the red emitter concentration and features a very low roll off.*

For OLEDs comprising two different phosphorescent emitters in a single emission layer one can summarise as follows: In order to optimise an OLED for emission at a specific colour point, in a first step one should fix the concentration of the emitter with the larger triplet gap to a value, which ensures good energy transfer to the emitter, but which is low enough to avoid quenching effects between the single emitter molecules. In the discussed system this is a concentration of 8 wt% for Ir(ppy)$_3$. In the next step the concentration of the emitter with the lower triplet gap can be varied until the desired spectrum is achieved, because no loss in the quantum efficiency is expected. In case of Ir(MDQ)$_2$acac, a concentration of 8 wt% is sufficient to transfer almost all excitons to the red emitter, whereas balanced emission of both emitters can be achieved with an Ir(MDQ)$_2$acac concentration of 0.5 wt%.

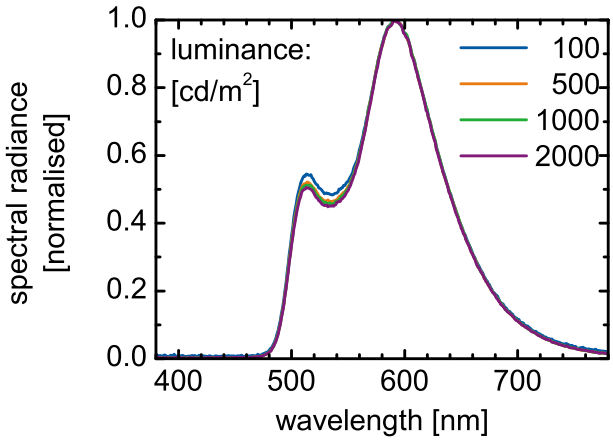

Figure 5.33: *Spectra measured at different brightness values. The $Ir(ppy)_3$ and the $Ir(MDQ)_2acac$ concentration are 8 wt% and 1 wt%, respectively. The spectral shape is almost independent of the driving conditions.*

5.3.2 Combination of a Highly with a Less Efficient Emitter

$Ir(dhfpy)_2acac$ is a yellow phosphorescent emitter, which features a photoluminescence spectrum with the maximum at 557 nm (Section 3.2.4). Hence, it is not suitable as green emitter in three-colour white OLEDs. However, its emission fills the gap between $Ir(ppy)_3$ and $Ir(MDQ)_2acac$. It is obvious that combining a three-colour device with $Ir(dhfpy)_2acac$ will lead to an increased CRI. Because the spectrum of this emitter fits very well to the maximum of the V_λ function, this will lead additionally to an increase of the luminous efficacy. However, a decreased quantum efficiency in comparison with $Ir(MDQ)_2acac$ was observed [105]. Given that only a small contribution of this emitter is required in a four-colour white OLED, a small loss of quantum efficiency might be acceptable. Whether $Ir(dhfpy)_2acac$ is still suitable for application in white OLEDs will be discussed in the following paragraphs.

Influence of the $Ir(dhfpy)_2acac$ Concentration

The experiments in this section are based on a stack similar to that examined in section 5.3.1 (For details see Table 5.10). The concentration of $Ir(ppy)_3$ is fixed to 8 wt% and the cavity length is adjusted to enhance the outcoupling of $Ir(dhfpy)_2acac$ emission. Due to the lower yield of $Ir(dhfpy)_2acac$, a decrease of external quantum efficiency is expected in comparison with a device with only $Ir(ppy)_3$ doped into the emission layer. However, the external quantum efficiencies strongly increase instead, because of a positive influence of the $Ir(dhfpy)_2acac$ molecules on the charge carrier balance. As shown in Figure 5.34, the external quantum efficiencies increase from 12 % to 16 % (at 1 000 cd/m^2) by mixing a low concentration of 0.1 wt% $Ir(dhfpy)_2acac$ into the emission layer. The external quantum efficiency rises further to 16.5 %, when the concentration is increased to 0.5 wt%, and drops again for higher values.

Figure 5.35 illustrates that this efficiency increase is not due to a higher yield of the yellow emission, but rather an increase of the green $Ir(ppy)_3$ emission. As mentioned above, the primarily hole conduction of a TCTA layer is even more pronounced in the presence of $Ir(ppy)_3$. Hence, an improvement of the charge carrier balance could be achieved by enhanced electron injection. However, the low concentrations do not allow an additional electron transport channel on the $Ir(dhfpy)_2acac$ molecules. This is supported by the fact that the current voltage dependence does not increase with the concentration of the yellow emitter (Figure 5.34). One can conclude that the improved charge carrier balance is based on an interference of the hole transport by $Ir(dhfpy)_2acac$.

Material	d [nm]
Glass substrate	
ITO	90
MeO-TPD: NDP-2	50: (2 wt%)
Spiro-TAD	10
TCTA: $Ir(ppy)_3$: $Ir(dhfpy)_2acac$	10: (8 wt%): (X wt%)
TPBi	10
BPhen:Cs	50
Al	100

Table 5.10: *Common structure of the devices investigated in this section. The yield of $Ir(dhfpy)_2acac$ is considerably lower than that of $Ir(MDQ)_2acac$. The concentration of $Ir(dhfpy)_2acac$ is varied, in order to estimate the strength of loss mechanisms induced thereby in such a mixed layer.*

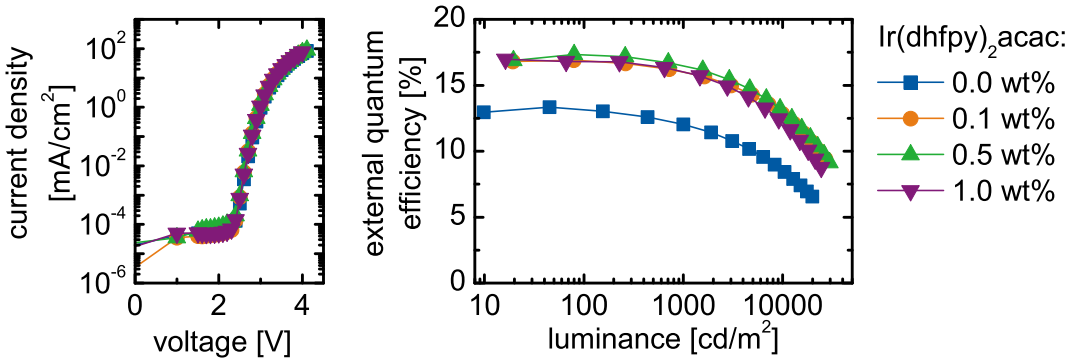

Figure 5.34: *Influence of the $Ir(dhfpy)_2acac$ concentration on the device characteristics. The external quantum efficiencies are determined by goniometer measurement. The corresponding stack is presented in Table 5.10. Although the influence on the current voltage dependence is very weak, the effect on the charge carrier balance is not neglectable as indicated by the strong increase of the external quantum efficiencies in the presence of $Ir(dhfpy)_2acac$.*

Comparison to $Ir(MDQ)_2acac$ Containing Devices

A comparison to the $Ir(MDQ)_2acac$ containing samples of section 5.3.1 will provide a deeper inside into the strength of the loss mechanisms induced by $Ir(dhfpy)_2acac$. Here, three OLEDs with an $Ir(ppy)_3$ concentration of 8 wt% are compared. The focus is on a pure $Ir(ppy)_3$ and an $Ir(dhfpy)_2acac$ (1 wt%) doped OLED. Additionally, an

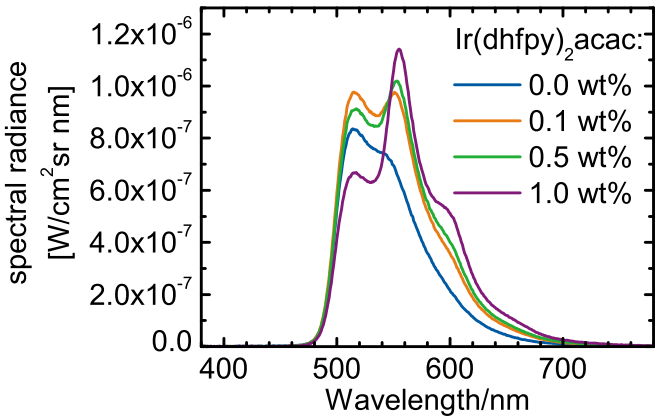

Figure 5.35: *Electroluminescence spectra of OLEDs based on the stack presented in Table 5.10. All spectra are measured at the same current density of $j = 0.77$ mA/cm^2. At first, Ir(ppy)$_3$ emission increases with Ir(dhfpy)$_2$acac concentration due to improved charge carrier balance and than decreases as more excitons are transferred to the yellow emitter.*

Ir(MDQ)$_2$acac OLED based on the stack presented in Table 5.9 is taken into account. Ir(dhfpy)$_2$acac as well as Ir(MDQ)$_2$acac positively affect the charge carrier balance. In case of Ir(MDQ)$_2$acac, the external quantum efficiency at 1 000 cd/m^2 is increased from 12 % to 17 % in comparison with the pure Ir(ppy)$_3$ device (Figure 5.36). Due to the lower yield of Ir(dhfpy)$_2$acac this gain is less pronounced for the corresponding device and results in an external quantum efficiency of 16 %. Despite the decreased external quantum efficiency, the Ir(dhfpy)$_2$acac OLED is characterised by a luminous efficacy at 1000 cd/m^2 of 58 lm/W, which is a strong gain compared with the 42 lm/W of the Ir(MDQ)$_2$acac device. The slightly higher driving voltage in case of the Ir(MDQ)$_2$acac OLED is caused by the thicker emission layer of this device. However, this is not the reason for the strong difference in the luminous efficacy. Assuming the same current voltage characteristics for the Ir(MDQ)$_2$acac as for the Ir(dhfpy)$_2$acac OLED, the luminous efficacy would only increase to 45 lm/W[5].

By plotting the spectra of these OLEDs together with the V_λ function (as done in Figure 5.37), it becomes clear that the increase of the luminous efficacy in case of the Ir(dhfpy)$_2$acac is due to its better position with respect to the sensitivity of the human eye. The results in this section strongly endorse the application of Ir(dhfpy)$_2$acac in white OLEDs, because an increase of the luminous efficacy is possible without shifting

[5]Which is shown by the following calculation: The Ir(MDQ)$_2$acac device reaches a luminance of 1 000 cd/m^2 at a current density of 2.27 mA/cm^2. For this current density a voltage of 3.31 V needs to be applied. The Ir(dhfpy)$_2$acac device reaches the same current density at a voltage of 3.08 V. The corrected luminous efficacy follows as: $\eta_{v,\text{corrected}} = \eta_v \cdot U_{\text{measured}}/U_{\text{assumed}} = 42\ \text{lm/W} \cdot 3.31\ \text{V}/3.08\ \text{V} \simeq 45\ \text{lm/W}$.

the colour point into the green region.

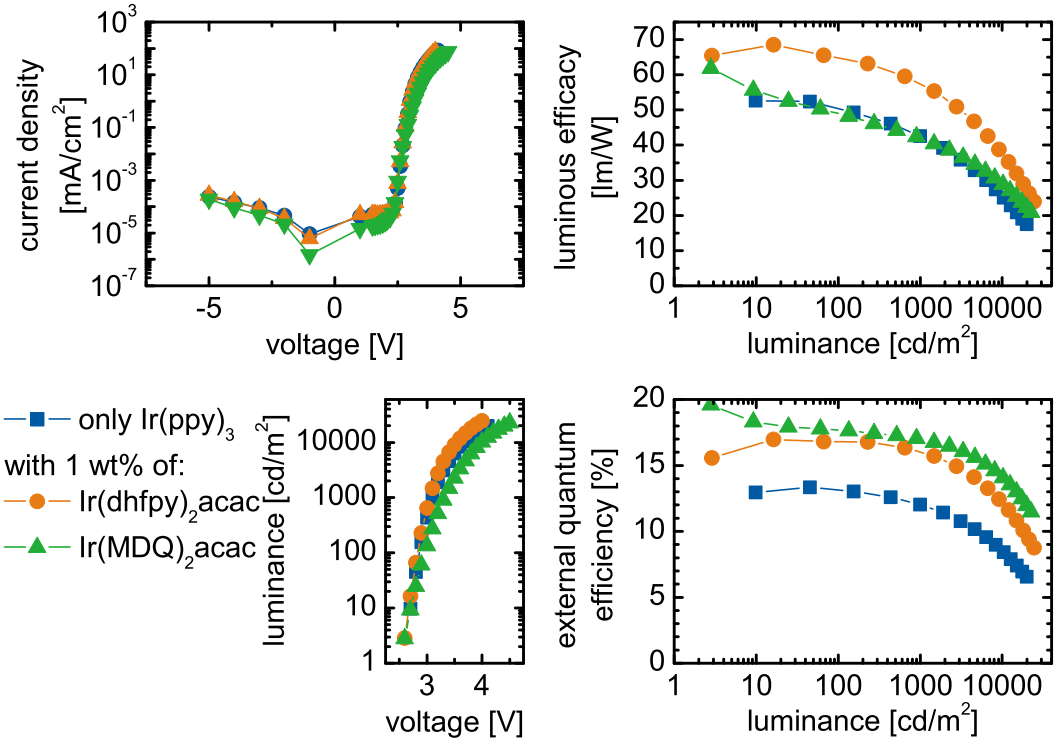

Figure 5.36: *Comparison of $Ir(ppy)_3$ OLEDs with and without additional phosphorescent emitters mixed into the emission layer. $Ir(dhfpy)_2acac$ as well as $Ir(MDQ)_2acac$ affect the charge carrier balance positively. Although, the quantum efficiency of the $Ir(dhfpy)_2acac$ device is lower than that of $Ir(MDQ)_2acac$ device, the luminous efficacy is strongly increased.*

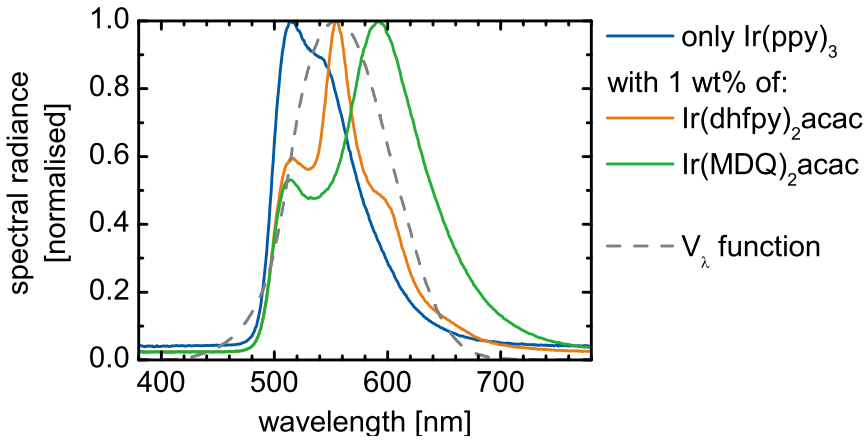

Figure 5.37: *Plot of the electroluminescence spectra of $Ir(ppy)_3$ OLEDs with and without additional phosphorescent emitters mixed into the emission layer together with the V_λ function.*

5.4 Single Emission Layer White OLED

In this section a white OLED is presented, which combines the emission of a fluorescent and two phosphorescent emitters in a single emission layer.

White OLEDs are typically composed of two or three emission layers, with different molecules in each layer contributing to emission in a broad wavelength region [24, 44]. In order to accelerate the production process of a white OLED, it is convenient to reduce the number of its layers. This can be achieved by combining all emitters in a single layer. For this purpose a stack is examined which is based on the experiments in the previous section, where the phosphorescent emitters $Ir(ppy)_3$ and $Ir(MDQ)_2acac$ were combined in a mixed emission layer. Here, the spectrum of this emission layer is extended by the emission of the fluorescent blue dopant TBPe (Table 5.11). In Section 5.3.1 an optimum value of 8 wt% was derived for the $Ir(ppy)_3$ concentration. At this concentration all excitons are transferred to the phosphorescent emitters and singlet emission is suppressed. With the intention to reduce the quenching of singlet emission, the concentration of the phosphorescent emitters is reduced to ≈ 1 wt%.

Material	d [nm]
Glass substrate	
ITO	90
MeO-TPD: F_4-TCNQ	25: (4 mol%)
Spiro-TAD	10
TCTA: TBPe: $Ir(ppy)_3$: $Ir(MDQ)_2acac$	20: (2.0 wt%): (1.2 wt%): (1.0 wt%)
TPBi	10
BPhen:Cs	55
Al	100

Table 5.11: *Architecture of a single emission layer white OLED. The combination of all emitter molecules in a single emission layer results in a very high colour stability against varying brightness.*

As for the OLEDs in the previous section, the homogeneous distribution of the different emitter molecules in the emission layer results in a high colour stability against varying brightness. The spectrum of this white OLED is almost independent of the luminance, which is emphasised by a very low shift of the corresponding colour coordinates from $(x,y) = (0.478, 0.463)$ at 357 cd/m^2 to $(x,y) = (0.477, 0.455)$ at 2 858 cd/m^2 (Figure 5.38). The correlated colour temperature is CCT $= 2\,800$ K and the colour rendering index is CRI $= 69$.

A major drawback of this device is its low external quantum efficiency of $\eta_q = 8$ % at 1 000 cd/m^2. Although the exact value of the triplet gap of TBPe is unknown, it

can be concluded from the low efficiency that triplet harvesting is not taking place. A fluorescent blue emitter with an energetically higher triplet gap has to be chosen. The triplet gap of 4P-NPD allows for triplet transfer to $Ir(MDQ)_2acac$ (Section 5.2.1). Hence, green triplets which are transferred to this emitter would be transferred to the red emitter afterwards. However, it was not possible to find an appropriate matrix material for 4P-NPD. Another problem of this approach is that it is hard to control the individual deposition rates of 4 different materials at the same time. The concentration of one emitter is equally influencing the emission of all other emitters. Therefore, the reproducibility of this stack is very low and an optimisation with regard to efficiency and a certain colour point is hardly possible.

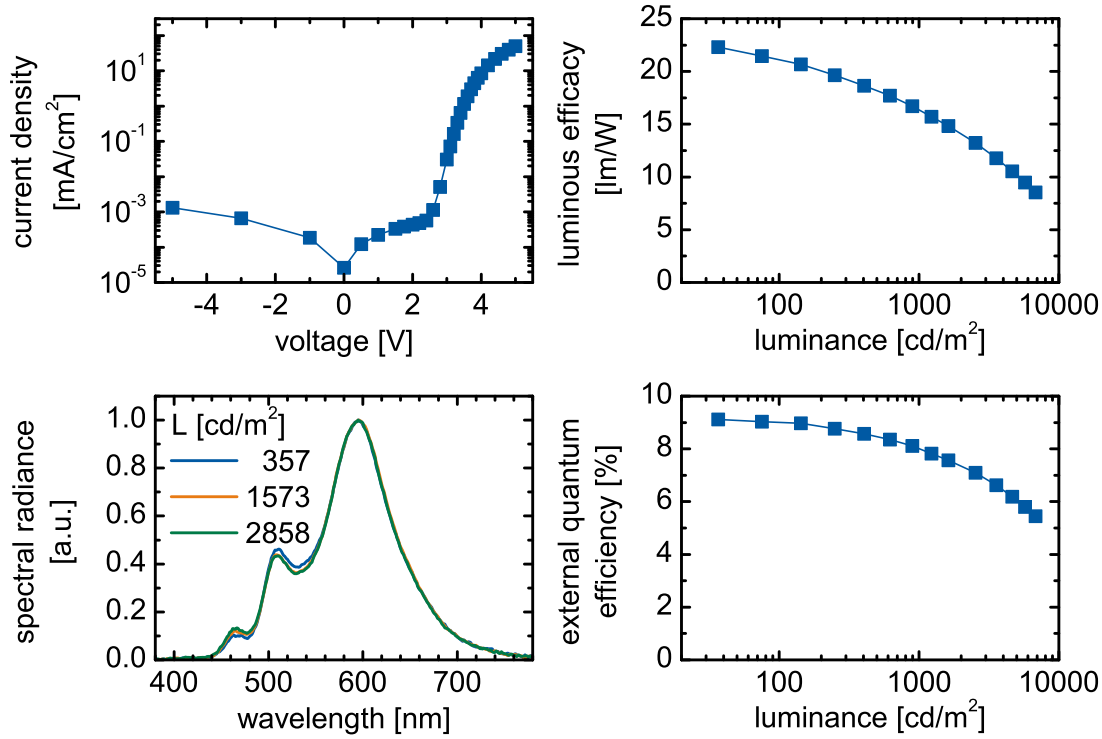

Figure 5.38: *Most important properties of a white OLED comprising three emitter materials in a single emission layer. The device is characterised by a very low colour shift from* $(x,y) = (0.478, 0.463)$ *at 357 cd/m*^{2} *to* $(x,y) = (0.477, 0.455)$ *at 2858 cd/m*^{2}*. However, low efficiencies and poor reproducibility are the major drawbacks of this device.*

5.5 Stacked OLEDs

The concept of stacked OLEDs is utilised to circumvent the limitations of triplet harvesting regarding the triplet transfer to phosphorescent green emitters. A fully phosphorescent unit comprising the emission of a yellow and a green emitter is stacked on top of a triplet harvesting OLED, which combines a fluorescent blue and a phosphorescent red emitter. An independent optimisation of the connecting charge generation layer, results in a strong decrease of the driving voltages. The efficiencies are further improved by the use of a substrate with enhanced refractive index and outcoupling enhancement by a macro extractor and a pyramid pattern.

In Section 5.2 the concept of triplet harvesting was introduced. By efficiently transferring otherwise lost triplets from the fluorescent to a phosphorescent emitter, internal quantum efficiencies up to 100 % are possible. For this purpose, the triplet state of the fluorescent emitter must be energetically higher than the triplet state of the corresponding phosphorescent emitter. Most fluorescent blue emitters do not satisfy this requirement for triplet transfer to phosphorescent green emitters. Therefore, white emission is usually achieved by direct recombination of a part of the excitons on the green emitter [23]. The disadvantage of this method is the loss of singlets which are needed for blue emission.

Another approach is the reduction of singlet-triplet splitting. This may result in fluorescent emitters allowing for triplet harvesting to green phosphorescent emitters, which, however, introduces another problem. By reducing the energetic difference between first excited singlet and triplet state, the inter system crossing rate is increased [64]. Although, the total efficiency in a triplet harvesting OLED may remain high, the blue emission is reduced.

A possibility to extend the spectrum of the blue/red triplet harvesting OLED in the green spectral region is the stacking of a second OLED on top of this device. The devices are sandwiched between anode and cathode and are connected by a charge generation layer, where pairs of electrons and holes are separated [46, 47]. It has been shown that this charge generation layer can be realised by a pn-junction formed by electrically doped layers [46]. Because of the strong band-bending, charges are separated at the interface between the hole and the electron conducting layer, when an electric field is applied. The resulting stack is electrically equivalent to a monolithic series connection of two independent OLEDs. Because external quantum efficiency and driving voltage of the individual units add up, the luminous efficacy of a stacked OLED is comparable to the single OLEDs.

The general advantages of stacked OLEDs are as follows. In the ideal case an additional

electron is generated at every charge generation layer for every injected one. Hence, the current density applied to reach a certain luminance is decreased proportional to the number of units stacked on top of each other. This reduction of the current density is an important feature for lighting applications, where devices with an large active area are needed. The usual current densities for luminances around 1 000 cd/m^2 would lead to currents of several Amperes. It is obvious, that the stacking of OLEDs does not completely solve this problem, but it helps to reduce the current densities. Because each unit is driven at reduced current density and reduced brightness, stacked OLEDs are characterised by prolonged lifetimes [115]. Another benefit is the gain of colour stability at varying brightness. In a conventional white OLED, a spatial shift of the recombination zone is often connected to a strong spectral change [116]. It is comprehensible that the electrical behaviour and the position of the recombination zone of each unit do not change, when they are combined to a stacked OLED. Therefore, a composition of several colour stable units will again result in a colour stable OLED. Hence, three or more emitters can be combined in a single OLED without putting much effort into the design of the OLED regarding a stable position of the exciton recombination zone.

5.5.1 Three Colour Stacked Devices

In a first experiment the blue/red triplet harvesting OLED from Section 5.2.3 is extended by an OLED comprising the phosphorescent green emitter Ir(ppy)$_3$. A pn-junction formed by a NDP-2 doped MeO-TPD layer and a Cs doped BPhen layer is used as charge generation layer. The complete architecture of this device is presented in Table 5.12.

The features of 4P-NPD (435 nm) and Ir(MDQ)$_2$acac (620 nm) as well as of Ir(ppy)$_3$ (510 nm) are present in the electroluminescence spectrum of this device (Figure 5.39). One can conclude that the materials applied in the pn-junction form a working charge generation layer. However, the green emission of this OLED is too strong. By simply surpressing the green emission, the overall efficiency of this device would strongly decrease. A possible way to reduce the green emission without a loss of efficiency is to transfer a part of the excitons to another emitter. As demonstrated in Section 5.3 efficient exciton transfer between different phosphorescent emitters can be achieved by coevaporation of two emitters in a common matrix material. The colour point of such devices can be chosen freely between both emitters. Here, 1 wt% of Ir(MDQ)$_2$acac is added to the phosphorescent unit. Hence, green emission is decreased and red emission increased. The thickness of each transport layer is adjusted to the new spectral shape (Table 5.12). However, this OLED is characterised by too intense red emission (Figure 5.39) and white colour coordinates might only be achieved for very low Ir(MDQ)$_2$acac concentrations. Because already a concentration of 1 wt% is very low,

Material	d [nm]
Glass substrate	
ITO	90
MeO-TPD: NDP-2	55/50: (2 wt%)
Spiro-TAD	10
4P-NPD: $Ir(MDQ)_2acac$	5: (5 wt%)
4P-NPD	5
BPhen	10
BPhen:Cs	90
MeO-TPD: NDP-2	80/75: (2 wt%)
Spiro-TAD	10
TCTA: $Ir(ppy)_3$: $Ir(MDQ)_2acac$	10: (8 wt%): (1 wt%)
TPBi: $Ir(ppy)_3$: $Ir(MDQ)_2acac$	10: (8 wt%): (1 wt%)
TPBi	10
BPhen:Cs	50/100
Al	100

Table 5.12: *Architectures of stacked OLEDs with an electrically doped pn-junction serving as charge generation layer. A first device was produced by stacking of a blue/red triplet harvesting and a green phosphorescent unit. By mixing an amount of* 1 *wt% of the red emitter into the emission layer of the phosphorescent unit (changes are highlighted with blue), a second device with enhanced red emission was produced.*

these devices will not be processable in a reproducible manner.

5.5.2 Four-Colour Stacked Devices

With the intention to reduce the green emission without enhancing the red emission, the red emitter is replaced by the yellow emitter $Ir(dhfpy)_2acac$ in the phosphorescent unit (Table 5.13). The emitter system of $Ir(ppy)_3$ and $Ir(dhfpy)_2acac$ was already introduced and examined in Section 5.3.2. In this section it was found that the luminous efficacy in case of $Ir(dhfpy)_2acac$ is strongly enhanced in comparison with Ir(MDQ)2acac, which was attributed to its beneficial position regarding the maximum of the V_λ function.

The spectral shape of the OLED with an $Ir(dhfpy)_2acac$ concentration of 1 wt% fits very well to the emission of the triplet harvesting OLED (Figure 5.40). The emission of the four different emitters aligns in a way that white colour coordinates $(x,y) = (0.489, 0.419)$ are achieved. The contribution of the $Ir(dhfpy)_2acac$ fills the spectral

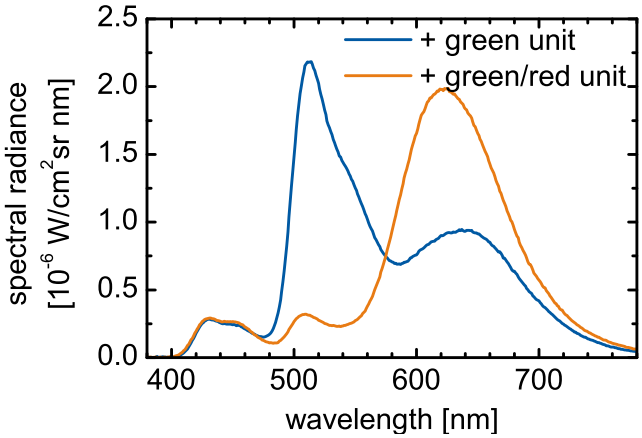

Figure 5.39: *Spectra of the stacked OLEDs as introduced in Table 5.12 measured at a constant current density of $j = 1.54$ mA/cm^2. An amount of 1 wt% Ir(MDQ)$_2$acac is mixed into the emission layer of the phosphorescent unit in order to decrease green emission and increase red emission. White colour coordinates may only be achieved for lower Ir(MDQ)$_2$acac concentrations.*

Material	d [nm]
Glass substrate	
ITO	90
MeO-TPD: NDP-2	35: (2 wt%)
Spiro-TAD	10
4P-NPD: Ir(MDQ)$_2$acac	5: (5 wt%)
4P-NPD	5
BPhen	10
BPhen:Cs	90
MeO-TPD: NDP-2	70: (2 wt%)
Spiro-TAD	10
TCTA: Ir(ppy)$_3$: Ir(dhfpy)$_2$acac	10: (8 wt%): (1 wt%)
TPBi	10
BPhen:Cs	60
Al	100

Table 5.13: *Architecture of a four-colour white stacked OLED. In comparison to the previous devices, the red emitter in the phosphorescent unit is replaced by the yellow emitter Ir(dhfpy)$_2$acac.*

gap between $Ir(ppy)_3$ and $Ir(MDQ)_2acac$.

Although only a CRI of 75.6 is reached by this device, a further optimisation of this stack may lead to an enhanced CRI in comparison with three-colour white OLEDs. A goniometer measurement reveals that the luminous efficacy $\eta_v = 27.6$ lm/W (at 1 000 cd/m^2) of this OLED is too low, which can be explained by the poor current voltage characteristics. In Figure 5.41 current density is plotted against voltage for the single units (as presented in Section 5.2.3 and Section 5.3.2) and the stacked OLED. The dotted line represents the calculated characteristics of a connection in series of the single OLEDs. At a current density of 1 mA/cm^2, the voltage of the stacked OLED $U(1\ \mathrm{mA/cm^2}) = 6.6$ V is increased by 0.7 V in comparison with the sum of the single units $U(1\ \mathrm{mA/cm^2}) = 5.9$ V. This voltage increase can be attributed to the charge generation layer. A way to improve the pn-junction is discussed in the next paragraph.

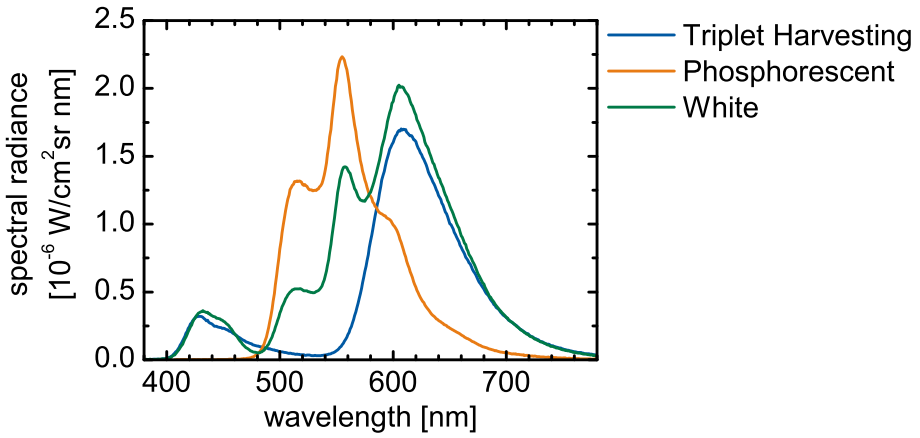

Figure 5.40: *Spectra of the single units and the stacked device. The emission of the four different emitters aligns very well to a spectrum with warm white colour coordinates* $(x,y) = (0.489, 0.419)$ *and a colour rendering index of* 75.6.

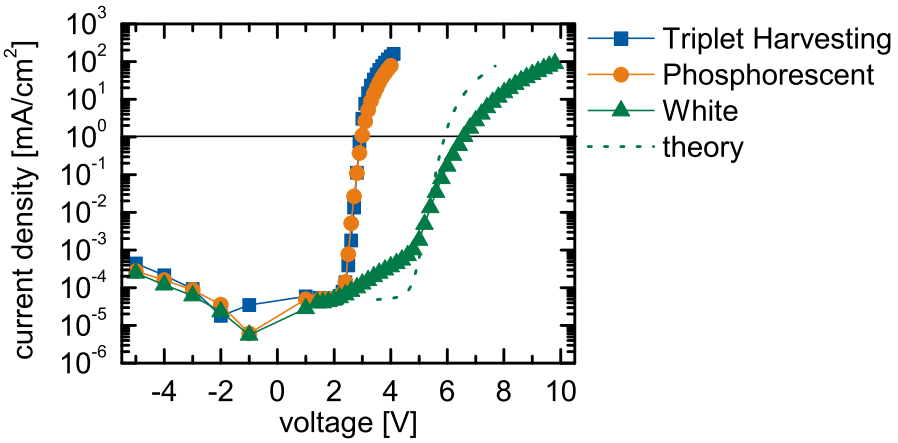

Figure 5.41: *Current-voltage characteristics of the stacked OLED and the individual units. At a current density of* 1 *mA/cm*^{2} *the voltage of the stacked OLED is increased by* 0.7 *V in comparison with the sum of the single units (dotted line). This voltage increase can be attributed to a malfunction of the charge generation layer.*

Improvement of the pn-Junction

It is known from tandem organic solar cells that the contact between p- and n-type doped layer will become quasi-ohmic if a very thin metal layer is sandwiched between those [117]. At a thickness of only a few Angstrom, the metal rather forms cluster-like shapes than continuous layers [118, 119]. These clusters affect the pn-junction in two ways. They hinder dopant diffusion and thereby the formation of a compensated region. On the other hand, gap states are introduced which assist the charge separation [117]. Here, aluminium is chosen, in order to keep the impact on the emitted spectrum as small as possible. Aluminium very likely hinders the Cs diffusion by the formation of [BPhen + Al]$^+$ and [2BPhen + Al]$^+$ complexes [120].

A series of simple test devices will exhibit the effect of aluminium on the characteristics of the above discussed pn-junction. The stack as well as a plot of current density against voltage is presented in Figure 5.42. The thickness variation starts at 0.5 nm, because lower values are not reproducible. The measurement reveals that already at this low thickness the current-voltage characteristics of the pn-junction are significantly improved. The voltage which is needed to reach a current density of $j = 1$ mA/cm^2 decreases by 1.1 V from 7.4 V to 6.3 V in the presence of aluminium.

The improved pn-junction is now employed in a stacked OLED (Table 5.14). The most important properties of this OLED are summarised in Figure 5.43. For better comparison, the measurement of the OLED from the previous section without the aluminium

Material	d [nm]
Glass substrate	
ITO	90
MeO-TPD: NDP-2	20: (2 wt%)
α-NPD	20
BPhen:Cs	20
Al	X
MeO-TPD: NDP-2	20: (2 wt%)
α-NPD	20
BPhen:Cs	20
Al	100

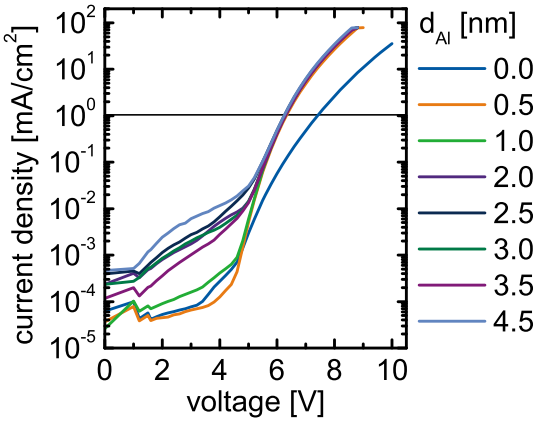

Figure 5.42: *Improvement of the current-voltage characteristics of the pn-junction. With the intention to improve the current voltage characteristics, a thin aluminium layer is inserted. Already at a thickness of* 0.5 *nm the voltage which is needed to reach a current density of* $j = 1$ *mA/cm*^{2} *is decreased by* 1.1 *V.*

interlayer is presented too. For the device with the aluminium clusters, the voltage for a current density of 1 mA/cm^2 decreases by 0.6 V from 6.6 V to 6.0V. This is almost the same voltage as calculated from the single OLEDs above, which is one cause for the improvement of the luminous efficacy from 27.6 lm/W to 33.0 lm/W at 1 000 cd/m^2. On the other hand, the OLED with the aluminium interlayer benefits from improved charge balance. Hence, the external quantum efficiency increases from 24 % to 26 % at 1 000 cd/m^2.

For a stacked OLED a value around 40 % would have been expected. To understand this discrepancy, thin film optics have to be taken into account. Here, four emitters are combined in a common cavity. Although there is some freedom concerning the choice of the position of the emission zones inside the cavity, the total cavity length is the same for all emitters. Hence, it is not possible to optimise the optics of this OLED to all emitters at the same time. A more detailed explanation is given in Section 4.4.2.

Material	d [nm]
Glass substrate	
ITO	90
MeO-TPD: NDP-2	45: (2 wt%)
Spiro-TAD	10
4P-NPD: $Ir(MDQ)_2acac$	5: (5 wt%)
4P-NPD	5
BPhen	10
BPhen:Cs	90
Al	0.5
MeO-TPD: NDP-2	85: (2 wt%)
Spiro-TAD	10
TCTA: $Ir(ppy)_3$: $Ir(dhfpy)_2acac$	10: (8 wt%): (1 wt%)
TPBi	10
BPhen:Cs	60
Al	100

Table 5.14: *Application of the improved pn-junction in the four-colour white stacked OLED. Because the aluminium in the pn-junction does not form a closed layer, it should have weak influence on the optics of the OLED.*

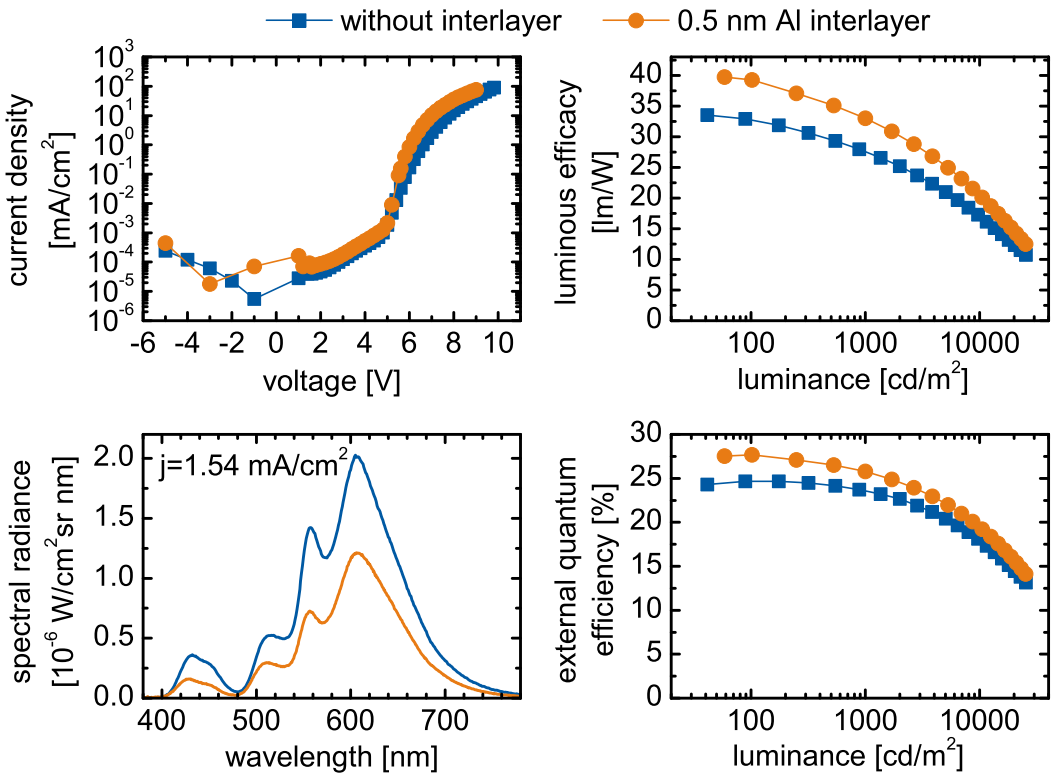

Figure 5.43: *Properties of white OLEDs with and without additional aluminium interlayer. Spectra are measured in forward direction and efficiencies are determined by goniometer measurement. Driving voltage as well as luminous efficacy and external quantum efficiency are significantly improved by the aluminium layer.*

Transfer to High-Refractive-Index Substrates

By replacing the standard glass substrate with a substrate with enhanced refractive index, the mismatch between the refractive indices of ITO and glass is decreased (Figure 5.44). Thus, more light is coupled into the substrate. By optimising the cavity for glass modes and an intelligent choice of an outcoupling structure, the light extraction can be notably improved. This can be visualised by means of the critical angles of total reflection at the boundary between ITO and glass. For instance, the critical angle of total reflection of green light with a wavelength of 510 nm (corresponds to $Ir(ppy)_3$ emission) changes according to Snell's law from $\vartheta = 50.0\,^\circ$ to $\vartheta = 64.6\,^\circ$ if the refractive index of the substrate changes from $n_d = 1.51$ to $n_d = 1.78$ (Figure 5.44).

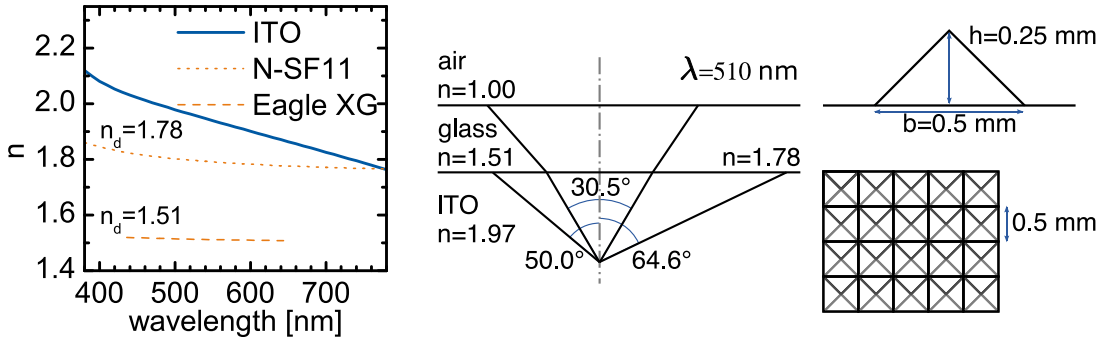

Figure 5.44: *Left: Refractive index of ITO, standard glass (*Corning Inc.*: Eagle XG), and high-refractive index glass (*SCHOTT AG*: N-SF11). By the use of high-refractive index glass the mismatch between the refractive index of ITO and glass can be reduced. Middle: The critical angles for the coupling of green light from ITO to glass and to air. In case of high-refractive-index glass significantly more light can be coupled into the substrate. Right: A scalable pattern of square pyramids which is applied to enhance the extraction of light trapped inside the glass.*

The influence of the substrate on the emission of an OLED is illustrated by a simulation (Section 4.4) of a green OLED on standard glass and high-refractive-index glass. The following stack is used for the calculation: 1 mm Substrate/ 90 nm ITO/ 25 nm MeO-TPD: F_4-TCNQ (2 wt%)/ 10 nm S-TAD/ 20 nm TCTA:$Ir(ppy)_3$/ 10 nm TPBi/ 40 nm n-BPhen/ 100 nm Ag. The emission is assumed to take place with an internal efficiency of 100 % at the interface between TCTA and TPBi.

The influence of the cavity is reduced if the refractive index of the substrate is increased from $n_d = 1.51$ to $n_d = 1.78$. This reduction is revealed by a change in the emission affinity in forward direction (Figure 5.45). In case of the high-refractive-index glass, the emission affinity is less selective with regard to the wavelength of the emitted light.

This is very convenient, if the light extraction of three or more emitters is necessary as it is in white OLEDs.

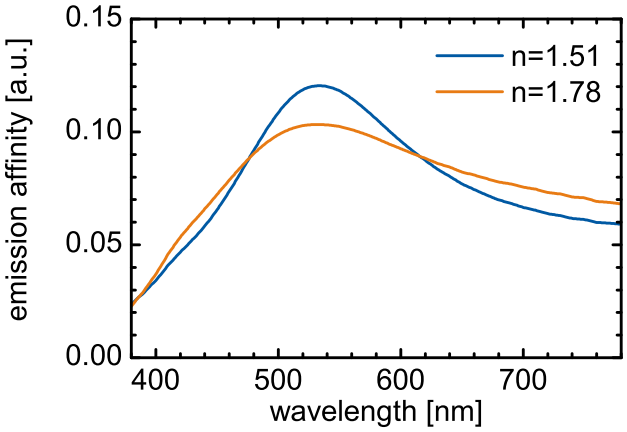

Figure 5.45: *Emission affinity of green OLEDs on standard and high-refractive-index glass. In case of high-refractive-index glass, the influence of the cavity is reduced and the emission affinity is less selective with regard to the wavelength of the emitted light.*

Furthermore, the change of the cavity results in a decrease of the number of extracted photons to 91 %. However, by outcoupling the whole light which is trapped in the glass, the photon flux of the OLED on standard glass is increased by a factor of 1.62, whereas it is increased by a factor of 1.81 in case of the OLED on high-refractive-index glass. The extraction of almost all glass modes is possible by attaching a hemisphere to the substrate. Here, a hemisphere with a diameter of 14.8 mm, a height of 6.4 mm and a refractive index of $n_d = 1.78$ as well as an index matched immersion oil (*Cargille-Sacher Laboratories Inc.*) are applied. However, the mass of a glass hemisphere for an OLED with an lighting relevant active area of 1 m^2 would exceed 1 000 kg. Therefore, it is reasonable to investigate high-refractive-index substrates in combination with flat scalable outcoupling structures. A structure which meets this requirement is the pyramid pattern which is presented in Figure 5.44. This structure is made of N-LAF21 glass (*SCHOTT AG*). The pyramids have a quadratic base with an edge length of 0.5 mm and a height of 0.25 mm. Because of geometrical reasons, a goniometer measurement is not possible for OLEDs with attached outcoupling structure. Therefore, the integrated efficiencies are measured in an Ulbricht sphere.

As mentioned above, it is beneficial to optimise the cavity of an OLED on high-refractive-index glass for enhanced substrate modes. The adapted stack is presented in Table 5.15. The colour coordinates of the spectrum emitted in forward direction are $(x,y) = (0.462, 0.429)$ at 1 000 cd/m^2 and the corresponding colour rendering index is CRI = 80.1. Figure 5.46 emphasises the high stability of the spectral shape

against varying brightness. The colour coordinates exhibit only a slight shift from $(x,y) = (0.466, 0.438)$ at 418 cd/m^2 to $(x,y) = (0.447, 0.411)$ at 6665 cd/m^2. The integrated efficiencies and the spectra measured in the Ulbricht sphere are plotted in Figure 5.47. Because the stack is optimised for a maximum fraction of glass modes, the efficiency of the flat device is reduced in comparison with the OLED on standard glass. The measurement with the hemisphere demonstrates how much light can be extracted from the device. A luminous efficacy of 90.5 lm/W and an external quantum efficiency of 75.8 % is achieved at 1000 cd/m^2, which is an increase of extracted photons by a factor of 2.9 compared with the flat OLED on standard glass. In case of the pyramid pattern, this factor is reduced to 1.6 and the efficiencies of the OLED are $\eta_v = 47.5$ lm/W and $\eta_q = 41.6$ %. Hence, a large amount of the substrate modes are lost. The critical angle for the total reflection of green light ($\lambda = 510$ nm) at the boundary between glass ($n_d = 1.78$) and air is $\vartheta_{\mathrm{c,glass}} = 34.2$ °. Therefore, the rectangular shape of the pyramids should secure light outcoupling up to a critical angle of $\vartheta_{\mathrm{c,pyramids}} = 79.2$ °. Hence, it can be assumed that a gross of the light is coupled into the substrate with an angle above $\vartheta = 80$ °and a further optimisation of the OLED especially for the pyramid pattern is possible.

Material	d [nm]
Glass substrate	$n_d = 1.78$
ITO	90
MeO-TPD: NDP-2	40: (2 wt%)
Spiro-TAD	10
4P-NPD: Ir(MDQ)$_2$acac	5: (5 wt%)
4P-NPD	5
BPhen	10
BPhen:Cs	90
Al	0.5
MeO-TPD: NDP-2	65: (2 wt%)
Spiro-TAD	10
TCTA: Ir(ppy)$_3$: Ir(dhfpy)$_2$acac	10: (8 wt%): (1 wt%)
TPBi	10
BPhen:Cs	75
Al	100

Table 5.15: *Architecture of the four colour white OLED on high-refractive-index glass. In order to improve the light-outcoupling with hemisphere and pyramid pattern, the stack is optimised for glass modes.*

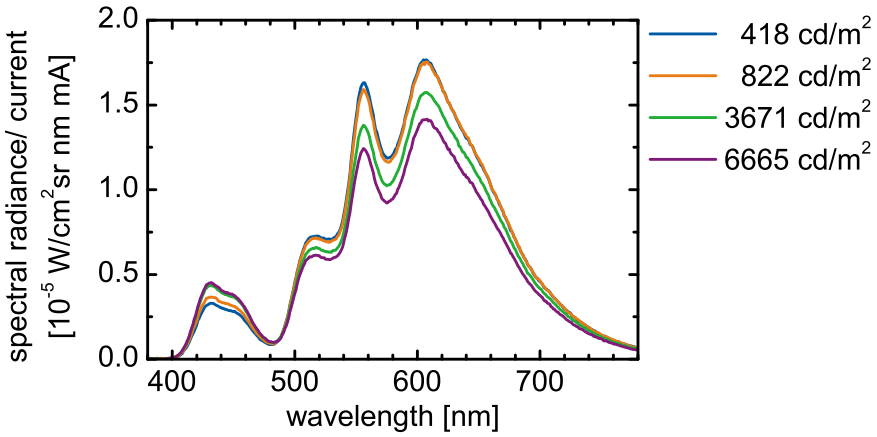

Figure 5.46: *Spectra of a four-colour white OLED on high-refractive-index glass (Table 5.15). The spectra are divided by the driving current and describe a spectral efficacy. The colour coordinates exhibit only a slight shift from* $(x,y) = (0.466, 0.438)$ *at* 418 *cd/m*^{2} *to* $(x,y) = (0.447, 0.411)$ *at* 6665 *cd/m*^{2}.

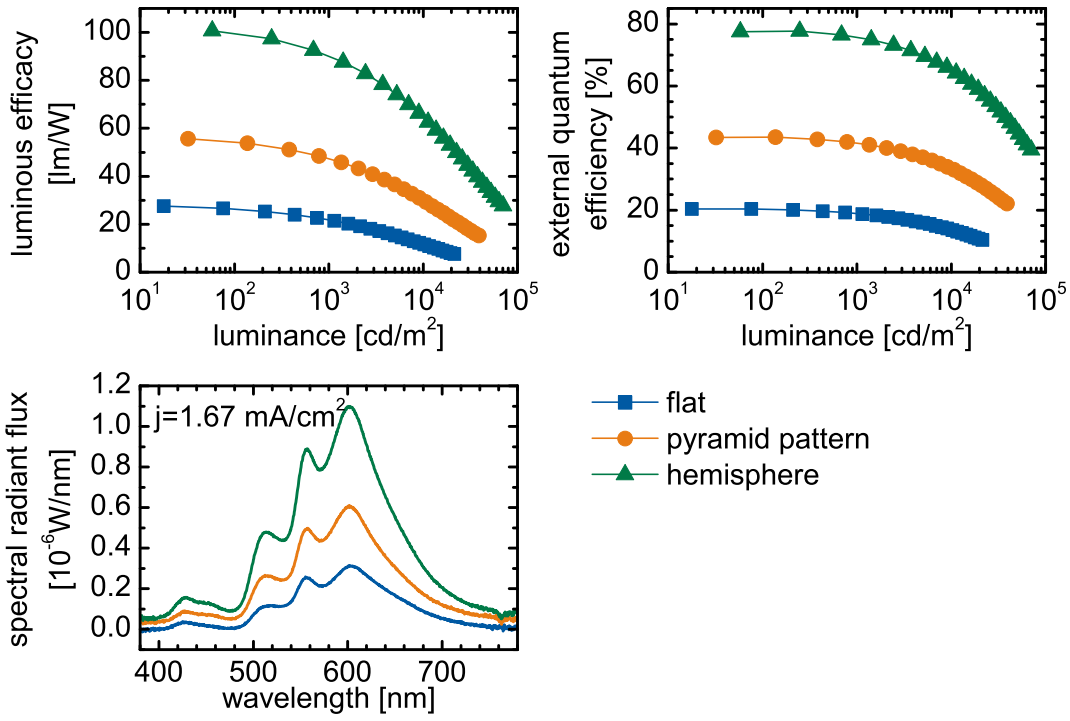

Figure 5.47: *Ulbricht sphere measurements of the device introduced in Table 5.15. By the use of a hemisphere a luminous efficacy of* 90 *lm/W at* 1000 *cd/m*^{2} *is achieved.*

6 Conclusion and Outlook

6.1 Conclusion

Three approaches were taken in order to achieve reproducible and highly efficient white OLEDs with excellent colour quality.

The first approach is based on the triplet harvesting concept. Otherwise unused triplet excitons are transferred from a fluorescent to a phosphorescent emitter with a smaller triplet energy. Because a blue emitter allowing for triplet transfer to a phosphorescent green emitter was not available, a model system for a three-colour white OLED was developed and investigated. This model device consists of the fluorescent blue emitter 4P-NPD and the phosphorescent emitters Ir(dhfpy)$_2$acac and Ir(MDQ)$_2$acac emitting in the yellow and red region, respectively. Here, it was shown that both phosphorescent emitters are excited by triplet diffusion and not by direct charge carrier recombination. A special feature of this OLED is that precise colour point control can be accomplished by layer thickness variation in the order of magnitude of a typical layer thickness in an OLED. Hence, no special requirements concerning the precision have to be met by the deposition tools. If a blue emitter was developed, which allows for triplet transfer to a phosphorescent green emitter, a highly efficient white OLED can be designed on the basis of this device.

The second approach is based on a hybrid white OLED with a single emission layer. This layer is a combination of a fluorescent blue and two phosphorescent emitters in a common matrix material. Because of the above mentioned lack of a blue emitter, which allows for triplet transfer to a green phosphorescent emitter, the concentrations of all emitters were chosen in a way that exciton transfer between the emitters was suppressed. The result is a non-radiative recombination of triplet excitons on the fluorescent blue emitter and an accordingly low quantum efficiency. However, a remarkable colour stability against varying brightness was achieved with this OLED.

The most successful approach is based on a stacked OLED. Here, the concept of triplet harvesting is limited to triplet transfer between a fluorescent blue and a phosphorescent

red emitter. The resulting spectral gap is filled by a full phosphorescent unit comprising the emission of a green and a yellow emitter, which is stacked on top of the triplet harvesting OLED. By individually optimising both units, it was possible to reach lighting relevant luminous efficacies up to $\eta_v = 33$ lm/W at 1 000 cd/m^2 from flat device without outcoupling enhancement and $\eta_v = 90$ lm/W, if the OLED is transferred to high refractive index glass and a macro extractor is attached. Despite the use of a fluorescent blue emitter, these values are comparable to the efficiencies reached with the full phosphorescent approach [17, 18]. A partial result of this optimisation process is that the combination of two phosphorescent emitters in a common matrix results in improved charge carrier balance and increased quantum efficiency in comparison to an OLED with an emission layer with only a single emitter. Since the individual units are already designed for high colour stability against varying brightness, the stacked device represents a colour stable combination of the emission of four different emitters. The fourth emitter emits in the yellow region at 557 nm and fills the spectral gap between the red and green emission maximum. Since the emission peak of the yellow emitter fits very well to the maximum of the V_λ function, an additional increase of the luminous efficacy is accomplished. Furthermore, the well balanced emission of the four emitters results in a high CRI of 80. The stacking of two OLEDs is electrically equivalent to a monolithic series connection of two OLEDs. Hence, the current density needed for a luminance of 1 000 cd/m^2 is reduced. This reduction of the current density is an important feature for lighting applications, where devices with a large active area are needed. The usual current density for a luminance around 1 000 cd/m^2 would lead to currents of several Amperes, which would result in the melting of the thin electrodes.

Small variations in the peak heights of the emitters have a strong influence on the CRI of an OLED. Therefore, a high reproducibility is very important for the development of a future product. Hence, too low concentrations or layer thicknesses have been consciously avoided throughout this work.

6.2 Outlook

The approach of simultaneous triplet harvesting to two different phosphorescent emitters and the approach of a blend layer of all three emitters would benefit from a fluorescent blue emitter with reduced singlet/triplet-splitting. In a cooperation with the Institut für Physikalische Chemie und Elektrochemie at the Technische Universität Dresden, quantum chemical calculations were used to predict the influence of the molecular structure on the position of the first excited states. The simulation shows that it is possible to tune the singlet/triplet-splitting by the degree of the methylisation of 4P-NPD. This can be explained by the Equations 3.14 and 3.15, which show that the singlet/triplet-splitting is proportional to the exchange integral between the wave functions of HOMO and LUMO (Equation 3.13). With increasing methylisation, the 4P-NPD is twisted and the overlap between HOMO and LUMO decreases. However, the synthesis of a promising candidate (Figure 6.1) could not be completed during this work. It is important to continue the identification of suitable blue emitters, because the blue emitter is still the limiting factor with regard to efficiency and lifetime in white OLEDs.

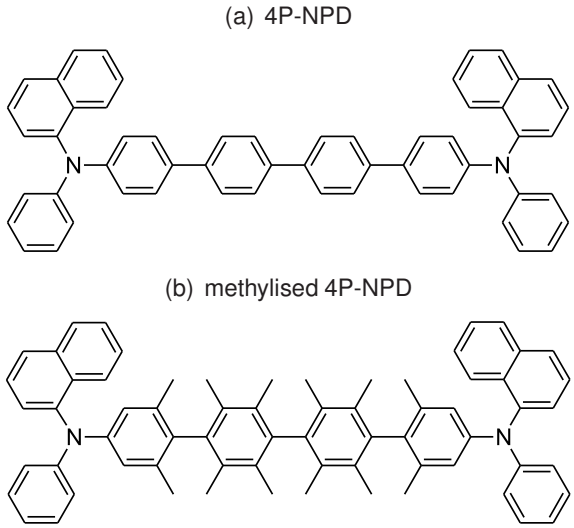

Figure 6.1: *(a) 4P-NPD and (b) a heavily methylised version of 4P-NPD being a promising candidate for having reduced singlet/triplet-splitting. The methyl groups force the molecule to twist, which leads to a decreased overlap between the wave functions of HOMO and LUMO.*

Because the triplet harvesting is limited to the transfer of excitons to the red emitter, it is not necessary to further decrease the singlet/triplet-splitting in case of the third approach. However, the stacked OLED would benefit in terms of luminous efficacy of a slightly green shifted blue emission. With a comparable singlet/triplet-splitting it is

possible to shift the maximum of the fluorescent emission to 450...460 nm without loosing the chance for triplet transfer to a red phosphorescent emitter.

The aluminium clusters in the charge generation layer of the stacked OLED lead to losses by absorption. These clusters would be obsolete if commercially available molecular n-dopants are used [48]. However, the molecule structures are not yet disclosed. Thus, these dopants are not used in this work.

The comparison between the hemisphere and the pyramid pattern show the large potential of improvement for the outcoupling structure. Although the values of the hemisphere are unlikely to be reached, an improved pattern may be able to increase the efficiency significantly. For better stack design an optical simulation tool is needed, which includes the outcoupling structure into the calculation.

The choice of materials was strongly limited by the low number of appropriate materials with known chemical structure. In some cases combinations of emitter and blocker materials were used, which are known for their irreversible reactions [121]. It is not possible to reach market relevant lifetimes with these materials. More suitable, longer living blocker materials as the *Merck* material TMM-004 are existing, but were not used due to the proprietary molecule structures [47]. However, the presented OLEDs are discussed in detail and allow for an easy transfer to more stable blocker and matrix materials.

Bibliography

[1] A. B. Chwang, M. A. Rothman, S. Y. Mao, R. H. Hewitt, M. S. Weaver, J. A. Silvernail, K. Rajan, M. Hack, J. J. Brown, X. Chu, L. Moro, T. Krajewski, and N. Rutherford. "Thin film encapsulated flexible organic electroluminescent displays". *Appl. Phys. Lett.* **83**, 413 (2003).

[2] A. P. Ghosh, L. J. Gerenser, C. M. Jarman, and J. E. Fornalik. "Thin-film encapsulation of organic light-emitting devices". *Appl. Phys. Lett.* **86**, 223503 (2005).

[3] S.-H. K. Park, J. Oh, C.-S. Hwang, J.-I. Lee, Y. S. Yang, H. Y. Chu, and K.-Y. Kang. "Ultra thin film encapsulation of organic light emitting diode on a plastic substrate". *ETRI Journal* **27**, 545 (2005).

[4] Y. Yuka and J. Ghassan. "Desktop ink-jet printer as a tool to print conducting polymers". *Synth. Met.* **156**, 779 (2006).

[5] Z. Li and H. Meng. "Organic light-emitting materials and devices". Taylor & Francis Group, Boca Raton (2007).

[6] A. Bernanose and G. Marquet. "Electroluminescence du carbazol par les champs electriques alternatifs; caracterisation de l'electrophotoluminescence organique". *J. Chim. Phys.* **51**, 255 (1954).

[7] C. W. Tang and S. A. Van Slyke. "Organic electroluminescent diodes". *Appl. Phys. Lett.* **51**, 913 (1987).

[8] M. Maitrot, G. Guillaud, B. Boudjema, J. J. André, and J. Simon. "Molecular material based junctions: formation of a schottky contact with metallophatlocyanine thin films doped by the cosublimation method". *J. Appl. Phys.* **60**, 2396 (1986).

[9] M. Pfeiffer. "Controlled Doping of Organic Vacuum Deposited Dye Layers: Basics and Applications". Dissertation, Institut für Angewandte Photophysik, Techn. Universität Dresden (1999).

[10] M. Pfeiffer, K. Leo, X. Zhou, J. S. Huang, M. Hofmann, A. Werner, and J. Blochwitz-Nimoth. "Doped organic semiconductors: physics and application in light emitting diodes". *Org. Electron.* **4**, 89 (2003).

[11] Q. Huang, S. Reineke, K. Walzer, M. Pfeiffer, and K. Leo. "Quantum efficiency enhancement in top-emitting organic light-emitting diodes as a result of enhanced intrinsic quantum yield". *Appl. Phys. Lett.* **89**, 263512 (2006).

[12] M. A. Baldo, D. F. O'Brien, Y. You, A. Shoustikov, S. Sibley, M. E. Thompson, and S. R. Forrest. "Highly efficient phosphorescent emission from organic electroluminescent devices". *Nature* **395**, 151 (1998).

[13] G. He, M. Pfeiffer, K. Leo, M. Hofmann, J. Birnstock, R. Pudzich, and J. Salbeck. "High-efficiency and low-voltage p-i-n electrophosphorescent organic light-emitting diodes with double-emission layers". *Appl. Phys. Lett.* **85**, 3911 (2004).

[14] R. Meerheim, S. Scholz, S. Olthof, G. Schwartz, S. Reineke, K. Walzer, and K. Leo. "Influence of charge balance and exciton distribution on efficiency and lifetime of phosphorescent organic light-emitting devices". *J. Appl. Phys.* **104**, 014510 (2008).

[15] N. Seidler. "Entwicklung einer Architektur für effiziente blaue OLEDs". Diplom, Institut für Angewandte Photophysik, Techn. Universität Dresden, (2009).

[16] N. Seidler, S. Reineke, K. Walzer, B. Lssem, A. Tomkeviciene, J. V. Grazulevicius, and K. Leo. "Influence of the hole blocking layer on blue phosphorescent organic light-emitting devices using 3,6-di(9-carbazolyl)-9-(2-ethylhexyl)carbazole as host material". *Appl. Phys. Lett.* **96**, 093304 (2010).

[17] S. Reineke, F. Lindner, G. Schwartz, N. Seidler, K. Walzer, B. Lüssem, and K. Leo. "White organic light-emitting diodes with fluorescent tube efficiency". *Nature* **459**, 234 (2009).

[18] T. Nakayama, K. Hiyama, K. Furukawa, and H. Ohtani. "Development of phosphorescent white OLED with extremely high power efficiency and long lifetime". *J. Soc. Inf. Display* **116**, 231 (2008).

[19] G. Lei, X. Yi, L. Duan, L. Wang, and Y. Qiu. "Multilayer white organic light-emitting diodes with a single host material". *Semicond. Sci. Technol.* **21**, 1455 (2006).

[20] Y. Hamada, K. Nishimura, and H. Kanno. "Organic electroluminescent element". United States Patent No. US 2005/0112404 A1 (26.05.2005).

[21] P. Shih, C. Chuang, E. W. Diau C. Chien, and C. Shu. "Highly efficient non-doped blue-light-emitting diodes based on an anthrancene derivative end-capped with tetraphenylethylene groups". *Adv. Funct. Mater.* **17**, 3141 (2007).

[22] J.-I. Lee, H. Y. Chu, Y. S. Yang, L.-M. Do, S. M. Chung, S.-H. K. Park, and C.-S. Hwang. "Harvest of triplet excitons in fluorescence emission layer based on a wide band gap host of TcTa for efficient white organic light emitting diodes". *Proc. SPIE* **6655**, 66550I (2007).

[23] G. Schwartz, S. Reineke, T. C. Rosenow, K. Walzer, and K. Leo. "Triplet harvesting in hybrid white organic light-emitting diodes". *Adv. Func. Mater.* **19**, 1 (2009).

[24] G. Schwartz, S. Reineke, K. Walzer, and K. Leo. "Reduced efficiency roll-off in high-efficiency hybrid white organic light-emitting diodes". *Appl. Phys. Lett.* **92**, 053311 (2008).

[25] A. Stockman and L. T. Sharpe. "Spectral sensitivities of the middle- and long-wavelength sensitive cones derived from measurements in observers of known genotype". *Vision Research* **40**, 1711 (2000).

[26] A. Roorda and D. R. Williams. "The arrangement of the three cone classes in the living human eye". *Nature* **397**, 520 (1999).

[27] C. A. Curcio, K. R. Sloan, R. E. Kalina, and A. E. Hendrickson. "Human photoreceptor topography". *J. Comp. Neurol.* **292**, 497 (1990).

[28] P. R. Boyce. "Human factors in lighting 2nd ed.". Taylor & Francis, London (2003).

[29] CIE. "Commission internationale de l'éclairage proceedings 1931". Cambridge University Press, Cambridge (1932).

[30] J. Guild. "The colorimetric properties of the spectrum". *Philosophical Transactions of the Royal Society of London* **A230**, 149 (1932).

[31] W.D. Wright. "A re-determination of the trichromatic coefficients of the spectral colours". *Transactions of the Optical Society* **30**, 141 (1928).

[32] CIE. "Method of measuring and specifying colour rendering properties of light sources". *CIE Publ.* **13.3** (1995).

[33] CIE. "Activity report". *Devision 1: Vision and Colour* **TC 1-69**, 21 (2008).

[34] K. S. Gibson and E. P. T. Tyndall. "Visibility of radiant energy". *Scientific Papers of the Bureau of Standards* **19**, 131 (1923).

[35] CIE. "Commission internationale de l'éclairage proceedings 1924". Cambridge University Press, Cambridge (1926).

[36] L. T. Sharpe, A. Stockman, W. Jagla, and H. Jägle. "A luminous efficiency function, V*(λ), for daylight adaptation". *Journal of Vision* **5**, 948 (2005).

[37] G. Wald. "Human vision and the spectrum". *Science* **101**, 653 (1945).

[38] B.H. Crawford. "The scotopic visibility function". *Proc. Phys. Soc. B* **62**, 321 (1949).

[39] R. V. Steele. "The story of a new light source". *Nature Photonics* **1**, 25 (2007).

[40] A. Žukauskas, M. S. Shur, and R. Gaska. "Introduction to solid-state lighting". John Wiley & Sons, Inc., New York (2002).

[41] N. Holonyak Jr. and S. F. Bevacqua. "Coherent (visible) light emission from Ga($As_{1-x}P_x$) junctions". *Appl. Phys. Lett.* **1**, 82 (1962).

[42] M.-F. Lin, L. Wang, W.-K. Wong, K.-W. Cheah, H.-L. Tam, M.-T. Lee, M.-H. Ho, and C. H. Chen. "Highly efficient and stable white light organic light-emitting devices". *Appl. Phys. Lett.* **91**, 073517 (2007).

[43] C.-H. Chang, C.-C. Chen, C.-C. Wua, S.-Y. Chang, J.-Y. Hung, and Y. Chi. "High-color-rendering pure-white phosphorescent organic light-emitting devices employing only two complementary colors". *Org. Electron.* **11**, 266 (2010).

[44] Y. Sun, N. C. Giebink, H. Kanno, B. Ma, M. E. Thompson, and St. R. Forrest. "Management of singlet and triplet excitons for efficient white organic light-emitting devices". *Nature* **440**, 908 (2006).

[45] M. E. Kondakova, J. C. Deaton, T. D. Pawlik, D. J. Giesen, D. Y. Kondakov, R. H. Young, T. L. Royster, D. L. Comfort, and J. D. Shore. "Highly efficient fluorescent-phosphorescent triplet-harvesting hybrid organic light-emitting diodes". *J. Appl. Phys.* **107**, 014515 (2010).

[46] L. S. Liao, K. P. Klubek, and C. W. Tang. "High-efficiency tandem organic light-emitting diodes". *Appl. Phys. Lett.* **84**, 167 (2004).

[47] H. Kanno, Y. Hamada, K. Nishimura, K. Okumoto, N. Saito, H. Ishida, H. Takahashi, K. Shibata, and K. Mameno. "High efficiency stacked organic light-emitting diodes employing Li_2O as a connecting layer". *Jap. J. Appl. Phys.* **45**, 9219 (2006).

[48] J. Birnstock, G. He, S. Murano, A. Werner, and O. Zeika. "White stacked oled with 35 lm/W and 100,000 hours lifetime at 1000 cd/m^2 for display and lighting applications". *SID 2008 Digest of Technical Papers* , 822 (2008).

[49] J. E. Lennard-Jones and C. A. Coulson. ”Part I.-homogeneous thermal reaction of hydrocarbons. the structure and energies of some hydrocarbon molecules”. *Trans. Faraday Soc.* **35**, 811 (1939).

[50] M. Pope and C. E. Swenberg. ”Electronic processes in organic crystals and polymers, 2nd Ed.”. Oxford University Press, New York (1999).

[51] W. Brütting. ”Physics of organic semiconductors”. Wiley-VCH, Weinheim (2005).

[52] F. Gutmann and L. Lyons. ”Organic semiconductors”. Wiley, New York (1967).

[53] H. Bässler. ”Charge transport in disordered organic photoconductors : a monte carlo simulation study”. *Phys. Stat. Sol. B* **175**, 15 (1993).

[54] P. I. Djurovich, E. I. Mayo, S. R. Forrest, and M. E. Thompson. ”Measurement of the lowest unoccupied molecular orbital energies of molecular organic semiconductors”. *Organic Electronics* **10**, 515 (2009).

[55] S. Krause, M. B. Casu, A. Schll, and E. Umbach. ”Determination of transport levels of organic semiconductors by ups and ips”. *New J. Phys.* **107**, 014515 (2010).

[56] L. Yan, Y. Wu, Z. Xu, and B. Hu. ”Positive and negative magnetic field effects in organic semiconducting materials”. *Synthetic Metals* **159**, 2323 (2009).

[57] M. Tian, J. Luo, and X. Liu. ”Highly efficient organic light-emitting devices beyond theoretical prediction under high current density”. *Optics Express* **17**, 21370 (2009).

[58] C. Ganzorig and M. Fujihira. ”A possible mechanism for enhanced electrofluorescence emission through triplet-triplet annihilation in organic electroluminescent devices”. *Appl. Phys. Lett.* **81**, 3137 (2002).

[59] D. Y. Kondakov. ”Characterization of triplet-triplet annihilation in organic light-emitting diodes based on anthracene derivatives”. *J. Appl. Phys.* **102**, 114504 (2007).

[60] H. Suzuki. ”Electronic absorption spectra and geometry of organic compounds”. Academic Press, New York (1967).

[61] J. Simon and J.-J. André. ”Molecular Semiconductors”. Springer-Verlag Berlin, Heidelberg (1985).

[62] T. Förster. ”Fluoreszenz organischer Verbindungen”. Vandenhoek und Ruprecht, Göttingen (1951).

[63] D. Dexter. "A theory of sensitized luminescence in solid". *J. Chem. Phys.* **21**, 836 (1953).

[64] M. Klessinger and J. Michl. "Excited states and photochemistry of organic molecules". VCH Publishers, New York (1995).

[65] V. I. Arkhipov, E. V. Emelianova, and H. Bässler. "Quenching of excitons in doped disordered organic semiconductors". *Phys. Rev. B* **70**, 205205 (2004).

[66] R. C. Powell and Z. G. Soos. "Singlet exciton energy transfer in organic solids". *J. Lumin.* **11**, 1 (1975).

[67] Y. C. Zhou, L. L. Ma, J. Zhou, X. M. Ding, and X. Y. Hou. "Effect of a sensing layer on triplet exciton diffusion in organic films". *Phys. Rev. B* **75**, 132202 (2007).

[68] M. A. Baldo, C. Adachi, and S. R. Forrest. "Transient analysis of organic electrophosphorescence. II. transient analysis of triplet-triplet annihilation". *Phys. Rev. B* **62**, 10967 (2000).

[69] S. Reineke, K. Walzer, and K. Leo. "Triplet-exciton quenching in organic phosphorescent light-emitting diodes with Ir-based emitters". *Phys. Rev. B* **75**, 125328 (2007).

[70] D. Hertel and K. Meerholz. "Triplet-polaron quenching in conjugated polymers". *J. Phys. Chem. B* **111**, 12075 (2007).

[71] S. H. Glarum. "Electron mobilities in organic semiconductors". *J. Phys. Chem. Solids* **24**, 1577 (1963).

[72] N. Karl. "Charge carrier transport in organic semiconductors". *Synthetic Metals* **133**, 649 (2003).

[73] V. I. Arkhipov and H. Bässler. "A model of weak-field quasi-equilibrium hopping transport in disordered materials". *Phil. Mag. Lett.* **67**, 343 (1993).

[74] M. Lampert and P. Mark. "Current injection in solids". Academic Press, New York (1970).

[75] J. Kido and T. Matsumoto. "Bright organic electroluminescent devices having a metal-doped electron-injecting layer". *Appl. Phys. Lett.* **73**, 2866 (1998).

[76] O. Solomeshch, Y. J. Yu, A. A. Goryunkov, L. N. Sidorov, R. F. Tuktarov, D. H. Choi, J.-I. Jin, and N. Tessler. "Ground-state interaction and electrical doping of fluorinated C60 in conjugated polymers". *Adv. Mater.* **21**, 4456 (2009).

[77] Selina Olthof. ”Photoelectron spectroscopy on doped organic semiconductors and related interfaces”. Dissertation, Institut für Angewandte Photophysik, Techn. Universität Dresden (2010).

[78] W. Gao and A. Kahn. ”Controlled p-doping of zinc phthalocyanine by coevaporation with tetrafluorotetracyanoquinodimethane: a direct and inverse photoemission study”. *Appl. Phys. Lett.* **79**, 4040 (2001).

[79] S. Olthof, R. Meerheim, M. Schober, and K. Leo. ”Energy level alignment at the interfaces in a multilayer organic light-emitting diode structure”. *Phys. Rev. B* **79**, 245308 (2009).

[80] P. Gemmern, V. Elsbergen, S. Grabowski, H. Boerner, H. Löbl, H. Bekcer, H. Kalisch, M. Heuken, and R. Jansen. ”Influence of carrier conductivity and injection on efficiency and chromaticity in small-molecule white organic light-emitting diodes based on 4,4’-bis(2,2’-diphenylvinyl)-1,1’-spirobiphenyl and rubrene”. *J. Appl. Phys.* **100**, 123707 (2006).

[81] M. Ikai, S. Tokito, Y. Sakamoto, T. Suzuki, and Y. Taga. ”Highly efficient phosphorescence from organic light-emitting devices with an exciton-block layer”. *Appl. Phys. Lett.* **79**, 156 (2001).

[82] M. Aonuma, T. Oyamada, T. Miki H. Sasabe, and C. Adachi. ”Material design of hole transport materials capable of thick-film formation in organic light emitting diodes”. *Appl. Phys. Lett.* **90**, 183503 (2007).

[83] I. G. Hill, D. Milliron, J. Schwartz, and A. Kahn. ”Organic semiconductor interfaces: electronic structure and transport properties”. *Appl. Surf. Sci.* **166**, 354 (2000).

[84] I. Tanaka, Y. Tabata, and S. Tokito. ”Observation of phosphorescence from tris(8-hydroxyquinoline) aluminum thin films using triplet energy transfer from iridium complexes”. *Phys. Rev. B* **71**, 205207 (2005).

[85] J. Jou, C. Wang, M. Wu, P. Chiang, H. Lin, H. Li, and R. Liu. ”Efficient fluorescent white organic light-emitting diodes with blue-green host of di(4-fluorophenyl)amino-di(styryl)biphenyl”. *Org. Electron.* **8**, 29 (2007).

[86] V. Bulović, A. Shoustikov, M. A. Baldo, E. Bose, V. G. Kozlov, M. E. Thompson, and S. R. Forrest. ”Bright, saturated, red-to-yellow organic light-emitting devices based on polarization-induced spectral shifts”. *Chem. Phys. Lett.* **287**, 455 (1998).

[87] M. A. Baldo, S. Lamansky, P. E. Burrows, M. E. Thompson, and S. R. Forrest. ”Very high-efficiency green organic light-emitting devices based on electrophosphorescence”. *Appl. Phys. Lett.* **75**, 4 (1999).

[88] S. Reineke, G. Schwartz, K. Walzer, M. Falke, and K. Leo. "Highly phosphorescent organic mixed films: The effect of aggregation on triplet-triplet annihilation". *Appl. Phys. Lett.* **94**, 163305 (2009).

[89] J. C. Deaton, D. W. Place, C. T. Brown, M. Rajeswaran, and M. E. Kondakova. "The blue aluminum and gallium chelates for OLEDs". *Inorg. Chim. Acta* **361**, 1020 (2008).

[90] D. Schneidenbach, S. Ammermann, M. Debeaux, A. Freund, M. Zöllner, C. Daniliuc, P. G. Jones, W. Kowalsky, and H.-H. Johannes. "Efficient and long-time stable red iridium(III) complexes for organic light-emitting diodes based on quinoxaline ligands". *Inorg. Chem.* **49**, 397 (2010).

[91] C. Adachi, R. Kwong, and S. R. Forrest. "Efficient electrophosphorescence using a doped ambipolar conductive molecular organic thin film". *Organic Electronics* **2**, 37 (2001).

[92] A. Hjortsberg. "Accurate determination of optical constants of absorbing materials: measurements of transmittance and reflectance of thin films on partially metallized substrates". *Thin Solid Films* **69**, L15 (1980).

[93] T. Fritz, J. Hahn, and H. Böttcher. "Determination of the optical constants of evaporated dye layers". *Thin Solid Films* **170**, 249 (1989).

[94] R. Meerheim, K. Walzer, M. Pfeiffer, and K. Leo. "Ultrastable and efficient red organic light emitting diodes with doped transport layers". *Appl. Phys. Lett.* **89**, 061111 (2006).

[95] H. Benisty, R. Stanley, and M. Mayer. "Method of source terms for dipole emission modification in modes of arbitrary planar structures". *J. Opt. Soc. Am. A* **15**, 1192 (1998).

[96] M. Furno, R. Meerheim, M. Thomschke, S. Hofmann, B. Luessem, and K. Leo. "Outcoupling efficiency in small-molecule OLEDs: from theory to experiment". *Proc. SPIE* **7617**, 761716 (2010).

[97] C. C. Katsidis and D. I. Siapkas. "General transfer-matrix method for optical multilayer systems with coherent, partially coherent, and incoherent interference". *Appl. Opt.* **41**, 3978 (2002).

[98] N. C. Greenham, R. H. Friend, and D. C. Bradley. "Angular dependence of the emission from a conjugated polymer light-emitting diode: implications for efficiency calculations". *Adv. Mater.* **6**, 491 (1994).

[99] S.-W. Wen, M.-T. Lee, and C. H. Chen. "Recent development of blue fluorescent oled materials and devices". *J. Disp. Techn.* **1**, 90 (2005).

[100] M. Ho, Y. Wu, S. Wen, M. Lee, T. Chen, C. H. Chen, K. Kwok, S. So, K. Yeung, Y. Cheng, and Z. Gao. "Highly efficient deep blue organic electroluminescent device based on 1-methyl-9,10-di(1-naphthyl)anthracene". *Appl. Phys. Lett.* **89**, 252903 (2006).

[101] I. G. Hill, A. J. Mäkinen, and Z. H. Kafafi. "Initial stages of metal/organic semiconductor interface formation". *J. Appl. Phys.* **88**, 889 (2000).

[102] K. Okumoto, H. Kanno, Y. Hamada, H. Takahashi, and K. Shibata. "High efficiency red organic light-emitting devices using tetraphenyldibenzoperiflanthene-doped rubrene as an emitting layer". *Appl. Phys. Lett.* **89**, 013502 (2006).

[103] K. Okumoto, H. Kanno, Y. Hamada, H. Takahashi, and K. Shibata. "Green fluorescent organic light-emitting device with external quantum efficiency of nearly 10%". *Appl. Phys. Lett.* **89**, 063504 (2006).

[104] F. Yen, C. Chiu, I. Lin, C. Teng, and X. Lin. "Efficient deep blue, blue, green, yellow, reddish-orange and red organic light-emitting device using 2,7-dipyrenespirofluorene (DPSF) as a fluorescent emitting host". *SID Symposium Digest of Technical Papers* **38**, 883 (2007).

[105] Gregor Schwartz. "Novel concepts for high-efficiency white organic light-emitting diodes". Dissertation, Institut für Angewandte Photophysik, Techn. Universität Dresden (2007).

[106] G. Schwartz, M. Pfeiffer, S. Reineke, K. Walzer, and K. Leo. "Harvesting triplet excitons from fluorescent blue emitters in white organic light-emitting diodes". *Adv. Mater.* **19**, 3672 (2007).

[107] R. Pudzich, T. Fuhrmann-Lieker, and J. Salbeck. "Spiro compounds for organic electroluminescence and related applications". *Adv. Polym. Sci.* **199**, 83 (2006).

[108] L. Peter and G. Vaubel. "Triplet exciton lifetime in crystalline pyrene". *Chem. Phys. Lett.* **18**, 531 (1973).

[109] A. D. Walser, R. Priestley, and R. Dorsinville. "Temperature dependence of the singlet excited state lifetime in Alq_3". *Synthetic Metals* **102**, 1552 (1999).

[110] R. G. Kepler, J. C. Caris, P. Avakian, and E. Abramson. "Triplet excitons and delayed fluorescence in anthracene crystals". *Phys. Rev. Lett.* **10**, 400 (1963).

[111] S. Singh, W. J. Jones, W. Siebrand, B. P. Stoicheff, and W. G. Schneider. "Laser generation of excitons and fluorescence in anthracene crystals". *J. Chem. Phys.* **42**, 330 (1965).

[112] W. Holzer, A. Penzkofer, and T. Tsuboi. "Absorption and emission spectroscopic characterization of Ir(ppy)$_3$". *Chemical Physics* **308**, 93 (2005).

[113] B. W. D' Andrade, S. Datta, S. R. Forrest, P. Djurovich, E. Polikarpov, and M. E. Thompson. "Relationship between the ionization and oxidation potentials of molecular organic semiconductors". *Organic Electronics* **6**, 11 (2005).

[114] K. Fehse, K. Walzer, K. Leo, W. Lövenich, and A. Elschner. "Highly conductive polymer anodes as replacements for inorganic materials in high-efficiency organic light-emitting diodes". *Adv. Mater.* **19**, 441 (2007).

[115] H.-D. Lee, S. J. Lee, K. Y. Lee, B. S. Kim, S. H. Lee, H. D. Bae, and Y. H. Tak. "High efficiency tandem organic light-emitting diodes using interconnecting layer". *Jpn. J. Appl. Phys.* **48**, 082101 (2009).

[116] Y.-S. Wu, S.-W. Hwang, H.-H. Chen, M.-T. Lee, W.-J. Shen, and C. H. Chen. "Efficient white organic light emitting devices with dual emitting layers". *Thin Solid Films* **488**, 265 (2005).

[117] B. Maennig, J. Drechsel, D. Gebeyehu, P. Simon, F. Kozlowski, A. Werner, F. Li, S. Grundmann, S. Sonntag, M. Koch, K. Leo, M. Pfeiffer, H. Hoppe, D. Meissner, N.S. Saricifci, I. Riedel, and J. Parisi. "Organic p-i-n solar cells". *Appl. Phys. A - Mat. Sci. Process* **79**, 1 (2004).

[118] A. Yakimov and S. R. Forrest. "High photovoltage multiple-heterojunction organic solar cells incorporating interfacial metallic nanoclusters". *Appl. Phys. Lett.* **80**, 1667 (2002).

[119] M. Westphalen, U. Kreibig, J. Rostalski, H. Lüth, and D. Meissner. "Metal cluster enhanced organic solar cells". *Sol. Energy Mater. Sol. Cells* **61**, 97 (2000).

[120] S. Scholz, K. Walzer, and K. Leo. "Analysis of complete organic semiconductor devices by laser desorption/ionization time-of-flight mass spectrometry". *Adv. Funct. Mater.* **18**, 2541 (2008).

[121] S. Scholz, R. Meerheim, B. Lüssem, and K. Leo. "Laser desorption/ionization time-of-flight mass spectrometry: A predictive tool for the lifetime of organic light emitting devices". *Appl. Phys. Lett.* **94**, 043314 (2009).

Acknowledgements

An dieser Stelle möchte ich einigen Menschen danken, ohne die diese Arbeit nicht möglich gewesen wäre. Vor allen Anderen danke ich Prof. K. Leo für die Möglichkeit, dieses Thema am IAPP bearbeiten zu können. Sein Rat und seine Unterstützung waren mir stets eine große Hilfe.

Desweitern danke ich

- Prof. K. Meerholz dafür, dass er sich die Zeit genommen hat diese Arbeit als Zweitgutachter zu lesen und zu bewerten.
- Björn Lüssem für zahlreiche Diskussionen und konstruktive Denkanstöße.
- Karsten Walzer, der vor Björn unsere Arbeitsgruppe geleitet hat.
- Ajay Perumal for patiently correcting my grammar.
- Ansgar Werner, Andreas Haldi für so manches hilfreiches Gespräch.
- Mauro Furno for developing an exquisite tool for the optical simulation of OLEDs.
- Carsten Wolf und Christian Kolberg, ohne deren Unterstützung die Wartung der Vakuumanlagen nicht zu bewältigen gewesen wäre.
- Den Mitarbeiterinnen und Mitarbeitern des Lesker-Teams, welche für meine Proben nicht nur einmal Überstunden einlegen mussten.
- Sämtlichen anderen Mitarbeiterinnen und Mitarbeitern des IAPP für ihre Unterstützung und die angenehme Arbeitsatmosphäre.

Erklärung

Diese Dissertation wurde am Institut für Angewandte Photophysik an der Technischen Universität Dresden unter wissenschaftlicher Betreuung durch Prof. Dr. Karl Leo angefertigt.

Ich erkenne die Promotionsordnung der Fakultät Mathematik und Naturwissenschaften an der Technischen Universität Dresden vom 20. März 2000, in der Fassung der vom Fakultätsrat am 19.06.2002 und 12.07.2002 beschlossenen und mit Erlass des Sächsischen Staatsministeriums für Wissenschaft und Kunst vom 18.03.2003 genehmigten Änderungen gemäß Satzung vom 16.04.2003 sowie gemäß der Änderungssatzung vom 17.07.2008 an.

Hiermit versichere ich, dass ich die vorliegende Arbeit ohne unzulässige Hilfe Dritter und ohne Benutzung anderer als der angegebenen Hilfsmittel angefertigt habe; die aus fremden Quellen direkt oder indirekt übernommenen Gedanken sind als solche kenntlich gemacht. Die Arbeit wurde bisher weder im Inland noch im Ausland in gleicher oder ähnlicher Form einer anderen Prüfungsbehörde vorgelegt.

Thomas Rosenow
Dresden, den 11.06.2010

Kurzfassung

Die vorliegende Arbeit beschäftigt sich mit drei Ansätzen der hocheffizienten Erzeugung von weißem Licht mit organischen Leuchtdioden (OLEDs) auf der Basis kleiner Moleküle.

Ein Ansatz kombiniert die Emission eines fluoreszenten und zweier phosphoreszenter Emitter in einer einzelnen Emissionsschicht. Da das Triplettniveau des verwendeten Blauemitters niedriger ist als die Triplettniveaus der phosphoreszenten Emitter, werden die Konzentrationen der Emitter so gewählt, dass ein Exzitonenübertrag zwischen ihnen unterbunden wird. Die strahlungslose Rekombination von Tripletts auf dem fluoreszenten Blauemitter begrenzt die Effizienz dieses Ansatzes, jedoch besticht die resultierende weiße OLED durch eine bemerkenswerte Farbstabilität.

Der zweite Ansatz basiert auf dem "Triplet Harvesting" Konzept. Ansonsten ungenutzte Triplett Exzitonen werden von einem fluoreszenten Blauemitter auf phosphoreszente Emitter übertragen, wodurch interne Quanteneffizienzen bis zu 100 % möglich sind. Der zur Verfügung stehende Blauemitter 4P-NPD erlaubt aufgrund seines niedrigen Triplettniveaus nicht den Triplettübertrag auf einen grünen Emitter. Daher wird das "Triplet Harvesting" auf zwei unterschiedliche phosphoreszente Emitter, anhand des gelben Emitters Ir(dhfpy)$_2$acac und des roten Emitters Ir(MDQ)$_2$acac untersucht. Es wird gezeigt, dass beide phosphoreszente Emitter indirekt durch Exzitonendiffusion angeregt werden und nicht durch direkte Rekombination von Ladungsträgern auf den Emittermolekülen. Eine genaue Justage der Anregungsverteilung zwischen den phosphoreszenten Emittern ist durch Schichtdickenvariation in der Größenordnung üblicher Schichtdicken möglich. Spätere Produktionsanlagen brauchen daher keinen speziellen Genauigkeitsanforderungen gerecht zu werden.

Der dritte und zugleich erfolgreichste Ansatz beruht auf einer Weiterentwicklung des zweiten Ansatzes. Er besteht zunächst darin den Tripletttransfer auf den Übertrag von einem fluoreszenten blauen auf einen phosphoreszenten roten Emitter zu beschränken. Die sich ergebende spektrale Lücke wird durch direktes Prozessieren einer unabhängigen voll phosphoreszenten OLED auf diese erste OLED gefüllt. Verbunden sind beide OLEDs durch eine ladungsträgererzeugende Schicht, in welcher durch das angelegte

Feld Elektron/Loch-Paare getrennt werden. Dieser Aufbau entspricht elektrisch der Reihenschaltung zweier OLEDs, welche im Rahmen dieser Arbeit individuell untersucht und optimiert werden. Dabei ergibt sich, dass die Kombination von zwei verschiedenen phosphoreszenten Emittern in einer gemeinsamen Matrix die Ladungsträgerbalance in der Emissionszone sowie die Quanteneffizienz der vollphosphoreszenten OLED stark verbessert. Als Ergebnis steht eine hocheffiziente weiße OLED, welche durch die ausgewogene Emission von vier verschiedenen Emittern farbstabiles Licht mit warm weißen Farbkoordinaten $(x,y) = (0.462, 0.429)$ und ausgezeichneten Farbwiedergabeeigenschaften (CRI $= 80.1$) erzeugt. Dabei sind die mit diesem Ansatz erreichten Lichtausbeuten ($\eta_v = 90.5$ lm/W) mit denen von voll phosphoreszenten OLEDs vergleichbar.